Copyright Warning & Restrictions

The copyright law of the United States (Title 17, United States Code) governs the making of photocopies or other reproductions of copyrighted material.

Under certain conditions specified in the law, libraries and archives are authorized to furnish a photocopy or other reproduction. One of these specified conditions is that the photocopy or reproduction is not to be "used for any purpose other than private study, scholarship, or research." If a, user makes a request for, or later uses, a photocopy or reproduction for purposes in excess of "fair use" that user may be liable for copyright infringement,

This institution reserves the right to refuse to accept a copying order if, in its judgment, fulfillment of the order would involve violation of copyright law.

Please Note: The author retains the copyright while the New Jersey Institute of Technology reserves the right to distribute this thesis or dissertation

Printing note: If you do not wish to print this page, then select "Pages from: first page # to: last page #" on the print dialog screen

NJIT New Jersey's Science & Technology University

The Van Houten library has removed some of the personal information and all signatures from the approval page and biographical sketches of theses and dissertations in order to protect the identity of NJIT graduates and faculty.

ABSTRACT

NYSTRÖM METHODS FOR HIGH-ORDER CQ SOLUTIONS OF THE WAVE EQUATION IN TWO DIMENSIONS

by
Erli Wind-Andersen

An investigation of high order Convolution Quadratures (CQ) methods for the solution of the wave equation in unbounded domains in two dimensions is presented. These rely on Nyström discretizations for the solution of the ensemble of associated Laplace domain modified Helmholtz problems. Two classes of CQ discretizations are considered: one based on linear multistep methods and the other based on Runge-Kutta methods. Both are used in conjunction with Nyström discretizations based on Alpert and QBX quadratures of Boundary Integral Equation (BIE) formulations of the Laplace domain Helmholtz problems with complex wavenumbers. CQ in conjunction with BIE is an excellent candidate to eventually explore numerical homogenization to replace a chaff cloud by a dispersive lossy dielectric that produces the same scattering. To this end, a variety of accuracy tests are presented that showcase the high-order in time convergence (up to and including fifth order) that the Nyström CQ discretizations are capable of delivering for a variety of two dimensional single and multiple scatterers. Particular emphasis is given to Lipschitz boundaries and open arcs with both Dirichlet and Neumann boundary conditions.

NYSTRÖM METHODS FOR HIGH-ORDER CQ SOLUTIONS OF THE WAVE EQUATION IN TWO DIMENSIONS

by
Erli Wind-Andersen

A Dissertation
Submitted to the Faculty of
New Jersey Institute of Technology and
Rutgers, The State University of New Jersey – Newark
in Partial Fulfillment of the Requirements for the Degree of
Doctor of Philosophy in Mathematical Sciences

Department of Mathematical Sciences
Department of Mathematics and Computer Science, Rutgers-Newark

May 2022

Copyright © 2022 by Erli Wind-Andersen

ALL RIGHTS RESERVED

APPROVAL PAGE

NYSTRÖM METHODS FOR HIGH-ORDER CQ SOLUTIONS OF THE WAVE EQUATION IN TWO DIMENSIONS

Erli Wind-Andersen

Catalin Turc, Dissertation Co-Advisor — Date
Associate Professor of Mathematical Sciences, NJIT

Peter G. Petropoulos, Dissertation Co-Advisor — Date
Associate Professor of Mathematical Sciences, NJIT

Shahriar Afkhami, Committee Member — Date
Professor of Mathematical Sciences, NJIT

David Shirokoff, Committee Member — Date
Associate Professor of Mathematical Sciences, NJIT

Carlos Pérez Arancibia, Committee Member — Date
Assistant Professor of Applied Mathematics,
University of Twente, Enschede, Netherlands

BIOGRAPHICAL SKETCH

Author: Erli Wind-Andersen

Degree: Doctor of Philosophy

Date: May 2022

Undergraduate and Graduate Education:

- Doctor of Philosophy in Mathematical Sciences,
  New Jersey Institute of Technology, Newark, NJ, 2022
- Master in Mathematics,
  New York University, New York, NY, 2016
- Bachelor of Science in Mathematics,
  Fordham University, Bronx, NY, 2013

Major: Mathematical Sciences

Presentations and Publications:

Peter P. Petropoulos, Catalin Turc, and Erli Wind-Andersen. Nyström methods for high-order CQ solutions of the wave equation in two dimensions. *arXiv*, 2111.06829.

You have to know how to look even if you don't know what you're looking for.

Roberto Bolaño

Mam: for 33 år siden gav du digselv et løfte. Du forudså fremtiden med uhyggelig nøjagtighed. Tillykke, du har holdt dit løfte. Papa: din støtte, lige siden jeg rejste hjemmefra, og flyttede hjem igen, og ud og ind igen, og hjem og ud igen igen, har du altid været der. Du har altid været interesseret, selv når jeg har manglet gå på mod. Det gjorde altid arbejdet mere interresant at komme tilbage til.

I dedicate the following to them.

ACKNOWLEDGMENT

I don't have the linguistic skills to accurately describe what my advisors mean to me; nor is the section long enough to recount all the ways in which they have shaped and guided me. I will therefore just mention one: they set a standard that they were unwilling to compromise on, thankfully. They were always available to help make the research, and myself as an academic, better. Thank you for introducing me to such a beautiful subject that most likely will take a lifetime to fully absorb.

My deep appreciation also goes to my committee: Professor Shahriar Afkhami, Professor David Shirokoff, and Professor Carlos Pérez Arancibia. I am particularly indebted to Professor Perez, though he may be unaware of it. Research papers in this field are not always easy to digest, his papers, however, have always been clear and a pleasure to read. This has made my life much easier.

The DMS also deserves praise, in particular the administrative staff: Michelle, Will Pauline, Ray, and especially Allison. They have been beyond excellent at helping me navigate all non-academic tasks.

To my friends, thank you for making work feel like play. It was always a pleasure to toss around ideas, both mathematical and otherwise, with Connor, David, Binan, Jimmey, Diego, and Axel. I will never look at tea the same, thanks to Axel, which I am not sure is a good thing. James, Yair, and Morten: I don't think I could find a group of more sarcastic and inappropriate acquaintances than you. Wahlberger. Just Wahlberger. Gus, thank you for all the good times: one of these days the Mets are comming out on top.

Rolf, this is all your fault and Danya, you know what you did.

To all my family, I give all my love and appreciation. My brother, mother, and father have plenty to do with any of my past or future success.

TABLE OF CONTENTS

TABLE OF CONTENTS
(Continued)

Chapter **Page**

LIST OF TABLES

Table **Page**

LIST OF FIGURES

Figure **Page**

LIST OF FIGURES
(Continued)

Figure **Page**

List of Algorithms

CHAPTER 1

INTRODUCTION

Chaff is one of the simplest and cheapest radar counter measures. Chaff consists of a very large collection of metal wires or fibres that, once dispersed in the air, make a chaff cloud. Signals reflected from a chaff cloud are an effective means of disturbing a radar system, and as such, are commonly used in military defense. Hence, the study of electromagnetic scattering becomes important in the context of defensive means.

Towards this end, in this dissertation we will solve the problem of time-domain scattering of pulses incident on large collections of two-dimensional scatterers on the boundaries of which Dirichlet or Neumann boundary conditions are imposed. Additionally the case of when all scatterers do not have the same boundary conditions are also considered. The individual scatterer boundaries that will be considered are smooth, piecewise-smooth, closed curves, or open curves (with knife-edges). The most immediate application of this type of mathematical problem is to calculate the scattered field arising from a chaff cloud. We present the work accomplished thus far towards a robust, efficient, and highly-accurate numerical method to accomplish the goal of this dissertation.

Much literature exists on the numerical solution of time-domain scattering problems governed by the wave equation. The typical numerical approaches fall into three categories: Finite Difference Time-Domain methods (FDTD), Finite Element Time-Domain methods (FETD), and Time-Domain Boundary Integral Equation methods (TDBIE) using retarded potentials. A very brief discussion of these methods, and of their shortcomings for the scattering problems we wish to solve, is presented below.

The FDTD method is presented in detail in [86] and in hundreds of thousands of other publications. In this method, the time-domain Maxwell's Equations are discretized via finite differences in both time and space, and, in order to satisfy the Sommerfeld radiation condition that says "all waves outside a region of space occupied by scatterers must propagate out to infinity," a large computational domain must be utilized. Typically, one considers a smaller domain and makes use of absorbing boundary conditions, [37, 9, 11, 46, 53], to simulate the presence of infinite space surrounding the region that contains all the scatterers. Further, solutions obtained with the FDTD method, by virtue of the method being a simple second-order accurate in space and time Leapfrog scheme, suffer from numerical dispersion error; to get accurate results, fine spatial and temporal meshes are necessary in order to control the dispersion error; since dispersion errors accumulate, this aspect of FDTD methods is highly deleterious when the incident pulse spectrum is wide (short-duration pulses in the time-domain), when long time simulations are required (long time relative to some timescale, typically the incident pulse duration), or when a very large collection of scatterers is employed. Finally, FDTD methods require special differencing strategies when scatterer boundaries are not aligned with the cartesian mesh and when scatterers possess corners and/or edges. The FETD method, suffers from the same issues as FDTD, with the exception being that its finite elements aspect allows for handling the kind of geometries and boundary conditions we are interested in. A further downside of the FETD methods is that these techniques require the usage of meshes that can be difficult to generate depending on the geometry considered. Finally, TDBIE formulations for surface scattering problems involves working at the level of the retarded layer potentials of the wave equation, [8, 92, 40, 44]. In addition, it has also been shown to be difficult to obtain stability with these methods, [30, 29]. As a result, TDBIE methods have typically only been used with low-order accuracy (first-order at best).

To address all the shortcomings of the previously described methods, we will employ Convolution Quadratures (CQ), [67, 7, 68, 48, 62, 12], with very-high accuracy time-stepping schemes to solve the scattering problems of interest that we briefly described above. The CQ methods reduce the solution of TDBIEs to an ensemble of frequency domain solutions of modified Helmholtz equations. By making use of collocation Nyström schemes for solving the Helmholtz equation, we are thus able to reduce our computational dimension by one. In addition, by taking advantage of the reformulation of the Helmholtz equation as an integral equation, we satisfy the radiation condition. Such methods can deliver high-order accuracy in space and time that is preserved even for non-smooth scatterer geometries.

An efficient and accurate numerical solution of the wave equation in two dimensional unbounded domains based on the Convolution Quadrature for the time discretization and on Boundary Integral Equation methods for the spatial discretization will be presented. Additionally, a basic exposition of Convolution Quadrature (CQ) methods and their application to time domain boundary integral equations (TDBIE) will also be covered. Via Laplace transforms and FFTs, CQ methods reduce the solution of TDBIE to an ensemble of frequency domain solutions of modified Helmholtz equations. The latter, in turn, are solved using Boundary Integral Equation formulations and Nystrom methods based on Alpert quadratures. We present a variety of numerical examples that exhibit high-order convergence (up to and including fifth order) in time for Convolution Quadrature methods for the solution of the wave equation in two dimensions. This work consists of applying the computational machinery described above to the efficient simulation of the interaction of time domain pulsed waves with large ensembles of open/closed scatterers, with applications in remote sensing and radar (e.g., chaff countermeasures). In particular, our goal is to eventually explore numerical homogenization to replace a model chaff cloud by a dispersive lossy dielectric that produces the same scattering. Towards

this application, we have found that CQ with BIE to be an excellent candidate to tackle the chaff cloud scattering problem, which we have verified through numerical experimentation. Though the benefits and efficiency of this method is significant, more computational speed is needed to solver larger scale problems. Currently, the field can be computed with less than a hundred scatterers within a reasonable amount of time. Obviously fast evaluation methods are needed to scale the problem beyond hundreds of scatterers to thousands. This is the limitation we are currently dealing with.

The dissertation is structured as follows. In Chapter 2, we derive the basic CQ method with appropriate time-stepping schemes, where the algorithms are also presented. In this same section, a way to verify the CQ method independent of time is also presented. In Chapter 3, we investigate how to solve the frequency Helmholtz problem with different boundary conditions and a variety of geometries. Chapter 4 is dedicated to multiple scattering and the preconditioners needed to effeciently calculate the unknown densitues. Chapter 5 shows the numerical results of implementing the CQ method again under different geometries and boundary conditions. Chapter 6 gives a summation of the work described throughout the previous chapters as well as a brief discussion on the natural extensions to the current work.

CHAPTER 2

CQ FOR SOLVING THE WAVE EQUATION

We are interested in solving the wave equation in a two-dimensional infinite domain $\Omega^+ := \mathbb{R}^2 \setminus \overline{\Omega}$, where Ω is a bounded domain in $\mathbb{R}^2$:

$$\begin{cases} c^{-2}\frac{\partial^2 u}{\partial t^2} & = \Delta u \quad \text{in } \Omega^+ \times (0,\infty) \\ u(x,0) & = \frac{\partial u(x,0)}{\partial t} = 0 \quad \text{in } \Omega^+ \\ u(x,t) & = g(x,t) \quad \text{on } \Gamma \times (0,\infty), \end{cases}$$

and we denoted $\Gamma := \partial\Omega$. Using the formula for the fundamental solution of the wave equation in two dimensions

$$k_{2D}(x,t) := \frac{H(t - c^{-1}|x|)}{2\pi\sqrt{t^2 - c^{-2}|x|^2}}$$

we seek for a solution $u(x,t)$ of the wave equation in the form of a Time Domain Single-Layer (TDSL) potential:

$$\begin{aligned} u(x,t) &= (S * \lambda)(x,t) = \int_\Gamma \int_0^t k_{2D}(t-\tau, x-y)\lambda(y,\tau)ds(y)d\tau \\ &= \frac{1}{2\pi}\int_\Gamma \int_0^{t-c^{-1}|x-y|} \frac{\lambda(y,\tau)}{\sqrt{(t-\tau)^2 - c^{-2}|x-y|^2}} s(y)d\tau \end{aligned}$$

in terms of the unknown boundary density function λ. Imposing the Dirichlet boundary conditions leads to the following Time Domain Boundary Integral Equation (TDBIE)

$$\int_\Gamma \int_0^t k_{2D}(t-\tau, x-y)\lambda(y,\tau)ds(y)d\tau = g(x,t) \quad \text{on } \Gamma \times (0,\infty). \tag{2.1}$$

We solve the TDBIE (2.1) using the Convolution Quadrature (CQ) methodology which we describe in what follows. Our presentation is concerned exclusively with the algorithmic aspects of CQ and follows that in the textbook of Sayas [80].

2.1 Convolution Quadratures

CQ are hybrid methods that combine Laplace transforms and A-stable ODE solvers to produce approximations of convolution integrals

$$(f * g)(t) \coloneqq \int_0^t f(\tau)g(t-\tau)d\tau, \tag{2.2}$$

for values of t on an equidistant mesh $0 = t_0 \leq \cdots \leq t_n = n\Delta t$. For a given function f we define its Laplace transform

$$F(s) \coloneqq \int_0^\infty e^{-st} f(t)dt,$$

which we assume to exist for $s \in \mathbb{C},\ \Re s > 0$. We make use of the inversion formula for the Laplace transform

$$f(t) = \frac{1}{2\pi i} \int_{\sigma - i\infty}^{\sigma + i\infty} e^{st} F(s)ds$$

and obtain

$$\begin{aligned}(f * g)(t) &= \int_0^t \left\{ \frac{1}{2\pi i} \int_{\sigma - i\infty}^{\sigma + i\infty} e^{st} F(s)ds \right\} g(t-\tau)d\tau \\ &= \frac{1}{2\pi i} \int_{\sigma - \infty}^{\sigma + \infty} F(s) \left\{ \int_0^t e^{st} g(t-\tau)d\tau \right\} ds.\end{aligned}$$

We denote

$$y(t; s) \coloneqq \int_0^t e^{s\tau} g(t-\tau)d\tau,$$

and notice that $y(t; s)$ is the solution of the following linear first order differential equation:

$$\begin{cases} \frac{dy}{dt} &= sy + g \quad \text{ in } [0, \infty). \\ y(0) &= 0. \end{cases} \tag{2.3}$$

We use the Backward Euler method to solve the differential Equation (2.3) on the grid $0 = t_0 \leq \cdots \leq t_n = n\Delta t$ and we get

$$\frac{y_n - y_{n-1}}{\Delta t} = sy_n + g_n, \quad g_n = g(t_n),$$

where $y_n \approx y(t_n)$. We thus obtain the following recurrence relation

$$y_n = \frac{1}{1 - \Delta t\ s} y_{n-1} + \frac{\Delta t}{1 - \Delta t\ s} g_n, \quad 0 \leq n, \quad y_{-1} := 0.$$

In order to derive an explicit formula for y_n we express them in the form

$$y_n = \left(\frac{1}{1 - \Delta t\ s}\right)^n z_n, \quad n \geq 1, z_{-1} = z_0 = 0,$$

which, when used in the backward Euler recurrence formulas lead a simple recurrence formula for the new expressions $\{z_n\}_{n\geq 1}$:

$$z_n = z_{n-1} + \frac{\Delta t}{(1 - \Delta t\ s)^{1-n}} g_n, \quad z_{-1} = z_0 = 0, \quad n \geq .$$

Consequently, we immediately obtain the explicit formula

$$z_n = \Delta t \sum_{m=0}^{n} \frac{1}{(1 - \Delta t\ s)^{(1-n)}} g_m,$$

and thus, we derive

$$y_n = \Delta t \sum_{m=0}^{n} (1 - \Delta t\ s)^{m-1-n} g_m = \Delta t \sum_{m=0}^{n} \frac{1}{(1 - \Delta t\ s)^{m+1}} g_{n-m}.$$

We notice that the last formula above can be viewed as an approximation to the following integral

$$\int_0^{t_n} e^{s\tau} g(t_n - \tau) d\tau,$$

which, in turn, delivers an approximation of the convolution integral in the form

$$(f * g)(t_n) = \frac{1}{2\pi i} \int_{\sigma-\infty}^{\sigma+\infty} F(s) y(t_n; s) ds$$

$$
\begin{aligned}
&\approx \frac{1}{2\pi i}\int_{\sigma-\infty}^{\sigma+\infty} F(s)y_n(s)ds \\
&= \sum_{m=0}^{n}\left(\frac{\Delta t}{2\pi i}\int_{\sigma-\infty}^{\sigma+\infty}\frac{F(s)}{(1-\Delta t s)^{m+1}}ds\right)g_{n-m}.
\end{aligned}
$$

It is natural then to define the discrete convolution weights ω_m in the following manner

$$
\begin{aligned}
\omega_m(\Delta t) :&= \frac{\Delta t}{2\pi i}\int_{\sigma-i\infty}^{\sigma+i\infty}\frac{F(s)}{(1-\Delta t s)^{m+1}}ds \\
&= \frac{(-1)^m}{\Delta t^m}\frac{(-1)}{2\pi i}\int_{\sigma-i\infty}^{\sigma+i\infty}\frac{F(s)}{(s-\frac{1}{\Delta t})^{m+1}}ds \\
&= \frac{(-1)^m}{\Delta t^m}\frac{1}{m!}F^{(m)}\left(\frac{1}{\Delta t}\right) \\
&= \frac{1}{m!}\frac{d^m}{d\xi^m}\left(F\left(\frac{1-\xi}{\Delta t}\right)\right)\Big|_{\xi=0}.
\end{aligned}
$$

In conclusion, CQ produce approximations of convolution integrals in the form of discrete convolutions involving the weights ω_m

$$
\begin{cases}
(f*g)(t_n) & \approx \sum_{m=0}^{n}\omega_m(\Delta t)g_{n-m} \quad \text{where } g_n = g(t_n) \\
F\left(\frac{1-\xi}{\Delta t}\right) & = \sum_{m=0}^{\infty}\omega_m(\Delta t)\xi^m.
\end{cases}
\tag{2.4}
$$

The derivations above can be extended from the Backward Euler method to the case when general linear multistep methods are applied to the numerical discretization of Equation (2.3).

2.2 CQ with General Linear Multistep Methods

In the case when a more general multistep solver is applied to the ordinary differential equation in the Equation (2.3), that is

$$
\frac{1}{\Delta t}\left(\alpha_0 y_n + \alpha_1 y_{n-1} + \cdots + \alpha_N y_{n-N}\right) = \beta_0(s y_n + g_n) + \cdots + \beta_N(s y_{n_N} + g_{n-N}), \tag{2.5}
$$

we employ the ζ transform machinery to derive approximations to the convolution integral. For a sequence $(y_n)_{n\geq 0}$ we define its ζ-transform as

$$Y(\zeta) = \sum_{n=0}^{\infty} y_n \zeta^n.$$

We then apply the ζ-transform to both sides of Equation (2.5). Extending by 0 the coefficients $\alpha_0, \dots \alpha_N$ and $\beta_0 \dots \beta_N$ for indices larger than N, and using the fact that the ζ-transform of a convolution is a product in ζ-space, we arrive at:

$$\frac{1}{\Delta t} A(\zeta) Y(\zeta) = sB(\zeta) Y(\zeta) + B(\zeta) G(\zeta)$$

where

$$A(\zeta) := \alpha_0 + \alpha_1 \zeta + \cdots + \alpha_N \zeta^N$$
$$B(\zeta) = \beta_0 + \beta_1 \zeta + \cdots + \beta_N \zeta^N.$$

If we denote by

$$P(\zeta) = \frac{A(\zeta)}{B(\zeta)} = \frac{\alpha_0 + \alpha_1 \zeta + \cdots + \alpha_N \zeta^N}{\beta_0 + \beta_1 \zeta + \cdots + \beta_N \zeta^N},$$

we then obtain an explicit formula for the ζ transform of $\{y_n\}_{0\leq n}$

$$Y(\zeta) = \left(\frac{P(\zeta)}{\Delta t} - s \right)^{-1} G(\zeta). \tag{2.6}$$

The coefficients $\{y_n\}_{0\leq n}$ are then retrieved via Cauchy's integral formula

$$y_n = \frac{1}{2\pi i} \int_{|\zeta|=\lambda} \frac{Y(\zeta)}{\zeta^{n+1}} d\zeta.$$

Consequently, we derive the following approximation for the values $y(t_n, s)$:

$$y(t_n; s) \approx \frac{1}{2\pi i} \int_{|\zeta|=\lambda} \left(\frac{P(\zeta)}{\Delta t} - s \right)^{-1} \frac{G(\zeta)}{\zeta^{n+1}} d\zeta,$$

assuming that λ is small enough so that $B(\lambda)$ is included in domain of analyticity of the integrand in the expression above. Finally, we derive the CQ approximation of

the convolution integral

$$
\begin{aligned}
(f*g)(t_n) &\approx \frac{1}{2\pi i}\int_{\sigma-i\infty}^{\sigma+i\infty} F(s)\left[\frac{1}{2\pi i}\int_{|\zeta|=\lambda}\left(\frac{P(\zeta)}{\Delta t}-s\right)^{-1}\frac{G(\zeta)}{\zeta^{n+1}}d\zeta\right]ds \\
&= \frac{1}{2\pi i}\int_{|\zeta|=\lambda}\frac{G(\zeta)}{\zeta^{n+1}}\left[\frac{1}{2\pi i}\int_{\sigma-i\infty}^{\sigma+i\infty}\left(\frac{P(\zeta)}{\Delta t}\right)^{-1}F(s)ds\right]d\zeta \\
&= \frac{1}{2\pi i}\int_{|\zeta|=\lambda}\frac{G(\zeta)}{\zeta^{n+1}}F\left(\frac{P(\zeta)}{\Delta t}\right)d\zeta,
\end{aligned}
$$

given that

$$
F\left(\frac{P(\zeta)}{\Delta t}\right) = \frac{1}{2\pi i}\int_{\sigma-i\infty}^{\sigma+i\infty}\frac{F(s)}{\frac{P(\zeta)}{\Delta t}-s}ds.
$$

The CQ approximation derived above can be viewed as a discrete convolution with weights defined as

$$
F\left(\frac{P(\zeta)}{\Delta t}\right) = \sum_{m=0}^{\infty}\omega_m(\Delta t)\zeta^m \quad \text{where } \omega_m(\Delta t) = \frac{1}{m!}\frac{d^m}{d\zeta^m}\left(F\left(\frac{P(\zeta)}{\Delta t}\right)\right)\Big|_{\zeta=0}, \tag{2.7}
$$

and thus

$$
(f*g)(t_n) \approx \sum_{m=0}^{n}\omega_m(\Delta t)g_{n-m} \quad \text{where } g_n = g(t_n).
$$

The analysis of the CQ scheme presented above reveals that the convergence of the discrete convolutions to the continuous ones can be established under the assumption that A-stable linear multi-step schemes are used for the solution of the differential Equation (2.3). Therefore, the convergence of linear multi-step schemes CQ is at most second-order in time, and the highest order can be achieved when BDF2 is used for the solution of (2.3).

2.3 Runge-Kutta Convolution Quadrature

Thus far we have looked at CQ methods based on linear multistep schemes. In order for the discrete convolutions produced by CQ methods to converge to the continuous ones, the underlying linear multistep schemes must be A-stable. On account of the

Dalquist barrier theorem, CQ methods based on linear multistep schemes cannot achieve higher than second order in time convergence. In order to bypass this limitation, we present in what follows CQ methods based on Runge-Kutta ODE solvers for the solution of the wave equation. Our exposition follows closely the paper by Betcke et al [12]. We start by writing the wave equation as a first order linear system:

$$\begin{cases} \frac{\partial Y(x;t)}{\partial t} = \mathcal{L}Y(x;t) & (x,t) \in \Omega^+ \times (0,\infty) \\ Y(x;0) = 0 & x \in \Omega^+ \\ BY(x;t) = F(x;t) & (x;t) \in \Gamma \times (0,\infty) \end{cases}$$

where we have introduced the following notations

$$Y(x;t) = \begin{bmatrix} u(x;t) \\ \frac{\partial u(x;t)}{\partial t} \end{bmatrix} \qquad \mathcal{L} = \begin{bmatrix} 0 & I \\ \Delta_x & 0 \end{bmatrix}$$
$$B = \begin{bmatrix} I & 0 \\ 0 & 0 \end{bmatrix} \qquad F(x;t) = \begin{bmatrix} g(x;t) \\ 0 \end{bmatrix}.$$

We apply an m stage Runge-Kutta (RK) scheme to the solution of the first order system above. The RK scheme can be described using the following matrix and vectors:

$$A = [a_{ij}]_{1 \le i,j \le m} \quad b = [b_j]_{1 \le j \le m} \quad c = [c_j]_{1 \le j \le m},$$

which define the Butcher Tableau associated with the RK scheme and can be found in Appendix A. Then, the RK scheme can be written in the form

$$\begin{cases} V_i(x;t_n) & = Y_d(x;t_n) + \Delta t \sum_{j=1}^m a_{ij} \mathcal{L} V_j(x;t_n) \quad i \in 1,\dots,m \\ Y_d(x;t_{n+1}) & = Y_d(x;t_n) + \Delta t \sum_{j=1}^m b_j \mathcal{L} V_j(x;t_n). \end{cases} \tag{2.8}$$

Applying the $\zeta-$transform to the Equations (2.8) we obtain

$$\begin{cases} V_i(x;\zeta) & = Y_d(x;\zeta) + \Delta t \sum_{j=1}^{m} a_{ij} \mathcal{L} V_j(x;\zeta) \quad i \in 1,\dots,m \\ \frac{Y_d(x;\zeta)}{\zeta} & = Y_d(x;\zeta) + \Delta t \sum_{j=1}^{m} b_j \mathcal{L} V_j(x;\zeta). \end{cases} \tag{2.9}$$

The A-stability requirement on the underlying ODE solver of CQ methods motivates the choice of *stiffly accurate* RK schemes (2.8). Thus, the last row of the matrix A must coincide with the vector b. Consequently, it holds that

$$V_m(x;\zeta) = \frac{Y_d(x;\zeta)}{\zeta}. \tag{2.10}$$

The second Equation in (2.9) leads to

$$Y_d(x;\zeta) = \frac{\zeta}{1-\zeta} \Delta t \sum_{j=1}^{m} b_j \mathcal{L} V_j(x;\zeta), \tag{2.11}$$

which, in turn, when plugged in the first Equation in (2.9), yields

$$V_i(x;\zeta) = \Delta t \sum_{j=1}^{m} \left(\frac{\zeta}{1-\zeta} b_j + a_{ij} \right) \mathcal{L} V_j(x;\zeta), \ i = 1,\dots,m. \tag{2.12}$$

Writing the vector quantities V_j in explicit form as $[R_j(x;\zeta)\ S_j(x;\zeta)]^\top$, we derive the following relations:

$$\begin{aligned} R_i(x;\zeta) &= \Delta t \sum_{j=1}^{m} \left(\frac{\zeta}{1-\zeta} b_j + a_{ij} \right) S_j(x;\zeta) \\ S_j(x;\zeta) &= \Delta t \sum_{\ell=1}^{m} \left(\frac{\zeta}{1-\zeta} b_j + a_{j\ell} \right) \Delta_x R_\ell(x;\zeta). \end{aligned}$$

Let us denote $\mathcal{R}(x;\zeta) := [R_1(x;\zeta),\dots,R_m(x;\zeta)]$. The last two equations above can then be written in compact form as

$$\left(\frac{\Delta(\zeta)}{\Delta t} \right)^2 \mathcal{R}(x;\zeta) = \Delta_x \mathcal{R}(x;\zeta). \tag{2.13}$$

where $\Delta(\zeta)$ is an operator defined by

$$\Delta(\zeta) = \left(A + \frac{\zeta}{1-\zeta} \mathbb{1} b^T \right)^{-1}$$

with $\mathbb{1} = [1, \ldots, 1]^T$. We note that (2.13) is a system of Helmholtz equations. A natural idea is to attempt to diagonalize this system in order to decouple the Helmholtz equations. To this end, we begin by diagonalizing the operator $\Delta(\zeta)$. Let $\mathbb{P}(\zeta)$ be the matrix consisting of the eigenvectors of $\Delta(\zeta)$ and define $\mathbb{D}(\zeta) = diag(\gamma_1(\zeta), \ldots, \gamma_m(\zeta))$ a diagonal matrix with the corresponding eigenvalues of $\Delta(\zeta)$; thus $\Delta(\zeta) = \mathbb{P}(\zeta)\mathbb{D}(\zeta)\mathbb{P}(\zeta)^{-1}$. Thus, the system (2.13) is decoupled into m Helmholtz equations

$$\left(\frac{\gamma_j(\zeta)}{\Delta t} \right)^2 W_j(x;\zeta) = \Delta_x W_j(x;\zeta), \ 1 \leq j \leq m \tag{2.14}$$

where

$$W_j(x;\zeta) = \sum_{\ell=1}^{m} \mathbb{P}^{-1}_{j\ell}(x;\zeta) R_\ell(x;\zeta).$$

Boundary conditions ought to be provided to the Helmholtz Equations (2.14). First we provide boundary conditions for the intermediate RK stages V_j; these take on the form

$$BV_j = F(x; t_n + c_j \Delta t) \quad x \in \Gamma$$
$$F(x;t) = \begin{bmatrix} g(x;t) \\ 0 \end{bmatrix}.$$

Applying the $\zeta-$transform to the boundary conditions above we get

$$R_\ell(x;\zeta) = G_\ell(x;\zeta) g(x; t_n + c_\ell \Delta t) \zeta^n \quad x \in \Gamma \tag{2.15}$$

and thus we derive the corresponding boundary conditions for the Helmholtz solutions W_j

$$W_j(x;\zeta) = \sum_{\ell=1}^{m} \mathbb{P}_{j\ell}^{-1}(\zeta) G_\ell(x;\zeta), \quad x \in \Gamma. \tag{2.16}$$

Consequently, the following modified Helmholtz equations must be solved in the Laplace domain

$$\begin{cases} \Delta_x W_j(x;\zeta) - \left(\frac{\gamma_j(\zeta)}{\Delta t}\right)^2 W_j(x;\zeta) = 0 & x \in \Omega^+ \\ W_j(x;\zeta) = \sum_{\ell=1}^{m} \mathbb{P}_{j\ell}^{-1}(\zeta) G_\ell(x;\zeta) & x \in \Gamma. \end{cases} \tag{2.17}$$

Once the Helmholtz equations above are solved, the ζ-transform of the solution of the wave equation is retrieved via the formula

$$U_d(x;\zeta) = \zeta R_m(x;\zeta) = \zeta \sum_{j=1}^{m} \mathbb{P}_{mj}(\zeta) W_j(x;\zeta). \tag{2.18}$$

Finally, reverting to the physical domain from the Laplace domain is performed in the same manner as in the case of linear multistep methods.

We will use in practice two-stage and three-stage Implicit RK Radau IIA methods. The two-stage RK Radau IIA method gives rise to third order in time CQ and will be denoted by the acronym IRK3. The three-stage RK Radau IIA method gives rise to fifth order in time CQ and will be denoted by the acronym IRK5. We note that the higher order in time convergence that can be achieved by RK CQ methods entail commensurately more solutions of frequency domain modified Helmholtz equations.

2.4 Discrete Fourier Transforms and Convolution Quadratures

It is clear from the presentation above that a key ingredient in the CQ is the computation of the weights $\omega_n(\Delta t)$. To this end, Cauchy's integral formulas are used, and, given the analyticity of the function $F\left(\frac{P(\zeta)}{\Delta t}\right)$ in a ball around the origin,

the trapezoidal rule delivers a high-order quadrature for the numerical evaluation of the Cauchy integrals. The CQ algorithm that follows the prescriptions outlined above can be accelerated using FFTs, and we describe next the steps of this algorithm.

We remind the reader that the scope of CQ in this work is the solution of TDBIE. To that end, we shall apply CQ for the solution of a Volterra integral equation: given two functions f and g, find the unknown function φ such that

$$f * \varphi = g.$$

Using CQ to discretize the convolution integral in the left hand side of the equation above we arrive at a lower triangular linear system featuring the unknowns $\varphi_n \approx \varphi(t_n)$ and the CQ weights ω_n

$$\sum_{m=0}^{n} \omega_{n-m}(\Delta t)\varphi_m = g_n, \;\; g_n := g(t_n), \quad 0 \le n \le N. \tag{2.19}$$

Obviously, once the convolution weights $\omega_n(\Delta t)$ are computed, the linear system (2.19) can be solved using forward substitution. Instead, we will use Discrete Fourier Transforms that will allow us on the one hand to evaluate efficiently the convolution weights $\omega_n(\Delta t)$, and on the other to decouple in the Fourier space the linear system (2.19). We start with the computation of the convolution weights whose expression is given via the Cauchy integral formula

$$\omega_m(\Delta t) = \frac{1}{2\pi i}\int_{|\zeta|=\lambda} \frac{F\left(\frac{P(\zeta)}{\Delta t}\right)}{\zeta^{m+1}} d\zeta = \lambda^{-m}\int_0^1 F\left(\frac{P(\lambda e^{-2\pi i\theta})}{\Delta t}\right) e^{2\pi m i\theta} d\theta, \tag{2.20}$$

where we use the substitution $\zeta = \lambda e^{-2\pi i\theta}$. Let us now denote in what follows $\zeta_{N+1} := e^{\frac{2\pi i}{N+1}}$. We use the trapezoidal rule with $N+1$ nodes to approximate the integral in the right hand side of Equation (2.20) and we obtain

$$\omega_m(\Delta t) \approx \frac{\lambda^{-m}}{N+1}\sum_{\ell=0}^{N} F(s_\ell)\zeta_{N+1}^{-\ell m}, \quad \text{where } s_\ell = \frac{P(\lambda\zeta_{N+1}^{-\ell})}{\Delta t}, \; 0 \le m \le N. \tag{2.21}$$

We are now in the position to rewrite the linear system (2.19) in the following form:

$$\frac{\lambda^{-n}}{N+1}\sum_{\ell=0}^{N}F(s_\ell)\left(\sum_{m=0}^{N}\lambda^m\varphi_m\zeta_{N+1}^{\ell(n-m)}\right)=g_n,\ 0\le n\le N. \tag{2.22}$$

We can manipulate the last formula one step further and arrive at the following linear system

$$\frac{\lambda^{-n}}{N+1}\sum_{\ell=0}^{N}F(s_\ell)\zeta_{N+1}^{\ell n}\left(\sum_{\ell=0}^{N}\lambda^m\varphi_m\zeta_{N+1}^{-\ell m}\right)=g_n,\ 0\le n\le N. \tag{2.23}$$

At this stage, we make use of the Discrete Fourier Transform (DTF). Recall that given a sequence $\{\varphi_j\}$, $0\le j\le N$, its DFT is defined as follows

$$\hat{\varphi}_l=\sum_{j=0}^{N}\zeta_{N+1}^{-\ell j}\varphi_j,\quad 0\le\ell\le N.$$

Furthermore, the inversion formula

$$\varphi_\ell=\frac{1}{N+1}\sum_{j=0}^{N}\zeta_{N+1}^{\ell j}\hat{\varphi}_j\quad 0\le j\le N$$

allows us to go back from the Fourier domain to the physical domain. With these notations in place, we recognize that

$$\sum_{m=0}^{N}\lambda^m\varphi_m\zeta_{N+1}^{-\ell m}=(\widehat{\lambda\varphi})_\ell,\quad \text{where } \{\lambda\varphi\}:=\lambda^j\varphi_j,\ 0\le j\le N.$$

Obviously, the inversion formula for DFT yields

$$\varphi_j=\frac{\lambda^{-j}}{N+1}\sum_{\ell=0}^{N}(\widehat{\lambda\varphi})_\ell\zeta_{N+1}^{\ell j}.$$

The linear system (2.23) can be recast then in the form

$$\frac{1}{N+1}\sum_{\ell=0}^{N}\zeta_{N+1}^{\ell n}F(s_\ell)(\widehat{\lambda\varphi})_\ell=\lambda^n g_n\quad 0\le n\le N,$$

which, in turn, leads to

$$\frac{1}{N+1}\sum_{\ell=0}^{N}\zeta_{N+1}^{(\ell-j)n}F(s_\ell)(\widehat{\lambda\varphi})_\ell=\lambda^n\zeta_{N+1}^{-nj}g_n\quad 0\le n\le N. \tag{2.24}$$

Summing up both sides of Equations (2.24) for all values of the index $0 \leq n \leq N$ we derive:

$$\frac{1}{N+1}\sum_{n=0}^{N} F(s_\ell)(\widehat{\lambda\varphi})_\ell \sum_{\ell=0}^{N} \zeta_{N+1}^{(\ell-j)n} = \sum_{n=0}^{N} \lambda^n \zeta_{N+1}^{nj} g_n \quad 0 \leq j \leq N. \tag{2.25}$$

Given that

$$\sum_{n=0}^{N} \lambda^n g_n \zeta_{N+1}^{-nj} = (\widehat{\lambda g})_j$$

$$\sum_{n=0}^{N} \zeta_{N+1}^{(\ell-j)n} = \begin{cases} N+1 \text{ if } \ell = j, \\ 0 \text{ otherwise} \end{cases}$$

Equations (2.25) reduce to *decoupled* equations in the Fourier domain

$$F(s_j)(\widehat{\lambda\varphi})_j = (\widehat{\lambda g})_j \quad \text{for all } 0 \leq j \leq N.$$

Consequently, the discrete Fourier coefficients of the sequence $\{\lambda\varphi\}$ are computed explicitly

$$(\widehat{\lambda\varphi})_j = (F(s_j))^{-1}(\widehat{\lambda g})_j \quad \text{for all } 0 \leq j \leq N. \tag{2.26}$$

Finally, an application of the inversion formula for DFT leads to explicit formulas for φ_ℓ

$$\varphi_\ell = \frac{\lambda^{-\ell}}{N+1}\sum_{j=0}^{N} \left[(F(s_j))^{-1}(\widehat{\lambda g})_j\right] \zeta_{N+1}^{\ell j} \quad \text{for all } 0 \leq \ell \leq N. \tag{2.27}$$

All of the DFT in the derivations above are effected in practice with FFTs.

2.5 CQ Solutions of TDBIE

We assume in what follows that the wave speed is $c = 1$. We will solve the TDBIE

$$\int_0^t \int_\Gamma k_{2D}(x-y, t-\tau)\varphi(y,\tau) ds(y) d\tau = g(x;t) \quad \text{for all } t > 0,\ x \in \Gamma. \tag{2.28}$$

The Laplace transform of the wave equation Green function $k_{2D}(x,t)$ is

$$K(x,s) = \frac{i}{4} H_0^{(1)}(is|x|).$$

Making use of Laplace transform techniques similar to the ones used in the derivation of CQ above we obtain

$$\begin{aligned}
&\int_0^t \int_\Gamma k_{2D}(x-y,t-\tau)\varphi(y,\tau)ds(y)d\tau \\
&= \frac{1}{2\pi i}\int_{\sigma-i\infty}^{\sigma+i\infty} \int_0^t e^{\tau s}\left[\int_\Gamma K(x-y,s)\varphi(y,t-\tau)ds(y)\right]d\tau ds \\
&= \frac{1}{2\pi i}\int_{\sigma-i\infty}^{\sigma+i\infty} \int_0^t e^{\tau s}\left(V(s)\varphi(\cdot,t-\tau)\right)(x)d\tau ds,
\end{aligned}$$

where $V(s)$ denotes the single layer BIO

$$\left(V(s)\varphi\right)(x) = \int_\Gamma K(x-y,s)\varphi(y)ds(y), \quad x \in \Gamma. \tag{2.29}$$

We note that the single layer potential

$$w(x;s) := \int_\Gamma K(x-y,s)\varphi(y)ds(y), \quad x \in \mathbb{R}^2 \setminus \Gamma$$

is a radiative solution of the modified Helmholtz equation

$$\Delta_x w(x;s) - s^2 w(x;s) = 0 \quad x \in \mathbb{R}^2 \setminus \Omega.$$

We apply the CQ machinery to solve the TDBIE

$$\frac{1}{2\pi i}\int_{\sigma-i\infty}^{\sigma+i\infty} \int_0^t e^{\tau s}\left(V(s)\varphi(\cdot,t-\tau)\right)(x)d\tau ds = g(x,t) \quad t>0 \quad x \in \Gamma. \tag{2.30}$$

In this context, the Laplace domain function $F(s)$ from the previous sections is replaced by the operator $V(s)$. Denoting by

$$\varphi_j^{\Delta t}(x) = \varphi^{\Delta t}(x,t_j), \quad 0 \le j \le N$$

the CQ methodology leads us to the following linear system of boundary integral equations

$$\sum_{j=0}^{n} \left(\omega_{n-j}^{\Delta t}\varphi_j\right)(x) = g_n(x), \quad n = 1, \cdots, N \quad x \in \Gamma, \tag{2.31}$$

where

$$V\left(\frac{P(\zeta)}{\Delta t}\right) = \sum_{n=0}^{\infty} \omega_n^{\Delta t}\zeta^n, \quad |\zeta| \leq 1, \tag{2.32}$$

where $P(\zeta) = \frac{1}{2}(\zeta^2 - 4\zeta + 3)$ is the characteristic polynomial of BDF2. The operator convolution weights are computed using the formula

$$\begin{aligned}\omega_j^{\Delta t}(V) &= \frac{1}{2\pi i}\int_{|\zeta|=\lambda} \frac{V(\frac{P(\zeta)}{\Delta t})}{\zeta^{j+1}} d\zeta \\ &\approx \frac{\lambda^{-j}}{N+1}\sum_{\ell=0}^{N} V(s_\ell)\zeta_{N+1}^{\ell j}, \quad s_\ell = \frac{P(\lambda\zeta_{N+1}^{-\ell})}{\Delta t}.\end{aligned}$$

The DFT manipulations lead us to the following $N+1$ decoupled BIE:

$$\left(V(s_\ell)\hat{\varphi}_\ell\right)(x) = \hat{g}_\ell(x) \quad x \in \Gamma \quad \ell = 0, \ldots, N, \tag{2.33}$$

where

$$\begin{aligned}\hat{g}_\ell(x) &:= \sum_{n=0}^{N} \lambda^n g_n(x)\zeta_{N+1}^{-\ell n} \\ \hat{\varphi}_l(x) &:= \sum_{n=0}^{N} \lambda^n \varphi_n(x)\zeta_{N+1}^{-ln}.\end{aligned}$$

Once the densities $\hat{\varphi}_\ell(x)$ are computed by solving the sequence of frequency domain BIE for all wavenumbers s_ℓ, we retrieve the quantities $\varphi_\ell(x)$ which are approximations of $\varphi(x, \ell\Delta t)$ using the inverse DFT:

$$\varphi_\ell(x) = \sum_{j=0}^{N} \lambda^n \hat{\varphi}_n(x)\zeta_{N+1}^{\ell j}. \tag{2.34}$$

We note that in practice FFTs are used throughout the CQ algorithm. We discuss in what follows how we solve the sequence of Laplace domain BIE.

2.6 CQ TDBIE Algorithms

The BDF2 CQ algorithm for the solution of the TDBIE on the interval $[0, T]$ produces boundary densities $\varphi(\cdot, t_j)$, $t_j = j\Delta t$, $T = N\Delta t$ via solutions of the Laplace domain BIE (2.33) and the IDFT formula (2.34). Assuming that the ensemble of BIE (2.33) is solved with reasonably high spatial accuracy, the order of the BDF2 CQ solution of the TDBIE is then second order in time provided that λ is chosen per the prescription in [7]

$$\lambda = \max\left(\Delta t^{\frac{3}{N}}, \varepsilon^{\frac{1}{2N}}\right) \tag{2.35}$$

where ε is machine precision. Given that in applications of interest the boundary data g in the TDBIE is real valued, the conjugation symmetries

$$\hat{\varphi}_{N+2-j} = \overline{\hat{\varphi}_j} \quad j = 1, 2, \ldots, \left[\frac{N}{2} + 1\right]$$

are used to reduce by a half the number of frequency domain BIE (2.33). Further computational reductions can be achieved by exploiting sparsity in the frequency content of the boundary data $g(t, x)$. Specifically, for many incident fields that are encountered in practical applications, the magnitude of $\hat{g}_\ell(x)$ is small (uniformly in $x \in \Gamma$) for a wide range of frequencies ℓ. For those indices ℓ for which $\|\hat{g}_\ell\|_{\infty,\Gamma}$ falls below a specific threshold (e.g. 10^{-8}), the solution $\hat{\varphi}_\ell$ of the corresponding BIE (2.33) is assumed to be equal to zero.

Once we have solved the ensemble of Laplace domain BIE (2.33), a simple post processing step delivers the solution $u(x, t_n)$ of the wave equation for $x \in \Omega^+$ from the boundary densities $\hat{\varphi}_\ell$, $0 \le \ell \le N$. Indeed, fix an $x \in \Omega^+$ and evaluate the Single Layer potentials

$$\widehat{u}(x, s_\ell) = \int_\Gamma K(x - y, s_\ell)\widehat{\varphi}_\ell(y) ds(y) \quad \text{for each } \ell = 0, \ldots, N. \tag{2.36}$$

We note that none of the integral kernels $K(x-y, s_\ell)$ in Equation (2.36) are singular, and thus the evaluation of the quantities $\widehat{u}(x, s_\ell)$ can be effected vis simple quadrature rules. Finally, we obtain after applying IDFT

$$u(x, t_n) \approx \frac{\lambda^{-n}}{N+1} \sum_{j=0}^{N} \widehat{u}(x, s_j) \zeta_{N+1}^{jn}, \ 1 \leq n \leq N. \tag{2.37}$$

We provide in what follows the pseudocode for the BDF2 CQ solution of TDBIE.

Algorithm 1: BDF2 CQ Algorithm

Choose a time $T > 0$ up to which we simulate the solution of the wave equation and an equispaced mesh $t_n = n\Delta t, 0 \leq n \leq N, \ \Delta t = \frac{T}{N}$;
Choose a paramater λ in accordance with (2.35);
Use a boundary mesh $x_m = x(\theta_m), \ 1 \leq m \leq 2M$ on Γ where $\theta_m = (m-1)\pi/M$; all the BIE densities are sampled on this mesh.

Step 1: Sample $g(t_n, x_m)$ for $0 \leq n \leq N$ and apply FFT to the ensemble $\{\lambda^n g(t_n, x_m)\}_{0 \leq n \leq N}$ for all grid points x_m to produce the Fourier coefficients $\{\hat{g}_l(x_m)\}_{0 \leq l \leq N}$ for all grid points $\{x_m\}_{1 \leq m \leq 2M}$.

Step 2: Solve in parallel the frequency domain BIE using Nyström methods

$$\frac{i}{4} \int_\Gamma H_0^{(1)}(is_l|x-y|)\hat{\varphi}_\ell(y) ds(y) = \hat{g}_l(x), \ x \in \Gamma$$

for $0 \leq l \leq N$. The outcome of this step are the vectors $\hat{\varphi}_\ell(x_m), \ 1 \leq m \leq 2M$ for all $0 \leq \ell \leq N$.

Step 3: Apply IFFT to the vectors

$$\{\hat{\varphi}_\ell(x_m)\}_{0 \leq \ell \leq N}$$

for $1 \leq m \leq 2M$ and then multiply the ℓ-th outcome by $\lambda^{-\ell}$ to get an approximation of $\varphi(t_\ell, x_m)$ for all $0 \leq \ell \leq N$ and $1 \leq m \leq 2M$ grid points. Use post processing to obtain the solution of the wave equation $u(t_n, x)$ at points $x \in \Omega^+$.

The overall procedure for IRK is similar to that BDF2, but as can be seen in the derivation, the differences accumulate. Below is given the Algorithm for the Implicit Runge-Kutta time stepping scheme:

Algorithm 2: IRK Algorithm For Calculating Densities with CQ

Choose a $T > 0$ and the equispaced mesh $t_n = n\Delta t, \Delta t = \frac{T}{N}$;
Choose a λ in accordance with (2.35), with a larger N;
Use a mesh $\vec{x}(\theta_m)$ for $0 < \theta_m \leq 2\pi$.

Step 1: Pick a Implicit Runge-Kutta Radau-II scheme, filling in the matrix and vectore A, b, c.

Step 2: Sample $g(t_n + c_j\Delta t, x_i)$ for $0 \leq n \leq N$, $1 \leq j \leq m$ and construct the FFT of $\{\lambda^n g(t_n + c_j\Delta t, x_i)\}_{0\leq n\leq N}$ for all grid points x_i. This can be done at once and it produces $\{\hat{g}_j(z_l, x_i)\}_{0\leq l\leq N}$ for all grid points $\{x_i\}_{1\leq i\leq M}$, and $j \in \{1, \ldots, m\}$.

Step 3: let $z_l = e^{-2\pi il/(N+1)}$. Form all of the following matrices:

$$\Delta(z_l) = \left(A + \frac{z_l}{1 - z_l}\mathbb{1}b^T\right)^{-1},$$

Then diagonalize the system: $\Delta(z_l) = \mathbb{P}(z_l)\text{diag}(\gamma_j(z_l))\mathbb{P}^{-1}(z_l)$.

Step 4: Solve in parallel

$$\underbrace{\int_\Gamma K(i\gamma_j(z_l)|x - y|)\hat{\varphi_{jl}}(y)ds(y)}_{W_j(z_l;x)} = \sum_{q=1}^{m} \mathbb{P}_q^{-1}(z_l)\hat{g}_q(z_l, x)$$

for $0 \leq l \leq N$. Where K is the appropriate kernel for the layer representation and boundary condition. When the data is $g(t, x)$ is real, solve only those problems where the frequency is not within a neighborhood of zero.

Step 5: Once the densities φ_{jl} have been found, we invert the diagonalization: $U_d(z_l i, x) = \sum_{j=1}^{m} \mathbb{P}(z_l)_{mj} W_j(z_l; x)$

Step 6: Do the IFFT of

$$\{U_d(z_l, x_i)\}_{0\leq l\leq N}$$

and for $1 \leq i \leq M$ and then multiply it by λ^{-l} to get an approximation of $u(t_l, x_m)$ (original function of the wave equation) on all of its spatial and time grid points.

2.7 A Model Problem for CQ RK Methods

Several numerical tests have been proposed in the literature to validate the order of convergence of CQ methods. Typically, those tests rely on carefully constructed Volterra integral equations with known solutions. We investigate in what follows the convergence properties of RK CQ methods for certain Volterra integral equations that arise in connection with certain 3D TDBIE in geometrical configurations whereby separation of variables techniques are possible. Specifically, we consider the following TDBIE in the exterior of a spherical obstacle under the assumption incident fields that depend on the variable t only

$$\begin{aligned} g(t) &= \int_0^t \int_{\mathbb{S}^2} k_{3D}(\|x-y\|, t-\tau)\varphi(y,\tau) dS_y d\tau \\ &= \frac{1}{2\pi i}\int_{\sigma-i\infty}^{\sigma+i\infty} \int_0^t e^{s\tau} \int_\Gamma K_{3D}(\|x-y\|, s)\varphi(y, t-\tau) dS_y d\tau ds \quad \varphi(y,\tau) = \varphi(\tau) \\ &= \frac{1}{2\pi i}\int_0^t \int_{\sigma-i\infty}^{\sigma+i\infty} e^{s\tau} V(s)\varphi(t-\tau,\cdot)(x) d\tau ds \end{aligned}$$

where $k_{3D}(x,t) = \frac{\delta(t-\|x\|)}{4\pi t}$ and $K_{3D}(x,s) = \frac{e^{-s\|x\|}}{4\pi\|x\|}$. In spherical geometries the single layer BIE is diagonalizable in the orthonormal basis of spherical harmonics and as such we get

$$g(t) = \frac{1}{2\pi i}\int_{\sigma-i\infty}^{\sigma+\infty} \int_0^t e^{s\tau}\lambda_0(is)\varphi(t-\tau) d\tau ds$$

where

$$\lambda_0(is) = \frac{1-e^{-2s}}{2s}.$$

Clearly, we have

$$g(t) = \int_0^t \left(\frac{1}{2\pi i}\int_{\sigma-i\infty}^{\sigma+\infty} e^{s\tau}\lambda_0(is) ds\right)\varphi(t-\tau) d\tau.$$

Given that

$$\check{\lambda}_0(\tau) = \frac{1}{2\pi i}\int_{\sigma-i\infty}^{\sigma+\infty} e^{s\tau}\lambda_0(is) ds$$

the TDBIE reduces to the following Volterra integral equation

$$g(t) = \int_0^t \check{\lambda}_0(\tau)\varphi(t-\tau)d\tau. \tag{2.38}$$

A straightforward calculation gives

$$\begin{aligned}\int_{\sigma-i\infty}^{\sigma+i\infty} e^{s\tau}\lambda_0(is)ds &= \int_{\sigma-i\infty}^{\sigma+i\infty} e^{s\tau}\left(\frac{1-e^{-2s}}{2s}\right)ds \\ &= \frac{1}{2}(1-H(\tau-2)),\end{aligned}$$

where the function $H(\tau)$ is the Heaviside function. We now plug the last expression above into (2.38) and we solve for the density φ for all $0 < t \leq 2$:

$$\begin{aligned}2g(t) &= \int_0^t [1-H(\tau-2)]\varphi(t-\tau)d\tau \\ 2g(t) &= \int_0^2 \varphi(t-\tau)d\tau \\ 2g'(t) &= \int_0^2 \frac{d}{dt}\varphi(t-\tau)d\tau \\ &= -\int_0^2 \frac{d}{d\tau}\varphi(t-\tau)d\tau = \varphi(t)-\varphi(t-2), \quad 0 < t \leq 2.\end{aligned}$$

We thus obtain

$$\varphi(t) = 2g'(t), \quad 0 < t \leq 2.$$

We use this to test the convergence rate of the SL TDBIE solution for CQ with both BDF2 and the Radau-II scheme. All of the frequency domain problems that arise in the CQ algorithm are solved explicitly using the explicit value of the eigenvalues $\lambda_0(is_\ell)$. Thus, our numerical experiments simply test the time integrators. We present the plots of the convergence rates in Figure 2.1. As it can be seen, the CQ with IRK3 does not exhibit third order convergence. Unfortunately, we do not have yet an explanation for this rather peculiar behavior of the IRK3 CQ solver.

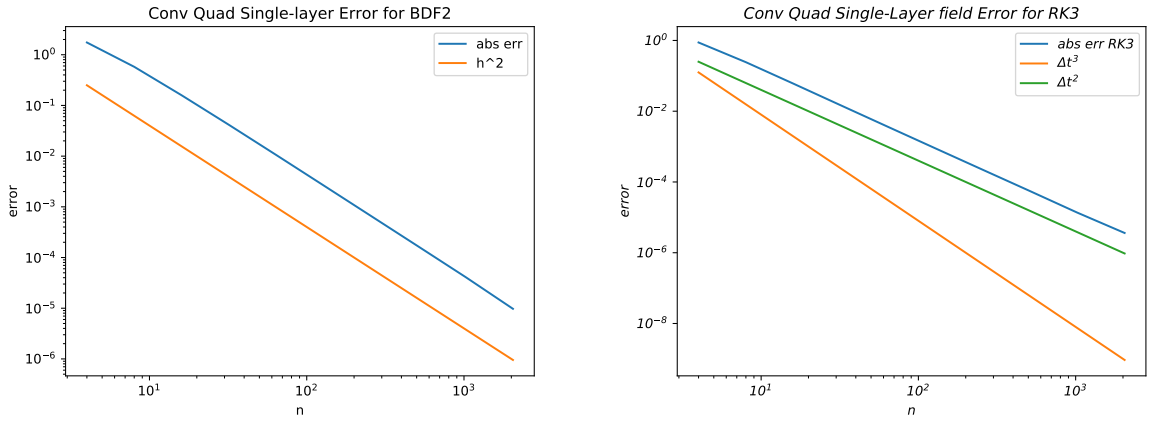

Figure 2.1 Convergence rate of BDF2 CQ and IRK3 CQ for the single Layer TDBIE model problem.

2.8 Double-Layer and Combined Field TDBIE

Puzzled by the unexpected behavior of the IRK3 CQ solution of the Single Layer TDBIE, we proceeded to investigate the case when a double layer TD formulation is used for the solution of the wave equation in the exterior of the unit sphere. The derivations are similar in this case, with two notable differences: (1) we are dealing now with a TDBIE of the second kind; and (2) the eigenvalues of the double layer Helmholtz operators are given by the formula

$$\mu_0(is) = -\frac{1}{2} + \left[\left(\frac{e^{-2s}+1}{2}\right) + \left(\frac{e^{-2s}-1}{2s}\right)\right].$$

Taking into account the formula for the inverse Laplace transform of the function $\mu_0(is)$

$$\begin{aligned}&\int_{\sigma-i\infty}^{\sigma+i\infty} e^{s\tau}\left(-\frac{1}{2} + \left[\left(\frac{e^{-2s}+1}{2}\right) + \left(\frac{e^{-2s}-1}{2s}\right)\right]\right) ds \\ &= \frac{\delta(\tau-2)}{2} + \frac{\delta(\tau)}{2} + \frac{1}{2}(H(\tau-2)-1)\end{aligned}$$

we arrive at the following Volterra integral equation for the density ψ of the TDBIE:

$$2g(t) = \int_0^t \left[\delta(\tau-2) + \delta(\tau) + (H(\tau-2)-1)\right]\psi(t-\tau)d\tau$$

$$
\begin{aligned}
2g(t) &= \psi(t-2) + \psi(t) - \int_0^2 \psi(t-\tau)d\tau \\
2g'(t) &= \psi'(t) - \int_0^2 \frac{d}{dt}\psi(t-\tau)d\tau \\
&= + \int_0^2 \frac{d}{d\tau}\psi(t-\tau)d\tau = \psi'(t) - \psi(t), \quad 0 < t \leq 2.
\end{aligned}
$$

Thus, we have to solve the following differential equation

$$
\psi'(t) - \psi(t) = 2g'(t), \quad 0 < t \leq 2
$$

from which we get

$$
\psi(t) = e^t \left(C + \int 2g'(t)e^{-t}dt \right), \ 0 < t \leq 2.
$$

In this case, we display the rates of convergence of CQ methods based on BDF2 and IRK3 in Figure 2.2. As it can be seen, third order convergence of IRK3 CQ methods is now observed in practice.

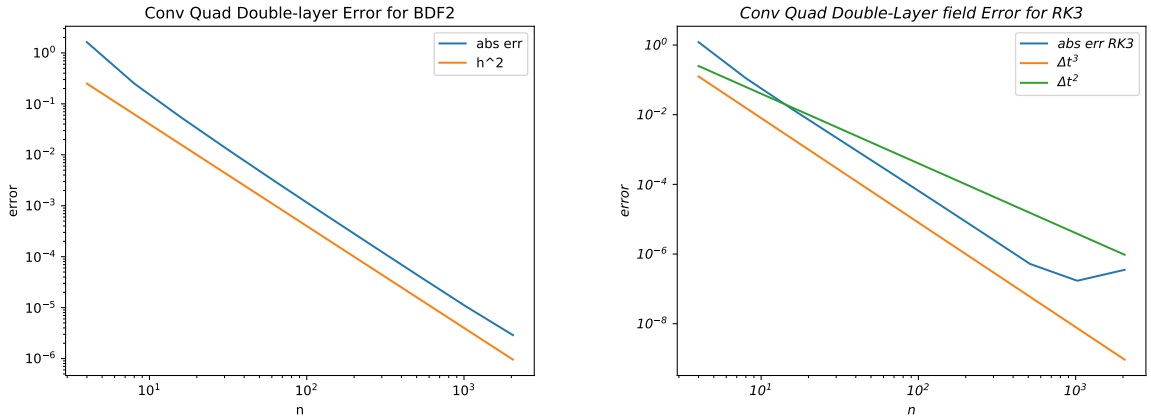

Figure 2.2 Convergence of CQ BDF2 and CQ IRK3 for the solution of the double layer TDBIE model problem.

We repeated the experiment in the case when the Combined Field approach is used to derive TDBIE. As illustrated in Figure 2.3, third order is again observed for the IRK3 CQ method.

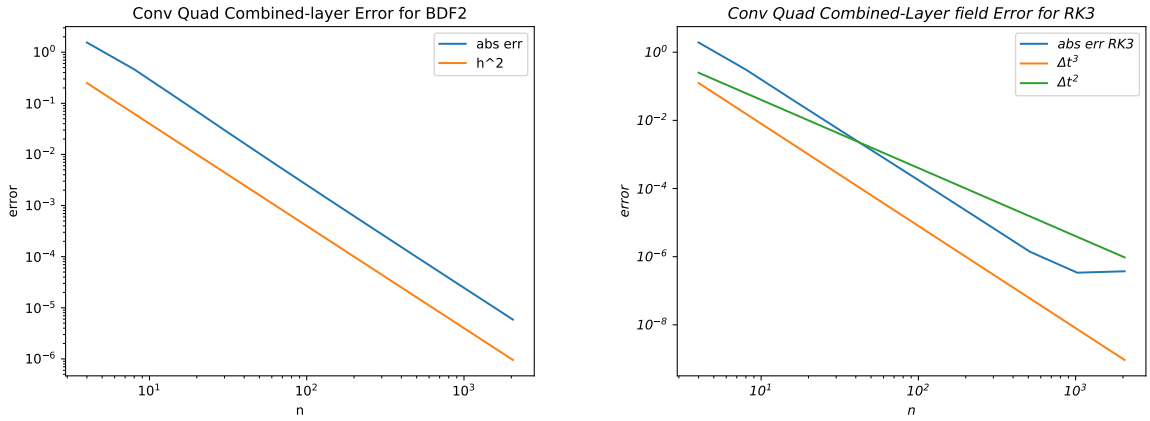

Figure 2.3 Convergence of CQ BDF2 and CQ IRK3 for the solution of the combined field TDBIE model problem.

CHAPTER 3

NYSTRÖM METHODS FOR THE MODIFIED HELMHOLZ BIE

As we have already remarked, a key component of CQ methods for the solution of TDBIE is solving ensembles of modified Helmholtz equations. We use the BIE machinery to solve such problems and we will highlight the additional challenges that are encountered in the Helmholtz problems that arise in the CQ context.

3.1 Dirichlet Boundary Conditions

We are interested in solving the Helmholtz boundary value problem

$$\begin{cases} \Delta u(x) + k^2 u(x) = 0 & x \in \Omega^+ \\ u(x) = g(x) & x \in \Gamma \\ \lim_{r\to\infty} \sqrt{r}(\frac{\partial}{\partial r} - ik)u(r,\theta) = 0. \end{cases} \tag{3.1}$$

We assume that the wavenumber $k \in \mathbb{C}$ with $\Im k \geq 0$. We pursue the solution of exterior Helmholtz problems based on layer potential formulations. One of the immediate benefits of this approach is the direct enforcement of the radiation condition through the choice of an outgoing Green function.

Single Layer Potential Let us seek for a solution of Equation (3.1) in the form of a Single-Layer (SL) potential:

$$u(x) = \underbrace{\int_\Gamma G_k(x-y)\varphi(y)ds(y)}_{(\mathcal{S}_k\varphi)(x)}, \quad x \in \mathbb{R}^2 \setminus \Gamma \tag{3.2}$$

where

$$G_k(x) = \frac{i}{4} H_0^{(1)}(k|x|) \tag{3.3}$$

is the Hankel function of order zero of the first kind. The single layer potential is continuous throughout $\mathbb{R}^2$, and thus, taking its limit on the boundary Γ we arrive at the BIE of the first kind:

$$(\mathcal{S}_k\varphi)(x) = g(x),\ x \in \Gamma. \tag{3.4}$$

Double Layer Potential Suppose now that we look for a solution of Equation (3.1) in the form of a Double Layer potential

$$u(x) = \underbrace{\int_\Gamma \frac{\partial G_k(x-y)}{\partial n(y)}\varphi(y)ds(y)}_{(\mathcal{K}_k\varphi)(x)}, \quad x \in \mathbb{R}^2 \setminus \Gamma. \tag{3.5}$$

The limit of the double layer on Γ gives rise to a jump condition and leads to the BIE of the second kind

$$(\mathcal{K}_k\varphi)(x) + \varphi(x) = 2g(x),\ x \in \Gamma. \tag{3.6}$$

Combined Field Formulations We can also take a linear combination of the two previous layer potentials:

$$u(x) = \underbrace{\int_\Gamma \frac{\partial G_k(x-y)}{\partial n(y)}\varphi(y)ds(y) - \eta\int_\Gamma G_k(x-y)\varphi(y)ds(y)}_{(\mathcal{C}_k\varphi)(x)}. \tag{3.7}$$

Normally we will pick the coupling parameter to be $\eta = ik$. The BIE we need to solve in this case is:

$$(\mathcal{C}_k\varphi)(x) + \varphi = 2g(x),\ x \in \Gamma \tag{3.8}$$

where once again the term φ comes from the jump condition of the double layer potential. Due to the types of boundaries that we consider, the Combined Field representation will not be a focus in what is to follow.

3.1.1 Smooth Boundaries

We give a brief overview of Nyström discretizations of the BIE Equations (3.4),(3.6), and (3.8). In these methods the densities are approximated by global trigonometric polynomials using equispaced interpolation nodes on the interval $[0, 2\pi]$ (we assume 2π periodic parametrizations of the closed curves Γ) and the BIE are collocated on the boundary mesh corresponding to the interpolation nodes. However, the kernels of the BIE under considerations are singular when the integration point y is equal to the target point x, and thus these singularities have to be handled carefully via specialized quadratures. A closer look at the kernel of the single layer formulations around its singularity at $x = 0$ reveals

$$H_\alpha^{(1)}(x) = J_\alpha(x) + iY_\alpha(x),$$

where

$$J_\alpha(x) \sim \frac{1}{\Gamma(\alpha+1)}\left(\frac{x}{2}\right)^\alpha \quad \alpha \geq 0 \quad x \to 0^+$$
$$Y_\alpha(x) \sim \frac{1}{\pi}\left(\frac{z}{2}\right)^{-\alpha}\sum_{k=0}^{\alpha-1}\frac{(\alpha-k-1)!}{k!}\left(\frac{x^2}{4}\right)^k + \frac{2}{\pi}J_\alpha(x)\ln\left(\frac{x}{2}\right) \quad x \to 0^+.$$

In the case of single layer BIE, we have to resolve logarithmic singularities. In the case of regular enough boundaries Γ (e.g. at least C^2), it turns out that the singularity of the double layer BIO is also logarithmic. The Nyström method proposed by Kussmaul and Martensen relies on the splittings above. Assuming that the wavenumber k is real, and that Γ is parametrized by a 2π periodic function x, the kernel of the single layer BIO

$$M_k(t,\tau) = \frac{i}{4}H_0^{(1)}(k|x(t) - x(\tau)|)$$

is split in the following form

$$M_k(t,\tau) = M_{k,1}(t,\tau)\ln\left(4\sin^2\left(\frac{t-\tau}{2}\right)\right) + M_{k,2}(t,\tau)$$

$$M_{k,1}(t,\tau) = \frac{-1}{4\pi} J_0(k|x(t) - x(\tau)|)$$

where the expressions $M_{k,1}(t,\tau)$ and $M_{k,2}(t,\tau)$ are regular with limiting values

$$M_{k,1}(t,t) = \frac{-1}{4\pi} \qquad M_{k,2}(t,t) = \frac{i}{4} - \frac{C}{2\pi} - \frac{1}{2\pi} \ln\left(\frac{k|x'(t)|}{2}\right).$$

Using the addition theorem, the integrals of the products of the logarithmic singularity $\ln\left(4\sin^2\left(\frac{t-\tau}{2}\right)\right)$ and the Fourier basis $e^{in\tau}$ can be computer explicitly, and this is the key ingredient in the Kussmaul and Martensen quadrature. Unfortunately, those quadratures cannot be applied directly in the case when the wavenumber k is complex because the Bessel function $J_0(z)$ grows exponentially as $|z| \to \infty$ in the case when the argument z is complex with positive imaginary part. In [62], Peréz-Arancibia and Labarca advocated for the use of Alpert quadrature rules for such wavenumbers. We recall that all the wavenumbers s_ℓ that feature in CQ are complex with possibly large imaginary parts. The main advantage of Alpert quadratures is that they can handle the logarithmic singularities of the Hankel functions in a manner that is agnostic to their arguments. As such, it can be applied to all the CQ BIE featuring various wavenumbers s_ℓ.

We describe briefly in what follows the mechanics of Alpert quadratures. They amount to

$$\begin{aligned}\int_0^T k(x_i,x')\sigma(x')dx' \approx h\sum_{p=0}^{N-2a} k(x_i, x_i + ah + ph)\sigma(x_i + ah + ph) \\ + h\sum_{p=1}^{m} w_p k(x_i, x_i + \chi_p h)\sigma(x_i + \chi_p h) \\ + h\sum_{p=1}^{m} w_p k(x_i, x_i + T - \chi_p h)\sigma(x_i + T - \chi_p h)\end{aligned}$$

where $\{x_i\}$ is an equispaced mesh on the interval $[0,T]$, the kernel $k(x_i,x')$ has a logarithmic singularity as $x' \to x_i$, σ is assumed to be a regular enough density, and the weights w_p and the nodes χ_p are selected so that the ensuing quadratures

achieves a prescribed rate of convergence. The weights and nodes are tabulated in Appendix B. The endpoint correction nodes χ_p are typically not integers, and as such the Alpert quadrature requires evaluation of the density σ outside of the equispaced mesh $\{x_i\}$. This is achieved by resorting to Lagrange interpolation that shifts the grid points around the non-grid point x where σ needs to be evaluated

$$\sigma(x) = \sum_{q=0}^{m=1} L_q^{(x_i)}(x)\sigma(x_i + qh) \qquad \text{where} \qquad L_q^{(x_i)}(x) = \prod_{r=0} \frac{x - (x_i + rh)}{(x_i + qh) - (x_i + rh)}.$$

Consequently, we have

$$\sigma(x_i + \chi_p h) \approx \sum_{q=0}^{m+3} L_q^{(x_i)}(x_i + \chi_p h)\sigma(x_i + qh)$$
$$\sigma(x_i + T - \chi_p h) \approx \sum_{q=0}^{m+3} L_q^{(x_i)}(x_i + T - \chi_p h)\sigma(x_i + T - qh).$$

Finally, the Alpert quadrature reads

$$\begin{aligned}
\int_0^T k(x_i, x')\sigma(x')dx' &\approx h\sum_{p=0}^{m+3} k(x_i, x_i + ah + ph)\sigma(x_i + ah + ph) \\
&+ h\sum_{q=0}^{m+3}\left(\sum_{p=1} w_p k(x_i, x_i + \chi_p h)L_q^{(x_i)}(x_i + \chi_p)\right)\sigma(x_i + qh) \\
&+ h\sum_{q=0}^{m+3}\left(\sum_{p=1} w_p k(x_i, x_i + T - \chi_p)L_q^{(x_i+T)}(x_i + T - \chi_p h)\right)\sigma(x_i + T - qh).
\end{aligned}$$

Assuming that the density σ is sampled at a mesh consisting of N equispaced nodes on the interval $[0, T]$, the Alpert quadratures applied to all of the integrals $\int_0^T k(x_i, x')\sigma(x')dx'$ for $1 \le i \le N$ leads to a matrix vector multiplication, where the N vector collects the values $\sigma(x_i),\ 1 \le i \le N$, and the $N \times N$ collocation/Nyström matrix has entries $a_{i,j},\ 1 \le i, j \le N$ that can be constructed explicitly via the formula $a_{i,j} = b_{i,j} + c_{i,j}$ where

$$b_{i,j} = \begin{cases} 0 & \text{if } |l(i,j)| < a \\ hk(x_i, x_j) & \text{if } |l(i,j)| \ge a, \end{cases}$$

and

$$c_{i,j} = \begin{cases} 0 & \text{if } |l(i,j)| > m+3 \\ h\sum_{p=1} w_p \begin{pmatrix} +k(x_i, x_i+\chi_p h) L^{(x_i)}_{l(i,j)}(x_i+\chi_p h) \\ +k(x_i, x_i+T-\chi_p h) L^{(x_i+T)}_{l(i,j)}(x_i+T-\chi_p h) \end{pmatrix} & \text{if } |l(i,j)| \leq m+3 \end{cases}$$

where

$$l(i,j) = (j-1)(\text{mod N}).$$

The numerical solution of the BIE in Equations (3.4), (3.6), or (3.8) rely on construction of Alpert Nyström matrices like the ones above. We note that is also possible to use trigonometric interpolation instead of Lagrange interpolation in order to evaluate densities at off grid points. Appendix C contains a presentation of this alternative interpolation method.

3.1.2 Piecewise Smooth Boundaries

In order to handle piecewise smooth domains with our layer potential formulation, we will make use of the following Sigmoid function, that polynomially bunches the discretization points toward corner points while maintaining a reasonable density of discretization points throughout the rest of the boundary Γ.

$$w(s) = \frac{T_{j+1}[v(s)]^p + T_j[1-v(s)]^p}{[v(s)]^p + [1-v(s)]^p} \quad T_j \leq s \leq T_{j+1}, 1 \leq j \leq P$$

$$v(s) = \left(\frac{1}{p} - \frac{1}{2}\right)\left(\frac{T_j + T_{j+1} - 2s}{T_{j+1} - T_j}\right)^3 + \frac{1}{p}\left(\frac{2s - T_j - T_{j+1}}{T_{j+1} - T_j}\right) + \frac{1}{2}$$

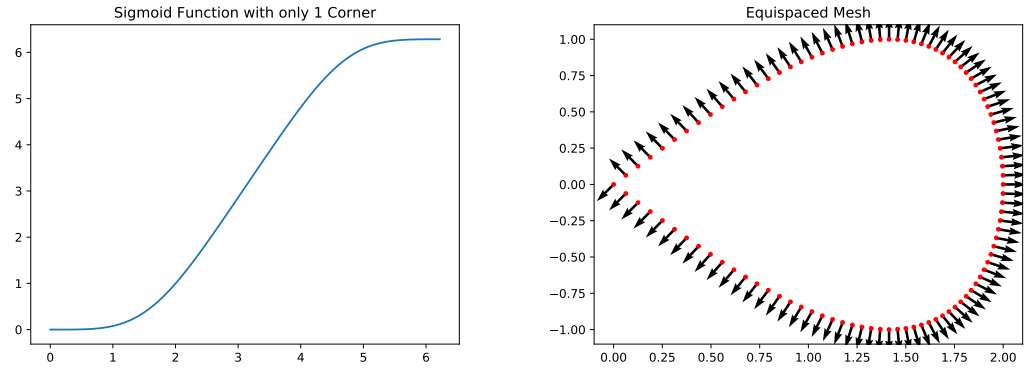

Figure 3.1 Effect of the sigmoid function on boundary discretization.

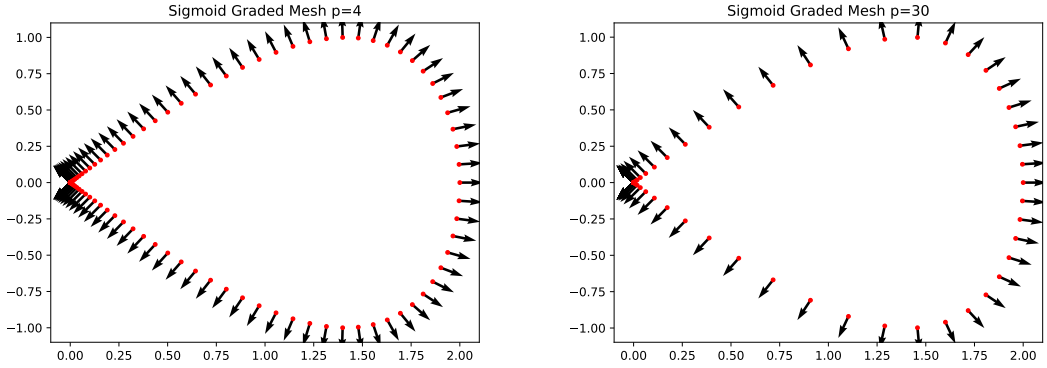

The assumption is that the domain Ω has corners at $x_1, x_2, \ldots, x_n$. The gradation works in conjunction with a parameterization for the boundary Γ, $x(\cdot) = (x_1(\cdot), x_2(\cdot))$. We compose the two, to get

$$x_w(t) = (x_1(w(t)), x_2(w(t)))\,.$$

In this approach we avoid having discretization points at the corners, by simply shifting the t-mesh

$$t_j = \frac{1}{2}(2j-1)\left(\frac{2\pi}{N}\right). \tag{3.9}$$

In addition to using graded meshes, we will also introduce weighted BIE formulations which we explain next.

Weighted Single-Layer Formulation Using graded meshes, the parametrized version of the Single Layer BIO reads

$$(\mathcal{S}_k\varphi)(t) = \int_0^{2\pi} G_k(x_w(t) - x_w(\tau))\varphi(\tau)|x'_w(\tau)|d\tau \tag{3.10}$$

where $\varphi(\tau) := \varphi(x_w(\tau))$. The ensuing parametrized BIE is:

$$(\mathcal{S}_k\varphi)(t) = g(x_w(t)).$$

Given that we are dealing with BIE of the first kind, it makes sense then to define a new weighted density in the form

$$\varphi^w(\tau) = \varphi(\tau)|x'_w(\tau)|,$$

which, given that x'_w vanishes polynomially at corners, makes the new density more regular than the original one. The weight formulation is then

$$\int_0^{2\pi} G_k(x_w(t) - x_w(\tau))\varphi^w(\tau)d\tau = g(x_w(t)). \tag{3.11}$$

The weighted Equation (3.11) is directly amenable to solutions via Alpert Nyström matrices.

Weighted Double-Layer Formulation We suppose now that the solution takes a DL form:

$$(\mathcal{K}_k\varphi)(t) = \int_0^{2\pi} \frac{\partial G_k(x_w(t) - x_w(\tau))}{\partial n(\tau)}\varphi(\tau)|x'_w(\tau)|d\tau$$

We add and subtract the Laplace free space kernel:

$$\begin{aligned}(\mathcal{K}_k\varphi) = &\int_0^{2\pi} \frac{\partial (G_k - G_0)(x_w(t) - x_w(\tau))}{\partial n(\tau)}\varphi(\tau)|x'_w(\tau)|d\tau \\ &+ \int_0^{2\pi} \frac{\partial G_0(x_w(t) - x_w(\tau))}{\partial n(\tau)}(\varphi(\tau) - \varphi(t))|x'_w(\tau)|d\tau \\ &+ \varphi(t)\int_0^{2\pi} \frac{\partial G_0(x_w(t) - x_w(\tau))}{\partial n(\tau)}|x'_w(\tau)|d\tau.\end{aligned}$$

Evaluating $\mathcal{K}_k$ on the boundary leads to the BIE:

$$\begin{aligned} g(x_w(t)) = \alpha(t)\varphi(t) &+ \int_0^{2\pi} \frac{\partial (G_k - G_0)(x_w(t) - x_w(\tau))}{\partial n(\tau)} \varphi(\tau)|x_w'(\tau)|d\tau \\ &+ \int_0^{2\pi} \frac{\partial G_0(|x_w(t) - x_w(\tau)|)}{\partial n(\tau)} (\varphi(\tau) - \varphi(t))|x_w'(\tau)|d\tau \\ &+ \varphi(t) \int_0^{2\pi} \frac{\partial G_0(x_w(t) - x_w(\tau))}{\partial n(\tau)} |x_w'(\tau)|d\tau \end{aligned}$$

where

$$\alpha(t) = \begin{cases} \frac{1}{2} & t \in [0, 2\pi] \setminus \{T_1, \ldots, T_N\} \\ \frac{\gamma_j}{2} & t = T_j, 1 \leq j \leq N, \end{cases}$$

in terms of the corner apertures γ_j. Further, we make use of the following identity:

$$\int_0^{2\pi} \frac{\partial G_0(x_w(t) - x_w(\tau))}{\partial n(\tau)} |x_w'(\tau)|d\tau = -\alpha(t)$$

and we reduce the BIE to

$$\begin{aligned} g(x_w(t)) = &\int_0^{2\pi} \frac{\partial (G_k - G_0)(|x_w(t) - x_w(\tau)|)}{\partial n(\tau)} \varphi(\tau)|x_w'(\tau)|d\tau \\ &+ \int_0^{2\pi} \frac{\partial G_0(x_w(t) - x_w(\tau))}{\partial n(\tau)} (\varphi(\tau) - \varphi(t))|x_w'(\tau)|d\tau. \end{aligned}$$

As a result of these manipulations, the first integral above can be evaluated using Alpert quadratures, while the second one can be evaluated using the trapezoidal rule. The key observation here is the fact that the density φ is Hölder continuous, the the simple trapezoidal rule suffices to deliver high order convergence.

Quadrature by Expansion The quadrature by expansion (QBX) method is another powerful and popular method used to evaluate the boundary layer potentials and operators that arise in Helmholtz problems. Just like the Alpert quadratures, QBX can be applied relatively easily to the evaluations of layer potentials whose

associated Green functions feature either real or complex wavenumbers. In what follows, we give an exposition of QBX in the case of evaluations of single layer potentials. The Quadrature by Expansion method relies on the addition formula

$$H_0^{(1)}(k|x-x'|) = \sum_{\ell=-\infty}^{\infty} H_\ell^{(1)}(k|x'-x^+|)e^{i\ell\theta'}J_\ell(k|x-x^+|)e^{-i\ell\theta},\ x' \in \Gamma \tag{3.12}$$

where θ and θ' are the angular coordinates of x and respectively x' in the polar coordinate system centered at $c = x^+$. The addition theorem (3.12) leads than to the following series representation for the single layer potential

$$(\mathcal{V}_k\varphi)(x) = \sum_{\ell=-\infty}^{\infty} \alpha_\ell J_\ell(k|x-x^+|)e^{-i\ell\theta}, \quad \alpha_\ell := \frac{i}{4}\int_\Gamma H_\ell^{(1)}(k|x'-x^+|)e^{i\ell\theta'}\varphi(x')ds(x'). \tag{3.13}$$

In practice a truncation parameter p is chosen in the series representation (3.13) leading to the following QBX approximation

$$(\mathcal{V}_k\varphi)(x) \approx \sum_{\ell=-p}^{p} \alpha_\ell J_\ell(k|x-x^+|)e^{-i\ell\theta} \tag{3.14}$$

where the coefficients α_ℓ have to be evaluated numerically for all $-p \le \ell \le p$. We note that the integrands in the definition (3.13) of the coefficients α_ℓ do not contain kernel singularities as $x^+ \notin \Gamma$. We will use in what follows Clenshaw-Curtis quadratures to evaluate numerically the coefficients α_ℓ in Equation (3.13). Indeed, we assume that Γ is piecewise smooth and the corners are located at $x_1, x_2, \ldots, x_P$ and thus

$$\alpha_\ell = \sum_m \alpha_{\ell,m}, \qquad \alpha_{\ell,m} := \frac{i}{4}\int_{\Gamma_m} H_\ell^{(1)}(k|x'-x^+|)e^{i\ell\theta'}\varphi(x')ds(x').$$

We apply Clenshaw-Curtis quadratures for the evaluation of each of the integrals in the definition of $\alpha_{\ell,m}$, that is

$$\alpha_{\ell,m} \approx \frac{i}{4}\sum_{j=1}^{N_m} \omega_j H_\ell^{(1)}(k|\gamma_m(t_j)-x^+|)e^{i\ell\theta'_j}\widetilde{\varphi}(\gamma_m(t_j)) \tag{3.15}$$

where we assume that Γ_m is parametrized in the form $\Gamma_m = \{\gamma_m(t) : t \in [-1,1]\}$ and $\gamma_m : [-1,1] \to \mathbb{R}^2$ is smooth, $\widetilde{\varphi}(\gamma_m(t_j)) = \varphi(\gamma_m(t_j))|\gamma_m'(t_j)|$, the quadrature points t_j are the Chebyshev zero points

$$t_j := \cos(\vartheta_j), \quad \vartheta_j := \frac{(2j-1)\pi}{2N_m}, \quad j = 1, \ldots, N_m$$

and the Fejér quadrature weights ω_j are given by

$$\omega_j := \frac{2}{N_m}\left(1 - 2\sum_{q=1}^{[N_m/2]} \frac{1}{4q^2-1}\cos(2q\vartheta_j)\right), \quad j = 1, \ldots, N_m.$$

The full QBX discretization of the single layer BIE (3.2) is given in what follows: (1) choose a grid on Γ such that $x_{j,m} = \gamma_m(t_j),\ 1 \le m \le P+1,\ 1 \le j \le n_m$ and $t_j := \cos(\vartheta_j), \quad \vartheta_j := \frac{(2j-1)\pi}{2n_m}, \quad j = 1, \ldots, n_m$; (2) for each x_j on Γ define the expansion centers $x_j^{\pm} := x_j \pm \varepsilon(x_j)n(x_j)$; (3) use the QBX approximation (3.14) for a given truncation parameter p; and (4) evaluate the ensuing coefficients $\alpha_{\ell,m}$ according to the Clenshaw-Curtis quadrature (3.15) using oversampling, that is choose $N_m = \beta n_m,\ \beta \ge 1$ in Equation (3.15) and use Chebyshev interpolation to access the values of the density φ^w on the fine Chebyshev grid with N_m nodes on each Γ_m. Finally, we choose $\varepsilon(x_j) = \min(|x_j - x_{j-1}|, |x_j - x_{j+1}|)$ in the definition of the centers $x_j^{\pm}$.

It is also possible to consider weighted formulations of the single layer BIE (3.2). Specifically, assuming the $\gamma_m : [-1,1] \to \mathbb{R}^2$ parametrizations of each Γ_m for $1 \le m \le P+1$, we define

$$\varphi_m^w(t) := \varphi(\gamma_m(t))|\gamma_m'(t)|\sqrt{1-t^2}, \quad -1 \le t \le 1, \quad 1 \le m \le P+1 \tag{3.16}$$

which, in turn, leads to a simpler Fejér quadrature rule for the evaluation of the coefficients $\alpha_{\ell,m}$ of the form

$$\alpha_{\ell,m} \approx \frac{i\pi}{4N_m}\sum_{j=1}^{N_m} H_\ell^{(1)}(k|\gamma_m(t_j) - x^+|)e^{i\ell\theta_j'}\varphi_m^w(t_j). \tag{3.17}$$

Table 3.1 QBX Clenshaw-Curtis Error and Order of Convergence

N	Teardrop		Boomerang		Strip		V-shaped	
	ε_∞	e.o.c.	ε_∞	e.o.c.	ε_∞	e.o.c.	ε_∞	e.o.c.
32	1.3×10^{-2}		4.4×10^{-2}		2.6×10^{-4}		4.7×10^{-4}	
64	6.5×10^{-6}	10.9	1.0×10^{-5}	12.01	5.9×10^{-5}	2.18	1.1×10^{-4}	1.99
128	1.0×10^{-6}	2.70	4.9×10^{-8}	7.73	1.3×10^{-5}	2.10	2.9×10^{-5}	1.99
256	1.6×10^{-7}	2.64	2.2×10^{-10}	7.80	3.3×10^{-6}	2.07	7.4×10^{-6}	1.99

Errors in the near field and estimated orders of convergence obtained from the QBX Nyström quadrature discretization of the single layer formulation for real wavenumber $k = 8$ and plane wave normal incidence. We used the weighted unknown (3.16) and the Clenshaw-Curtis quadratures (3.17) in the expansion (3.13), as well as the QBX parameters $p = 8$ and $\beta = 6$.

We report in Table 3.1 numerical results concerning QBX quadrature Nyström discretizations of the single layer formulation of the Helmholtz Equation (3.1) using the weighted unknown (3.16) and the Clenshaw-Curtis quadratures (3.17) in the expansion (3.13). Qualitatively similar results are obtained in the cases when the wavenumber is complex.

3.2 Neumann Boundary Conditions

In this section, we will solve the wave equation with Neumann boundary conditions:

$$\begin{cases} \frac{\partial^2 u(x,t)}{\partial t^2} = \Delta u(x,t) \quad x \in \Omega^+,\ t > 0 \\ \frac{\partial u(x,t)}{\partial n(x)} = \frac{\partial g(x,t)}{\partial n(x)} \quad x \in \Gamma. \end{cases}$$

We can apply CQ with any of the A-stable ODE solvers previously discussed, the details are the same. The main difference is that we would have to deal in the Laplace domain with modified Helmholtz equations with Neumann boundary conditions, that is boundary value problems of the type

$$\begin{cases} \Delta u(x) + k^2 u(x) = 0 \quad x \in \Omega \\ \frac{\partial u(x)}{\partial n(x)} = \frac{\partial g(x)}{\partial n(x)} \quad x \in \Gamma. \end{cases} \tag{3.18}$$

The solution of these problems will be obtained again through BIE.

3.2.1 Smooth Boundaries

Single-Layer Formulation If we suppose that the solution (3.18) takes on the form of a SL potential

$$u(x) = \int_\Gamma G_k(|x-y|)\varphi(y)ds(y),\ x \in \Omega^+,$$

we obtain the following BIE of the second kind

$$-\frac{\varphi}{2} + \mathcal{K}_k^\top \varphi = f \quad \text{on } \Gamma, \quad (\mathcal{K}_k^\top \varphi)(x) := \int_\Gamma \frac{\partial G_k(x-y)}{\partial n(x)}\varphi(y)ds(y),\ x \in \Gamma. \tag{3.19}$$

We note that the BIE formulation (3.19) is uniquely solvable whenever $\Im k > 0$. In order to make the BIE formulation (3.19) amenable to Nyström discretizations based on Alpert quadratures, we use the parametrization γ of the boundary curve Γ that incorporates the sigmoid transforms and we employ the following weighted formulation

$$-\frac{1}{2}\varphi^w(t) - \frac{ik}{4}\int_0^{2\pi} H_1^{(1)}(k|\gamma(t)-\gamma(\tau)|)\frac{(\gamma(t)-\gamma(\tau))\cdot(\gamma'(t))^\perp}{|\gamma(t)-\gamma(\tau)|}\varphi^w(\tau)d\tau = f(\gamma(t))|\gamma'(t)| \tag{3.20}$$

where $(\gamma'(t))^\perp = (\gamma_2'(t), -\gamma_1'(t))$ and again here $\varphi^w(t) := |\gamma'(t)|\varphi(\gamma(t))$. On the other hand, the application of QBX quadratures to the evaluation of the BIO $\mathcal{K}_k^\top \varphi$ relies on the classical jump formulas for the gradients of single layer potentials

$$\nabla_x(\mathcal{S}_k\varphi)(x) = \lim_{x^\pm \to x} \nabla_{x^\pm}(\mathcal{S}_k\varphi)(x^\pm) \pm \frac{1}{2}n(x)\varphi(x),\ x \in \Gamma,\ x^\pm = x \pm \varepsilon n(x),$$

which amounts to differentiating term by term the expressions

$$(\mathcal{S}_k\varphi)(x^{\pm}) \approx \sum_{\ell=-p}^{p} \alpha_\ell J_\ell(k|x^{\pm} - x|)e^{-i\ell\theta^{\pm}}$$

in the polar coordinate systems around the expansion centers [54]. Furthermore, per the prescription in [54], we average the derivatives of the expansions above with respect to both x^+ and x^- in order to evaluate the BIO expressions in Equation (3.19). Specifically, the QBX quadrature takes on the form

$$-\quad \frac{\varphi(x)}{2} + (\mathcal{K}_k^{\top}\varphi)(x) \tag{3.21}$$

$$\begin{aligned} \approx\quad & -\frac{1}{2}\lim_{x^+\to x}\sum_{\ell=-p}^{p} k\alpha_\ell \left(-J_{\ell+1}(k|x^+ - x| + \frac{\ell}{k|x^+ - x|}J_\ell(k|x^+ - x|)\right)e^{-i\ell\theta^+} \\ +\quad & \frac{1}{2}\lim_{x^-\to x}\sum_{\ell=-p}^{p} k\alpha_\ell \left(-J_{\ell+1}(k|x^- - x| + \frac{\ell}{k|x^- - x|}J_\ell(k|x^- - x|)\right)e^{-i\ell\theta^-} \end{aligned} \tag{3.22}$$

where the coefficients α_ℓ are in turn computed via the formulas (3.15). We present in Tables 3.2 and 3.3 numerical results concerning Alpert and QBX discretizations of the second kind formulation (3.19) in the case when the wavenumber $k = 8$ using reference solutions produced by the high-order kernel-splitting Nyström discretization in [2].

3.2.2 Hypersingular BIE Fomulation

If we seek the solution of Equation (3.18) in the form of a double layer potential

$$u(x) = \int_\Gamma \frac{\partial G_k(|x - y|)}{\partial n(y)}\varphi(y)ds(y),\ x \in \Omega^+$$

then the enforcement of Neumann boundary conditions results in the following BIE

$$(\mathcal{N}_k\varphi)(x) = g(x),\ x \in \Gamma \tag{3.23}$$

Table 3.2 Alpert Error and Order of Convergence

N	Teardrop		Boomerang	
	ε_∞	e.o.c.	ε_∞	e.o.c.
64	2.4×10^{-4}		6.2×10^{-3}	
128	5.7×10^{-6}	5.40	1.4×10^{-4}	5.40
256	1.9×10^{-7}	4.87	4.7×10^{-6}	4.91
512	7.7×10^{-9}	4.67	1.8×10^{-7}	4.71

Errors in the near field and estimated orders of convergence corresponding to the Alpert discretization of the weighted formulation (3.20) for real wavenumber $k = 8$ and plane wave normal incidence. We used the following Alpert quadrature parameters: $\sigma = 4$ in the sigmoid transform, and respectively $a = 2, m = 3$.

Table 3.3 QBX Clenshaw-Curtis Error and Order of Convergence

N	Teardrop		Boomerang	
	ε_∞	e.o.c.	ε_∞	e.o.c.
32	2.5×10^{-2}		3.3×10^{-1}	
64	3.0×10^{-3}	3.07	2.6×10^{-2}	3.65
128	3.6×10^{-4}	3.07	1.6×10^{-3}	4.03
256	3.1×10^{-5}	3.54	8.9×10^{-5}	4.16

Errors in the near field and estimated orders of convergence obtained with the QBX Nyström quadrature discretization of the single layer formulation for real wavenumber $k = 8$ and plane wave normal incidence. We used the QBX expansion (3.21) and the Clenshaw-Curtis quadratures (3.17) in the expansion (3.13), as well as the QBX parameters $p = 4$ and $\beta = 4$.

where the operator $\mathcal{N}_k$ is a BIO which has to be understood in the sense of Hadamard finite parts

$$(\mathcal{N}_k\varphi)(x) = f.p. \int_\Gamma \frac{\partial^2 G_k(|x-y|)}{\partial n(x)\partial n(y)}\varphi(y)ds(y),\ x \in \Gamma. \tag{3.24}$$

The operator $\mathcal{N}_k$ is a hypersingular, as the singularity is $\mathcal{O}(|x-y|^2)$. We can recast it in the following form

$$(\mathcal{N}_k\varphi)(x) = f.p. \int_\Gamma \frac{\partial^2 G_k(x-y)}{\partial n(x)\partial n(y)}\varphi(y)ds(y). \tag{3.25}$$

$$= \int_\Gamma \frac{\partial^2 (G_k - G_0)(x-y)}{\partial n(x)\partial n(y)}\varphi(y)ds(y) + f.p. \int_\Gamma \frac{\partial^2 G_0(x-y)}{\partial n(x)\partial n(y)}\varphi(y)ds(y) \tag{3.26}$$

where G_0 is the Green's function of the Laplace equation:

$$G_0(x) = -\frac{1}{2\pi}\log(|x|).$$

The kernel of the first integral term in the right hand side of (3.26) equals:

$$\frac{\partial^2 (G_k - G_0)(x-y)}{\partial n(y)\partial n(x)} = -n(x)\cdot\nabla^2_{xx}(G_k - G_0)(x-y)\ n(y), \tag{3.27}$$

where the notation ∇^2_{xx} stands for the Hessian matrix. Equation (3.27) can be further expressed as

$$n(x)\cdot\nabla^2_{xx}(G_k - G_0)(x-y)\ n(y) = \frac{-ik^2}{4}H_0^{(1)}(k|x-y|)\frac{(x-y)\cdot n(x)(x-y)\cdot n(y)}{|x-y|^2}$$
$$+\left(\frac{ik}{4}H_1^{(1)}(kx-y)|x-y| - \frac{1}{2\pi}\right)\left(\frac{2(x-y)\cdot n(x)(x-y)\cdot n(y)}{|x-y|^4} - \frac{n(x)\cdot n(y)}{|x-y|^2}\right).$$

In the light of the last calculation above, it can be seen that the singularity of the kernel of the first integral term in the right hand side of (3.26) is logarithmic. The Hadamard finite parts integral term in Equation (3.26) can be manipulated using integration by parts techniques starting from the identity

$$\frac{\partial^2 G_0(x-y)}{\partial n(x)\partial n(y)} = -\frac{\partial^2 G_0(x-y)}{\partial t(x)\partial t(y)},$$

where $t(x)$ is the unit tangent on Γ at x. We can expressed the hyper singular term in parametrized form

$$\begin{aligned} f.p.\int_\Gamma \frac{\partial^2 G_0(|x-y|)}{\partial n(x)\partial n(y)}\varphi(y)ds(y) &= -f.p.\int_\Gamma \frac{\partial^2 G_0(|x-y|)}{\partial t(x)\partial t(y)}\varphi(y)ds(y) \\ &= +\frac{1}{4\pi|x'(t)|}\int_0^{2\pi}\frac{\partial^2}{\partial t\partial\tau}\log(|x(t)-x(\tau)|^2)\varphi(\tau)d\tau. \end{aligned}$$

We add and subtract now the expression of the kernels in the case when $x(t) = (\cos t, \sin t)$ and obtain

$$\begin{aligned} &f.p.\int_\Gamma \frac{\partial^2 G_0(x-y)}{\partial n(x)\partial n(y)}\varphi(y)ds(y) \\ &= \frac{1}{4\pi|x'(t)|}\int_0^{2\pi}\frac{\partial^2}{\partial t\partial\tau}\left(\log\left(|x(t)-x(\tau)|^2\right) - \log\left(4\sin^2\left(\frac{t-\tau}{2}\right)\right)\right)\varphi(\tau)d\tau \\ &+ \frac{1}{4\pi|x'(t)|}\int_0^{2\pi}\frac{\partial^2}{\partial t\partial\tau}\left(\log\left(4\sin^2\left(\frac{t-\tau}{2}\right)\right)\right)\varphi(\tau)d\tau. \end{aligned}$$

Integrating by parts in the expressions above we get

$$\begin{aligned} &f.p.\int_\Gamma \frac{\partial^2 G_0(x-y)}{\partial n(x)\partial n(y)}\varphi(y)ds(y) \\ &= -\frac{1}{4\pi|x'(t)|}\int_0^{2\pi}\frac{\partial}{\partial t}\left(\log(|x(t)-x(\tau)|^2) - \log\left(4\sin^2\left(\frac{t-\tau}{2}\right)\right)\right)\varphi'(\tau)d\tau \\ &- \frac{1}{4\pi|x'(t)|}\int_0^{2\pi}\frac{\partial}{\partial t}\left(\log\left(4\sin^2\left(\frac{t-\tau}{2}\right)\right)\right)\varphi'(\tau)d\tau \\ &= \frac{1}{4\pi|x'(t)|}\int_0^{2\pi}\underbrace{\left(\frac{-2x'(t)\cdot(x(t)-x(\tau))}{|x(t)-x(\tau)|^2} - \cot\left(\frac{\tau-t}{2}\right)\right)}_{\eta(t,\tau)}\varphi'(\tau)d\tau \\ &+ \frac{1}{4\pi|x'(t)|}\int_0^{2\pi}\cot\left(\frac{\tau-t}{2}\right)\varphi'(\tau)d\tau. \end{aligned}$$

The expression $\eta(t,\tau)$ above can be seen to be regular

$$\eta(t,\tau) = \frac{-2x'(t)\cdot(x(t)-x(\tau))}{|x(t)-x(\tau)|^2} - \cot\left(\frac{\tau-t}{2}\right) \tag{3.28}$$

$$\lim_{\tau\to t}\eta(t,\tau) = -\frac{x'(t)\cdot x''(t)}{|x'(t)|^2}. \tag{3.29}$$

In conclusion, we expressed the hyper singular BIO in a form that is more amenable to Nyström discretizations:

$$(\mathcal{N}_k\varphi)(t) = -\int_0^{2\pi} n(t)\cdot\nabla^2_{tt}(G_k - G_0)(x(t)-x(\tau))n(\tau)\varphi(\tau)|x'(\tau)|d\tau \\ + \frac{1}{4\pi|x'(t)|}\int_0^{2\pi}\eta(t,\tau)\varphi'(\tau)d\tau + \frac{1}{4\pi|x'(t)|}\int_0^{2\pi}\cot\left(\frac{\tau-t}{2}\right)\varphi'(\tau)d\tau. \tag{3.30}$$

The first integral operator in the right hand side of Equation (3.30) is directly amenable to Alpert Nyström quadratures, given that its kernel exhibits only a logarithmic singularity. The next term features the derivative of the density which is effected in practice using the Fourier differentiation matrix who's entries are given by:

$$D_{ij} = \begin{cases} \frac{1}{2}(-1)^{i-j}\cot\left(\frac{(i-j)h}{2}\right) & i \neq j \\ 0 & i = j. \end{cases} \tag{3.31}$$

Given that the function $\eta(t,\tau)$ is regular in both its variables, the second integral in the right hand side of Equation (3.30) is evaluated simply using the trapezoidal rule, after the Fourier differentiation matrix has been applied to the density. Finally, the last term in the right hand side of Equation (3.30) is related to a Hilbert transform (see the [58] references on hyper singular integral equations) and can be evaluated in the following manner

$$\frac{1}{2\pi}\int_0^{2\pi}\cot\left(\frac{\tau-t}{2}\right)f'(\tau)d\tau \approx \sum_{j=0}^{2n} T_j^{(n)}(t)f(t_j^{(n)})$$

where

$$T_j^{(m)} = T_j^{(n)}(0) = \begin{cases} \frac{1}{2n\sin^2(t_j^{(n)}/2)} & j \in \text{Odd} \\ 0 & j \in \text{Even} \\ -n/2 & j = 0. \end{cases}$$

Piecewise Smooth Domains Given an incidence field $u^i(x)$ which satisfies the Helmholtz equation on the interior domain

$$\Delta u^i(x) + k^2 u^i(x) = 0 \quad x \in \Omega^-,$$

we want to find a solution $u^s(x)$ satisfying the Neumann boundary conditions in the exterior,

$$\begin{cases} \Delta u^s(x) + k^2 u^s(x) = 0 & x \in \Omega^+ \\ \frac{\partial u^s(x)}{\partial n(x)} = -\frac{\partial u^i(x)}{\partial n(x)} & x \in \Gamma. \end{cases} \tag{3.32}$$

For simplicity of the exposition we will assume that a single corner occurs at $x_0 \in \Gamma$. The goal is once again to find an integral representation for the solution of (3.32), but in this case instead of doing so for the scattered field, we look for an integral representation of the total field.

The advantage of the following technique is that the solution is bounded on Γ, unlike most other indirect formulations of the solution to (3.32), which are singular near x_0. The solutions u for these representations are Hölder continuous: $|u(x) - u(x_0)| = \mathcal{O}(|x - x_0|^\gamma)$, where γ can be determined from the angle of the corner.

The derivation and results of this section is based on [2] and will be partially reproduced here for completeness. A full proof invertability of the, yet to be described, operator can be found in the aforementioned paper. We start with Green's identity for both of the incidence and scattered field:

$$u^s(x) = \int_\Gamma \left(\frac{\partial G_k(x-y)}{\partial n(y)} u^s(y) - G_k(x-y) \frac{\partial u^s(y)}{\partial n(y)} dS_y \right) \tag{3.33}$$

$$u^i(x) = \int_\Gamma \left(\frac{\partial G_k(x-y)}{\partial n(y)} u^i(y) - G_k(x-y) \frac{\partial u^i(y)}{\partial n(y)} dS_y \right) = 0, \tag{3.34}$$

where $x \in \Gamma$. Adding (3.33) and (3.34) together gives us a representation for the scattered field, involving the total field,

$$u^s(x) = \int_\Gamma \frac{\partial G_k(x-y)}{\partial n(y)} \left(u^s(y) + u^i(y) \right) - G_k(x-y) \left(\frac{\partial u^s(y)}{\partial n(y)} + \frac{\partial u^i(y)}{\partial n(y)} \right) dS_y \tag{3.35}$$

$$= \underbrace{\int_\Gamma \frac{\partial G_k(x-y)}{\partial n(y)} u(y) dS_y}_{(\mathcal{K}_k \varphi)(x)} . \tag{3.36}$$

Notice that the second term above is zero due to the boundary conditions of (3.32), and $u(x) = u^s(x) + u^i(x)$. Taking the limit as x approaches the boundary and making use of the trace formulation for the DL potential, we arrive at an integral equation of the second kind,

$$\frac{1}{2} u(x) - (\mathcal{K}_k u)(x) = u^i(x) \quad x \in \Gamma. \tag{3.37}$$

Returning for a moment to (3.36), taking a normal derivative and similarly making use of the trace, resulting in an integral equation of the first kind involving the hypersingular operator

$$-(\mathcal{N}_k)(x) = \frac{\partial u^i(x)}{\partial n(x)} \quad x \in \Gamma. \tag{3.38}$$

As done in the previous section, we recast this integral equation as a Cauchy Principle value by making use of Maue's integration by parts identity. We now seek a uniquely solvable integral equation, but neither (3.37) or (3.38) are uniquely solvable for all wave numbers k. The usual way of overcoming this is to resort to a CFIE, consisting of a linear combination of the SL and DL. While such a formulation does fix the uniquely

saleability issue, we are in no better shape to resolve the issue of the hypersingular operator $\mathcal{N}_k$, which has spectrum that accumulates at infinity. To improve the spectral limitations amounts to regularizing the CFIE: the idea is to combine (3.38) with a regularizer, resulting in

$$\frac{1}{2}u(x) - (\mathcal{K}_k u)(x) - i\xi(\mathcal{R}\circ\mathcal{N}_k u)(x) = u^i(x) + i\xi\mathcal{R}\left(\frac{\partial u^i(x)}{n(x)}\right) \quad x\in\Gamma. \tag{3.39}$$

A wide variety of regularizers $\mathcal{R}$ can be used, however simple ones that are relatively easy to implement are preferred. The regularize considered in what follows will also work well in the CQ setting. An appropriate choice to this end is

$$(\mathcal{R}\varphi)(x) = (\mathcal{S}_\eta\varphi)(x) = \frac{i}{4}\int_\Gamma G_\eta(x-y)\varphi(y)dS_y. \tag{3.40}$$

With this regularizer, it can be proved that the choice of regularizer $\mathcal{R}=\mathcal{S}_\eta$ renders the left hand side of (3.39) renders invertible as an operator from $C^\gamma(\Gamma)$ to $C(\Gamma)$. The proof of this fact is given in [2], however only the relevant steps in the derivations of the invertible operator will be given. The following two identities will be useful in this pursuit

$$\mathcal{S}_\eta\circ\mathcal{N}_0 = -\frac{I}{4} + (\mathcal{K}_\eta)^2 \qquad \int_\Gamma\int_\Gamma \frac{\partial^2 G_0(x-y)}{\partial n(x)\partial n(y)}\varphi(y)dS_y dS_x = 0$$

The goal is to express the composition $\mathcal{R}\circ\mathcal{N}_k$, using the above, in a different form

$$\mathcal{S}_\eta\circ N_k = \mathcal{S}_\eta(\mathcal{N}_k - \mathcal{N}_0) - \frac{I}{4} + (\mathcal{K}_\eta)^2. \tag{3.41}$$

With this identity and a choice of $\xi = i$, we arrive at the final form of the integral operator,

$$u(x) - (\mathcal{K}_k u)(x) - (S_\eta(N_k - N_0)u)(x) - (\mathcal{K}_k u)^2(x) = u^i(x) + 2\mathcal{S}_\eta\left(\frac{\partial u^i(x)}{n(x)}\right) \tag{3.42}$$

It is worth noting that this formulation once discretized will need a graded mesh to account for the corner x_0, which can be handled with Alpert quadrature. QBX will

also be able to handle Equation (3.42), though an alternate procedure for QBX that applies for more general scatterers will be introduced in the following section. Finally, $\mathcal{S}_\eta$ can be precomputed once, making it an excellent choice as a regularizer given that CQ can require multiple frequency solves for each time step depending on the order of the method.

Open Arcs and Alpert Quadrature A special formulation is needed for the case of when we want to solve the problem with a double layer formulation and Neumann boundary conditions coupled with Alpert quadrature. A brief derivation will be derived in this subsection. To this end, we consider ther Hypersingular operator :

$$\mathcal{N}_k\varphi(x) = \int_\Gamma \frac{\partial^2 G_k(x-y)}{\partial n(x)\partial n(y)}\Psi(y)dS_y$$

As in the smooth case, we add and subtract the Laplace kernel, from which we get:

$$\mathcal{N}_k\varphi(x) = \int_\Gamma \bar{K}(x,y)\Psi(y)dS_y + \int_\Gamma \bar{K}_0(x,y)\Psi(y)dS_y$$

where

$$\begin{aligned}\bar{K}_0(x,y) &= \frac{\partial^2 G_0(x-y)}{\partial n(x)\partial n(y)} = -\frac{\partial^2 G_0(x-y)}{\partial t(x)\partial t(y)}\\ \bar{K}(x,y) &= \frac{\partial^2 \left(G_k - G_0\right)(x-y)}{\partial n(x)\partial n(y)}.\end{aligned}$$

Unlike in most of the other methods, we do not parameterize from 0 to 2π, but rather with

$$\Gamma = \left\{\gamma(t) : t \in [-1,1],\ \gamma : [-1,1] \to \mathbb{R}^2\right\}.$$

Much like we did in subsection 3.2.2, we and add and subtract the Laplace free space solution, to $\bar{K}_0$ and in the process define:

$$\begin{aligned}K_0(t,\tau) &= \frac{\partial^2}{\partial v^2}\left(G_0\left(\gamma(t)-\gamma(\tau)\right) - \ln\left(4\sin^2\left(\frac{t-\tau}{2}\right)\right)\right),\\ K(t,\tau) &= \frac{\partial^2 \left(G_k - G_0\right)\left(\gamma(t)-\gamma(\tau)\right)}{\partial n(t)\partial n(\tau)}.\end{aligned}$$

The hypersingular integral operator as can then be written as

$$(\mathcal{N}_k\varphi)(\gamma(t)) = \frac{1}{\pi|\gamma'(t)|}\int_{-1}^{1}\frac{\Psi'(\tau)}{\tau - t} + K_0(t,\tau)\Psi(\tau) + K(t,\tau)\Psi(\tau)d\tau.$$

With the change of variable $t = \cos(s)$ and $\tau = \cos(\sigma)$, we get

$$\frac{1}{\pi}\int_0^{\pi} \frac{\sin(s)\chi'(\sigma)}{\cos(s)-\cos(\sigma)} + H_0(s,\sigma)\chi(\sigma) + H(s,\sigma)\chi(\sigma)d\sigma = f(s)$$

where

$$\begin{aligned}
\chi(s) &= \Psi(\cos(s)) \\
f(s) &= |\gamma'(s)|\sin(s)g(\cos(s)) \\
H_0(s,\sigma) &= \sin(s)\sin(\sigma)K_0(\cos(s),\cos(\sigma)) \\
H(s,\sigma) &= \sin(s)\sin(\sigma)K(\cos(s),\cos(\sigma)).
\end{aligned}$$

From here we move on to make use of the following identity:

$$\frac{\sin(s)}{\cos(s)-\cos(\sigma)} = \frac{1}{2}\cot\left(\frac{\sigma-s}{2}\right) - \frac{1}{2}\cot\left(\frac{\sigma+s}{2}\right).$$

Taking advantage of an odd extension of the unknown density χ, the integral equation then becomes:

$$\frac{1}{2\pi}\int_0^{2\pi} \cot\left(\frac{\sigma-s}{2}\right)\chi'(\sigma) + H_0(s,\sigma)\chi(\sigma) + H(s,\sigma)\chi(\sigma)d\sigma = f(s). \tag{3.43}$$

This last formulation allows us to evaluate open arcs with Neumann boundary conditions and Alpert Quadrature.

Current and Charge Formulations We start with the Maue's integration by parts recasting of the BIO $N(k)$ in the form

$$(\mathcal{N}_k\varphi)(x) = k^2\int_\Gamma G_k(x-y)\hat{n}(x)\cdot\hat{n}(y)\varphi(y)ds(y) + \partial_s^x\int_\Gamma G_k(x-y)\partial_s\varphi(y)ds(y),\ x\in\Gamma \tag{3.44}$$

where ∂_s denote tangential differentiation, where $\varphi \in H^{1/2}(\Gamma)$ when Γ is closed and $\varphi \in \widetilde{H}^{1/2}(\Gamma)$ when Γ is open (we not that the integration by parts is still justified in the latter case since φ vanishes at the endpoints of Γ). We shall use in what follows

the $\hat{\cdot}$ notation to denote vector quantities. We employ in what follows the Current and Charge formulation of (3.23) starting from Equation (3.44) which is a variant of the formulations pioneered in [87] for 3D Maxwell equations and subsequently studied in the excellent contributions [10, 39]. First, we introduce the *charge* unknown ρ which is related to the *current* unknown φ in the following manner

$$\partial_s \varphi = ik\rho. \tag{3.45}$$

Replacing the tangential derivative $\partial_s\varphi$ by the new unknown ρ in the Maue formula (3.44) and enforcing the constraint (3.46) in an integral form, we arrive at the system of BIE

$$\begin{aligned} -ik\int_\Gamma G_k(x-y)\hat{n}(x)\cdot\hat{n}(y)\varphi(y)ds(y) + \partial_s\int_\Gamma G_k(x-y)\rho(y)ds(y) &= \frac{1}{ik}f(x) \\ \int_\Gamma G_k(x-y)\partial_s\varphi(y)ds(y) - ik\int_\Gamma G_k(x-y)\rho(y)ds(y) &= 0. \end{aligned}$$

Performing an integration by parts on the integral term that contains the quantity $\partial_s\varphi$ we obtain the following Current and Charge (CC) BIE formulation of the Helmholtz problem (3.18) whose unknowns are the densities $(\varphi,\rho)\in H^{1/2}(\Gamma)\times H^{-1/2}(\Gamma)$ in the case when Γ is closed and respectively $(\varphi,\rho)\in \widetilde{H}^{1/2}(\Gamma)\times \widetilde{H}^{-1/2}(\Gamma)$ when Γ is an open arc

$$\begin{aligned} -ik\int_\Gamma G_k(x-y)\hat{n}(x)\cdot\hat{n}(y)\varphi(y)ds(y) + \partial_s\int_\Gamma G_k(x-y)\rho(y)ds(y) &= \frac{1}{ik}f(x) \\ \nabla\cdot\int_\Gamma G_k(x-y)\hat{t}(y)\varphi(y)ds(y) - ik\int_\Gamma G_k(x-y)\rho(y)ds(y) &= 0. \end{aligned} \tag{3.46}$$

We note that the CC formulation (3.46) above features BIOs whose singularities are no longer integrable (i.e they exhibit Cauchy p.v. operators), and as such, they cannot be discretized directly using Alpert quadratues. On the other hand, the QBX methods can handle relatively seamlessly these new operators. In the QBX approach, the derivatives of the layer potentials that feature in the CC formulation (3.46) are

performed by differentiating term by term the expansions around the centers, via the formulas

$$\partial_s(\mathcal{S}_k\varphi)(x) \approx -i \lim_{x^+\to x} \sum_{\ell=-p}^{p} \ell\alpha_\ell \frac{J_\ell(k|x^+ - x|)}{|x^+ - x|} e^{-i\ell\theta^+}$$

and respectively

$$\begin{aligned}
&\nabla^x \cdot (\mathcal{S}_k\hat{t}\varphi)(x) \approx \\
- &\lim_{x^+\to x} \sum_{\ell=-p}^{p} k\hat{\alpha}_\ell \cdot \hat{n}(x) \left(-J_{\ell+1}(k|x^+ - x| + \frac{\ell}{k|x^+ - x|} J_\ell(k|x^+ - x|) \right) e^{-i\ell\theta^+} \\
- &\; i \lim_{x^+\to x} \sum_{\ell=-p}^{p} \ell\hat{\alpha}_\ell \cdot \hat{t}(x) \frac{J_\ell(k|x^+ - x|)}{|x^+ - x|} e^{-i\ell\theta^+}
\end{aligned}$$

where

$$\hat{\alpha}_\ell := \frac{i}{4} \int_\Gamma H_\ell^{(1)}(k|x' - x^+|) e^{i\ell\theta'} \hat{t}(x')\varphi(x') ds(x').$$

In the case when Γ is a smooth open arc with the usual $\gamma : [-1, 1] \to \mathbb{R}^2$, we can employ regularized unknowns that take into account the singular behavior of the functional densities (φ, ρ) in the BIE (3.46) as proposed in [17]. Specifically, we use in this case the weighted unknowns

$$\varphi(\gamma(t))|\gamma'(t)| = \varphi^w(t)\sqrt{1-t^2},\ \rho^w(t) := \rho(\gamma(t))|\gamma'(t)|\sqrt{1-t^2}, \quad -1 \le t \le 1 \quad (3.47)$$

in conjunction with the Fejér quadratures described above. The case when Γ is a piecewise smooth open arc, in turn, requires more care as the densities defined on the arc segments that contain open ends require special treatment. Indeed, since on those arc segments $\varphi \sim \mathcal{O}(\sqrt{d})$ and $\rho \sim \mathcal{O}(1/\sqrt{d})$ where d denotes the distance to the open ends, we consider $[0, 1]$ paramterizations of the open arc segments so that the open ends correspond in the parameter space to 0, we use the quadrature points v_n defined as

$$v_n := \frac{1}{2}(1 + \cos(\vartheta_n)), \quad \vartheta_n := \frac{(2n-1)\pi}{2N}, \quad n = 1, \ldots, N$$

and the modified Fejér quadratures

$$\int_0^1 \frac{f(v)}{\sqrt{v}} dv \approx \sum_{n=1}^{N}{}' \omega_n^{(1)} f(v_n),\ \omega_n^{(1)} := \frac{2}{N} \sum_{q=1}^{N} \frac{4}{1-4(q-1)^2} \cos((q-1)\vartheta_n) \tag{3.48}$$

for $n = 1, \ldots, N$ and respectively

$$\int_0^1 f(v)\sqrt{v}\ dv \approx \sum_{n=1}^{N}{}' \omega_n^{(2)} f(v_n), \tag{3.49}$$

$$\omega_n^{(2)} := \frac{2}{N} \sum_{q=1}^{N} \left(\frac{1}{1-4(q-1)^2} + \frac{3}{9-4(q-1)^2} \right) \cos((q-1)\vartheta_n). \tag{3.50}$$

where the prime notation denotes that the first term is halved. We present in Table 3.4 numerical results concerning QBX discretizations of the CC formulations (3.46) in the case when the wavenumber k is real; reference solutions were obtained via (a) the high-order kernel-splitting Nyström methods in [2, 17] in the case of smooth arcs and (b) refined QBX discretizations of the CC formulations with the modified Fejér quadratures (3.48) and (3.49). Similar orders of convergence were observed in the case when the wavenumbers are complex. Again, the advantage of the CC formulations (3.46) is that they are *universally* applicable to all types of boundaries Γ, including piecewise smooth open arcs. Finally, we mention that analytical preconditioners can be employed in order to speed up the iterative convergence of the discrete linear systems corresponding to Nyström discretizations of the CC formulations. Indeed, assuming that the Nyström CC sytem is expressed in the block matrix form

$$\begin{bmatrix} \mathcal{CC}_{11}^n & \mathcal{CC}_{12}^n \\ \mathcal{CC}_{21}^n & \mathcal{CC}_{22}^n \end{bmatrix} \begin{bmatrix} \varphi_n \\ \rho_n \end{bmatrix} = \frac{1}{ik} \begin{bmatrix} f_n \\ 0 \end{bmatrix}$$

we use the following preconditioned CC formulation

$$\begin{bmatrix} \mathcal{CC}_{22}^n & -\mathcal{CC}_{12}^n \\ -\mathcal{CC}_{21}^n & \mathcal{CC}_{11}^n \end{bmatrix} \begin{bmatrix} \mathcal{CC}_{11}^n & \mathcal{CC}_{12}^n \\ \mathcal{CC}_{21}^n & \mathcal{CC}_{22}^n \end{bmatrix} \begin{bmatrix} \varphi_n \\ \rho_n \end{bmatrix} = \frac{1}{ik} \begin{bmatrix} \mathcal{CC}_{22}^n & -\mathcal{CC}_{12}^n \\ -\mathcal{CC}_{21}^n & \mathcal{CC}_{11}^n \end{bmatrix} \begin{bmatrix} f_n \\ 0 \end{bmatrix}. \tag{3.51}$$

Table 3.4 QBX CC Error and Order of Convergence

N	Teardrop		Boomerang		Strip		V-shaped	
	ε_∞	e.o.c.	ε_∞	e.o.c.	ε_∞	e.o.c.	ε_∞	e.o.c.
32	2.1×10^{-1}		8.4×10^{-2}		1.2×10^{-2}		8.5×10^{-3}	
64	2.6×10^{-2}	3.03	7.6×10^{-3}	3.46	3.4×10^{-3}	1.89	2.2×10^{-3}	1.95
128	2.5×10^{-3}	3.32	5.1×10^{-4}	3.88	9.1×10^{-4}	1.89	5.4×10^{-4}	2.01
256	2.4×10^{-4}	3.42	6.1×10^{-5}	3.08	2.4×10^{-4}	1.89	1.3×10^{-4}	1.99

Errors in the near field and estimated orders of convergence obtained when the QBX Nyström discretization is applied to the CC formulation (3.46) with real wavenumber $k = 8$ and normal plane wave incidence. We used the QBX parameters $p = 4$ and $\beta = 4$.

CHAPTER 4

PRECONDITIONERS AND ITERATIVE SCHEMES

This chapter will be dedicated to the multiple time harmonic scattering regime and is based on the paper [88]. By multiple scattering, we mean that there are multiple obstacles, as opposed to the single scattering cases that have been covered so far.

We suppose that the solutions of the multiple scattering problem will take the form of a layer potential. The benefits of the BIE have already been covered, however to reiterate, when discretized the non-localness of the integral operator leads to a dense matrix. Further, the discretization needs to be sufficiently fine to capture the oscillatory nature of the wave, especially for larger wave numbers or a large collection of scatterers. In both of these cases, the linear system will grow and quickly become computationally intractable. Due to the computational complexity of the problems we are considering, direct solvers can no longer be utilized: instead we look to iterative methods, such as GMRES, to solve the discretized linear system in question.

4.1 Some Background and Notational Setup

In general, we cannot directly apply GMRES to the multiple scattering case and expect any speedup. The lack of accelerated convergence is expected to occur due to the non-positiveness of the Helmholtz operator, which becomes more pronounced at larger wave numbers. To recover the speedup from GMRES, a preconditioner is needed. In this context, a natural choice for preconditioner is one that captures the effect of a single scatterer.

4.2 Multiple Scattering

For M scatterers, the boundary of the problem is the collection of all the scatterers $\Gamma = \cup_{i=1}^{M} \Gamma_i$, where we also only consider disjointed scatterers $\cap_{i=1}^{M} \Gamma_i = \emptyset$. We seek

a layer potential solution, and for simplicity, the exposition of this section will just focus on the single layer representation of the Dirichlet problem,

$$u^s(x) = \underbrace{\int_{\cup_{i=1}^{M}\Gamma_i} G_k(x-y)\varphi(y)dS_y}_{\mathcal{S}\varphi} = \sum_{i=1}^{M}\int_{\Gamma_i} G_k(x-y)\varphi_i(y)dS_y \quad x \in \Gamma. \tag{4.1}$$

If we focus our attention on trying to evaluate the Γ_i boundary and also assume that $x \in \Gamma_i$, then this case reduces to the singular integrals that has been extensively covered thus far. In the case that $x \notin \Gamma_i$, this represents the reflection terms from the boundary Γ_i on the other boundaries. Continuing this reasoning for all the scatterers, we can write the problem as a linear system

$$\underbrace{\begin{bmatrix} \mathcal{S}_{\Gamma_1}^{x\in\Gamma_1} & \mathcal{S}_{\Gamma_2}^{x\in\Gamma_1} & \dots & \mathcal{S}_{\Gamma_M}^{x\in\Gamma_1} \\ \mathcal{S}_{\Gamma_1}^{x\in\Gamma_2} & \mathcal{S}_{\Gamma_2}^{x\in\Gamma_2} & \dots & \mathcal{S}_{\Gamma_M}^{x\in\Gamma_2} \\ \vdots & \vdots & \dots & \vdots \\ \mathcal{S}_{\Gamma_1}^{x\in\Gamma_j} & \mathcal{S}_{\Gamma_2}^{x\in\Gamma_j} & \dots & \mathcal{S}_{\Gamma_M}^{x\in\Gamma_j} \\ \vdots & \vdots & \dots & \vdots \\ \mathcal{S}_{\Gamma_1}^{x\in\Gamma_{M-1}} & \mathcal{S}_{\Gamma_2}^{x\in\Gamma_{M-1}} & \dots & \mathcal{S}_{\Gamma_M}^{x\in\Gamma_{M-1}} \\ \mathcal{S}_{\Gamma_1}^{x\in\Gamma_M} & \mathcal{S}_{\Gamma_2}^{x\in\Gamma_M} & \dots & \mathcal{S}_{\Gamma_M}^{x\in\Gamma_1} \end{bmatrix}}_{:=\boldsymbol{\mathcal{S}_M}} \underbrace{\begin{bmatrix} \varphi_1 \\ \varphi_2 \\ \vdots \\ \varphi_j \\ \vdots \\ \varphi_{M-1} \\ \varphi_M \end{bmatrix}}_{:=\boldsymbol{\varphi}} = \underbrace{\begin{bmatrix} g^{x\in\Gamma_1} \\ g^{x\in\Gamma_2} \\ \vdots \\ g^{x\in\Gamma_j} \\ \vdots \\ g^{x\in\Gamma_{M-1}} \\ g^{x\in\Gamma_M} \end{bmatrix}}_{:=\boldsymbol{g}} \tag{4.2}$$

Where the notation $\mathcal{S}_{\Gamma_j}^{x\in\Gamma_i}$ should be understood as the single layer operator on boundary Γ_j but x is located on the boundary Γ_i. In the case that $i = j$, the diagonal entries of the matrix above then result in our familiar singular integrals. Note that the wave number has been suppressed in layer representation for simplicity. Equation (4.2) is the system that we will precondition, once each of the operators $\mathcal{S}_{\Gamma_j}^{x\in\Gamma_i}$ have been discretized, for all $i, j \in \{1, \dots, M\}$. We refer the reader to [88] for the theoretical aspects of the similarity of the different representations and boundary conditions.

4.3 Single Scatter Preconditioner

As mentioned in the introduction of this chapter, we seek a preconditioner that corresponds to the scattering effect of a single scatterer, for each of the scatterers. This will correspond to the diagonal part of the of the matrix $\boldsymbol{\mathcal{S}_M}$. Therefor our single scatterer operator will be

$$\overline{\boldsymbol{\mathcal{S}}}_{\boldsymbol{M}} = \begin{bmatrix} \mathcal{S}_{\Gamma_1}^{x\in\Gamma_1} & 0 & 0 & \dots & 0 & 0 \\ 0 & \mathcal{S}_{\Gamma_2}^{x\in\Gamma_2} & 0 & \dots & 0 & 0 \\ \vdots & & \ddots & \dots & \dots & \vdots \\ 0 & \dots & \dots & \mathcal{S}_{\Gamma_j}^{x\in\Gamma_j} & \dots & 0 \\ \vdots & & \ddots & \dots & \dots & \vdots \\ 0 & \dots & \dots & \dots & \mathcal{S}_{\Gamma_{M-1}}^{x\in\Gamma_{M-1}} & 0 \\ 0 & \dots & \dots & \dots & & \mathcal{S}_{\Gamma_M}^{x\in\Gamma_M} \end{bmatrix}. \tag{4.3}$$

The diagonal components of $\overline{\boldsymbol{\mathcal{S}}}_{\boldsymbol{m}}$ represents the self interacting terms of the scatterer. If the scattering problem consisted only of one scatterer, say, Γ_j, then $\overline{\boldsymbol{\mathcal{S}}}_{\boldsymbol{M}} = \mathcal{S}_{\Gamma_j}^{x\in\Gamma_j}$. In what follows we will assume that none of the wave numbers are irregular, meaning that entries in $\overline{\boldsymbol{\mathcal{S}}}_{\boldsymbol{m}}$ will be invertible, further implying that $\overline{\boldsymbol{\mathcal{S}}}_{\boldsymbol{m}}$ as a whole will also be invertible.

$$\overline{\boldsymbol{\mathcal{S}}}_{\boldsymbol{M}}^{-1} = \begin{bmatrix} (S_{\Gamma_1}^{x\in\Gamma_1})^{-1} & 0 & 0 & \dots & 0 & 0 \\ 0 & (\mathcal{S}_{\Gamma_2}^{x\in\Gamma_2})^{-1} & 0 & \dots & 0 & 0 \\ \vdots & & \ddots & \dots & \dots & \vdots \\ 0 & 0 & \dots & (\mathcal{S}_{\Gamma_j}^{x\in\Gamma_j})^{-1} & \dots & 0 \\ \vdots & & \ddots & \dots & \dots & \vdots \\ 0 & 0 & 0 & 0\dots & (\mathcal{S}_{\Gamma_{M-1}}^{x\in\Gamma_{M-1}})^{-1} & 0 \\ 0 & 0 & 0 & 0\dots & 0 & (\mathcal{S}_{\Gamma_M}^{x\in\Gamma_M})^{-1} \end{bmatrix}$$

$\overline{\boldsymbol{S}}_{\boldsymbol{M}}^{-1}$ will then be the preconditioner that will be used in conjunction with GMRES. After Discretization of $\boldsymbol{\mathcal{S}}_{\boldsymbol{M}}$ an $\overline{\boldsymbol{S}}_{\boldsymbol{M}}^{-1}$, the resulting linear system that needs solving

$$\overline{\boldsymbol{S}}_{\boldsymbol{M}}^{-1}\boldsymbol{\mathcal{S}}_{\boldsymbol{M}}\boldsymbol{\varphi} = \overline{\boldsymbol{S}}_{\boldsymbol{M}}^{-1}\boldsymbol{g}. \tag{4.4}$$

We note that the operator $\overline{\boldsymbol{S}}_{\boldsymbol{M}}^{-1}\boldsymbol{\mathcal{S}}_{\boldsymbol{M}}$, has the following form

$$\overline{\boldsymbol{S}}_{\boldsymbol{M}}^{-1}\boldsymbol{\mathcal{S}}_{\boldsymbol{M}} = \begin{bmatrix} I & \dots & \dots & (S_{\Gamma_1}^{x\in\Gamma_1})^{-1}\mathcal{S}_{\Gamma_M}^{x\in\Gamma_1} \\ (S_{\Gamma_2}^{x\in\Gamma_2})^{-1}\mathcal{S}_{\Gamma_1}^{x\in\Gamma_2} & I & \dots & (S_{\Gamma_2}^{x\in\Gamma_2})^{-1}\mathcal{S}_{\Gamma_2}^{x\in\Gamma_2} \\ \vdots & \vdots & \dots & \vdots \\ (S_{\Gamma_j}^{x\in\Gamma_j})^{-1}\mathcal{S}_{\Gamma_1}^{x\in\Gamma_j} & \vdots & \dots & (S_{\Gamma_j}^{x\in\Gamma_j})^{-1}\mathcal{S}_{\Gamma_M}^{x\in\Gamma_j} \\ \vdots & \vdots & \dots & \vdots \\ (S_{\Gamma_{M-1}}^{x\in\Gamma_{M-1}})^{-1}\mathcal{S}_{\Gamma_1}^{x\in\Gamma_{M-1}} & \vdots & \dots & (S_{\Gamma_{M-1}}^{x\in\Gamma_{M-1}})^{-1}\mathcal{S}_{\Gamma_M}^{x\in\Gamma_{M-1}} \\ (S_{\Gamma_M}^{x\in\Gamma_M})^{-1}\mathcal{S}_{\Gamma_1}^{x\in\Gamma_M} & \dots & \dots & I \end{bmatrix} \tag{4.5}$$

This preconditioner will accelerate the convergence of GMRES: Figure 4.1, Figure 4.2, and numerical experiments in [88] show this to indeed be the case. The reader is referred to this paper for an in depth numerical treatment of the convergence speedup.

4.4 Preconditioner for SL and DL with Varying BC

A wonderful consequence of using this type of formulation to precondition a system like Equation (4.2) is that it generalizes easily to different layer potentials and boundary conditions. As an example, let us assume that we wish to solve the Dirichlet scattering problem with a DL potential. The equivalent system of Equation (4.2) is nearly the same

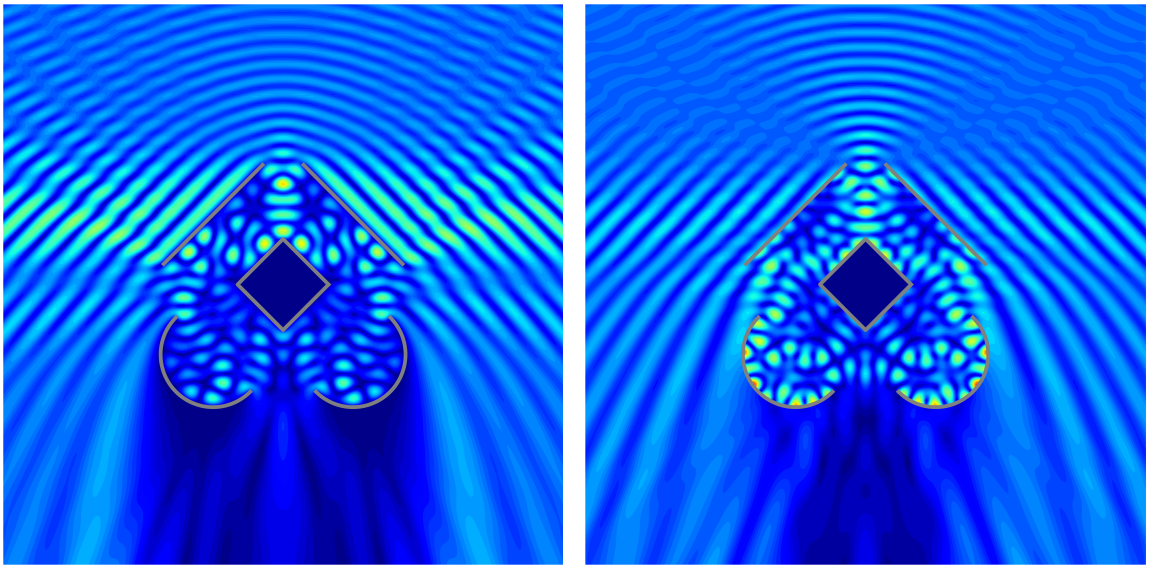

(a) Dirichlet BC. **(b)** Neumann BC.

Figure 4.1 The two images above show the total field resulting from a normal incidence plane wave with multiple scattering for different BC and with wavenumber $k = 15$.

$$\underbrace{\begin{bmatrix} \left(\frac{1}{2}I + \mathcal{K}_{\Gamma_1}^{x\in\Gamma_1}\right) & \mathcal{K}_{\Gamma_2}^{x\in\Gamma_1} & \dots & \mathcal{K}_{\Gamma_M}^{x\in\Gamma_1} \\ \mathcal{K}_{\Gamma_1}^{x\in\Gamma_2} & \left(\frac{1}{2}I + \mathcal{K}_{\Gamma_2}^{x\in\Gamma_2}\right) & \dots & \mathcal{K}_{\Gamma_M}^{x\in\Gamma_2} \\ \vdots & \vdots & \dots & \vdots \\ \mathcal{K}_{\Gamma_1}^{x\in\Gamma_j} & \mathcal{K}_{\Gamma_2}^{x\in\Gamma_j} & \dots & \mathcal{K}_{\Gamma_M}^{x\in\Gamma_j} \\ \vdots & \vdots & \dots & \vdots \\ \mathcal{K}_{\Gamma_1}^{x\in\Gamma_{M-1}} & \mathcal{K}_{\Gamma_2}^{x\in\Gamma_{M-1}} & \dots & \mathcal{K}_{\Gamma_M}^{x\in\Gamma_{M-1}} \\ \mathcal{K}_{\Gamma_1}^{x\in\Gamma_M} & \mathcal{K}_{\Gamma_2}^{x\in\Gamma_M} & \dots & \left(\frac{1}{2}I + \mathcal{K}_{\Gamma_M}^{x\in\Gamma_1}\right) \end{bmatrix}}_{:=\boldsymbol{\mathcal{K}_M}} \underbrace{\begin{bmatrix} \varphi_1 \\ \varphi_2 \\ \vdots \\ \varphi_j \\ \vdots \\ \varphi_{M-1} \\ \varphi_M \end{bmatrix}}_{:=\boldsymbol{\varphi}} = \underbrace{\begin{bmatrix} g^{x\in\Gamma_1} \\ g^{x\in\Gamma_2} \\ \vdots \\ g^{x\in\Gamma_j} \\ \vdots \\ g^{x\in\Gamma_{M-1}} \\ g^{x\in\Gamma_M} \end{bmatrix}}_{:=\boldsymbol{g}}. \quad (4.6)$$

Similarly, the preconditioner will be the inverse of the diagonal terms of Equation (4.6)

$$\overline{\boldsymbol{\mathcal{K}}}_{\boldsymbol{M}}^{-1} = \begin{bmatrix} (\frac{1}{2}I + \mathcal{K}_{\Gamma_1}^{x\in\Gamma_1})^{-1} & \dots & \dots & \dots & 0 \\ 0 & (\frac{1}{2}I + \mathcal{K}_{\Gamma_2}^{x\in\Gamma_2})^{-1} & \dots & 0 & 0 \\ \dots & & \ddots & & \\ \dots & & & \ddots & \\ 0 & 0 & 0\dots & (\frac{1}{2}I + \mathcal{K}_{\Gamma_{M-1}}^{x\in\Gamma_{M-1}})^{-1} & 0 \\ 0 & 0 & 0\dots & 0 & (\frac{1}{2}I + \mathcal{K}_{\Gamma_M}^{x\in\Gamma_M})^{-1} \end{bmatrix}$$

which will lead to the system

$$\overline{\boldsymbol{\mathcal{K}}}_{\boldsymbol{M}}^{-1}\boldsymbol{\mathcal{K}}_{\boldsymbol{M}}\boldsymbol{\varphi} = \overline{\boldsymbol{\mathcal{K}}}_{\boldsymbol{M}}^{-1}\boldsymbol{g}, \tag{4.7}$$

where $\overline{\boldsymbol{\mathcal{K}}}_{\boldsymbol{M}}^{-1}\boldsymbol{\mathcal{K}}_{\boldsymbol{M}}$ will have a similar form to (4.5). This overall procedure will work for any layer potential and boundary condition. In fact it can be generalized to the case where Γ_i and Γ_j do not have the same boundary condition. In general, the preconditioner will depend on the layer formulation and the corresponding trace of the Boundary condition, as can be seen above.

4.5 Discretization

As is perhaps obvious, but nonetheless worth stating, the diagonal terms of (4.2) or (4.6), will at best be singular and at worst hypersingular depending on the layer representation and boundary conditions. Meaning, that each of these terms should have special quadrature applied to it, as done in Chapter 3. The off-diagonal reflection terms however contain no singularity and are smooth, supposing of course that the scatterers are well separated. Stated differently, the orientation of the scatterers need to satisfy

$$\xi h > dist(\Gamma_i, \Gamma_j) \coloneqq \inf\{|x-y| : x \in \Gamma_i, y \in \Gamma_j\} \quad \text{for } i, j \in 1, \dots, M,$$

for some appropriately chosen ξ. Being that these are the only cases investigated, each of the off diagonal terms can be discretized by a simple trapezoidal rule. However, as the number of scatterers, M, grows, fast approximate methods will become essential. Finally, if each scatterer is discretized with N points, the size of the linear system in Equation (4.2) will be $NM \times NM$, with each operator $S_{\Gamma_j}^{x\in\Gamma_i}$ being of $N \times N$. Though, not all of the scatterers need the same resolution; if so, it becomes necessary to pad the system (4.2) to make it square.

Having described various discretization strategies of BIE formulations of Helmholtz equations that are oblivious to the nature of the wavenumber (be it real or complex), we present in the final section numerical results concerning CQ discretizations of the wave equation.

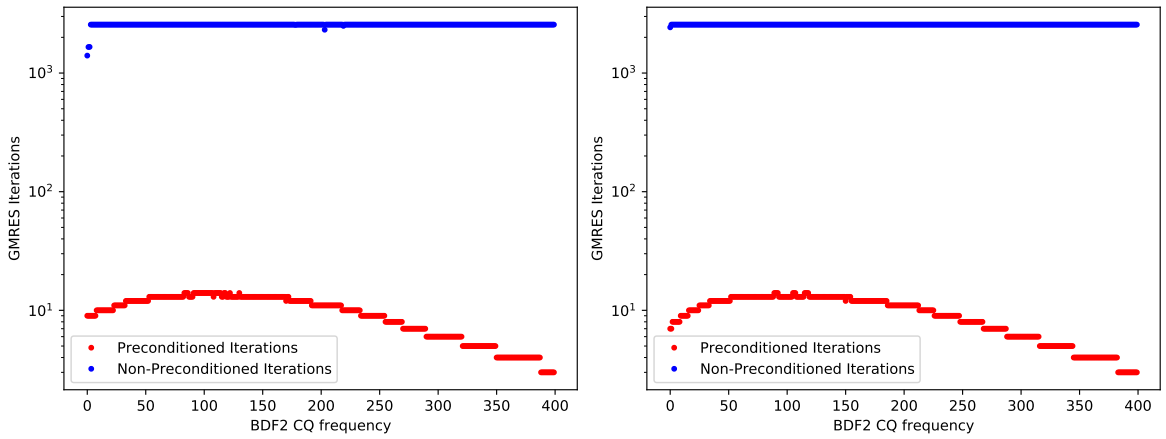

(a) Dirichlet BC. **(b)** Neumann BC.

Figure 4.2 Number of GMRES iterations for the geometric setup in Figure 4.1, with an incidence plane wave $\exp(-\frac{1}{2}(6^2(t - x \cdot d - \Omega)^2)$ and final time $T = 6$. Given is an ensemble of Laplace domain frequencies associated with the CQ BDF2 formulation with a total of 4096 time steps were used and 512 discretization points per boundary.

CHAPTER 5

CQ NUMERICAL EXPERIMENTS

To validate our method we perform numerical experiments for the BDF2, IRK3, and IRK5 time-stepping schemes with a fourth order Alpert quadrature. These experiments will be done over a variety of domains, boundary conditions, and spatial discretizations. The incoming pulsed plane considered will vary: we consider both smooth and non-smooth waves. The error will be calculated using a reference solution, in the norm defined in [7]:

$$\|u_D(x,t_n) - u_d(x,t_n)\| = \sqrt{\sum_{n=0}^{N} \Delta t |u_D(x,t_n) - u_d(x,t_n)|^2},$$

where

1. u_D is a reference solution, with discretization twice as fine in time and space as the last discretized iteration of the approximate solution.

2. u_d is an approximate solution.

Finally, all incoming plane waves will have unit speed.

5.1 Multiple Strips Convergence

Convergence is first tested on a smooth incoming plane wave,

$$u_{inc}(\vec{x},t) = \exp\left(-\frac{1}{2}\left(\frac{t-\vec{x}\cdot\vec{v}-\Omega}{\sigma}\right)^2\right)$$

with varying values of σ. The results are reasonable, showing the correct convergence rate. However, it should be noted that the convergence tapers out prior to its theoretical minimum. This is a common aspect in all the numerical experiments.

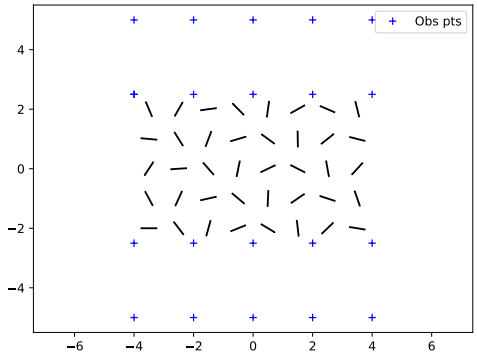

Figure 5.1 Orientation of the scatterers and the location of the obersavation points.

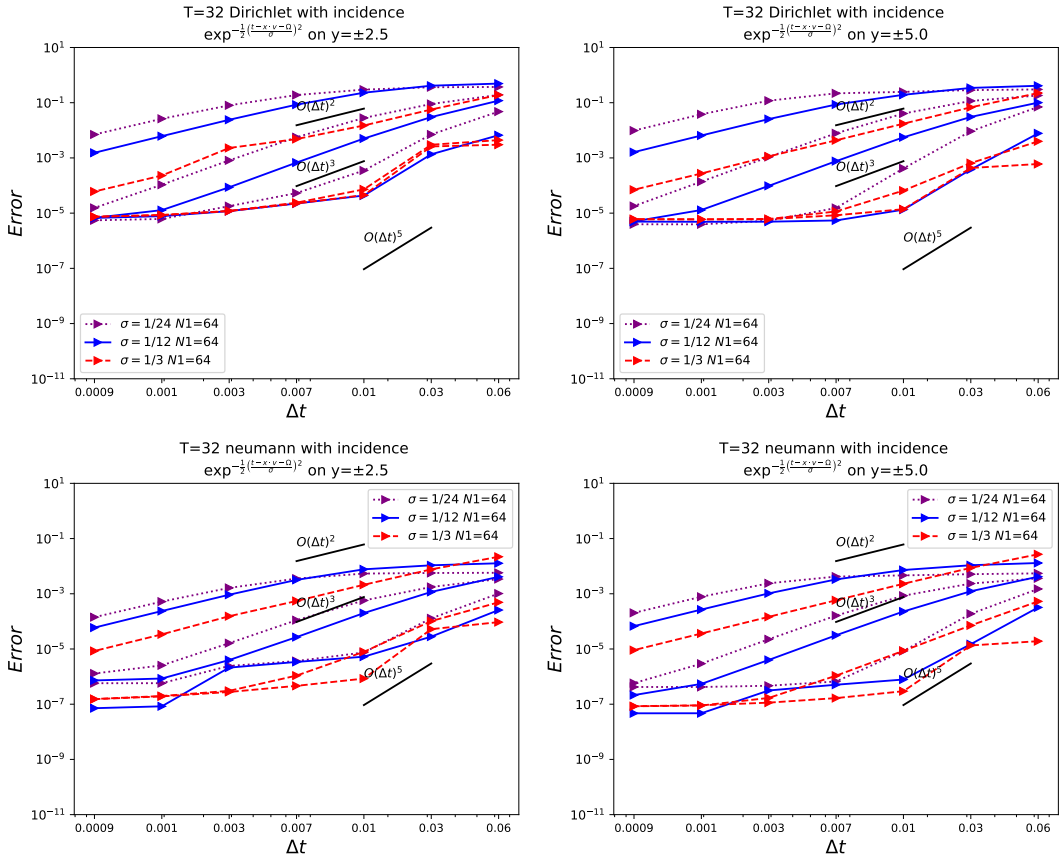

Figure 5.2 Convergence plot for the orientation of the scatterers and observation points 5.1. Different spatial discretization are tested to ensure the correct order of convergence in time.

There are two possible ways to overcome this shortcoming. First, a finer spatial discretization could be used, which is the typical way employed in this manuscript.

A second possibility is to over resolve the frequency domain solves [12]. This is more involved as it means introducing yet another parameter that needs fine tuning. For convenience, this approach has not been explored.

5.2 Grated Strips

This section is dedicated to reproducing results from the paper by Carin and Felsen in [23], and various other papers by the same authors. We first give the setup of the problem and then show the similarity between the two results.

5.2.1 Non-Smooth Incidence

In [23], the parameters are not specified exactly so considerable effort has gone into making the setup match as closely as possible. We use unit strip length oriented as seen in Figure 5.3. The distance between the strips is $2/3$, with the observation point located on the y-axis at the point $(0, 50/3)$. The incidence pulse consists of three sections of a sin function, with two lobes with amplitude below the zero axis and one lobe of amplitude 2 above the zero axis. Their τ parameter normalizes their time trace results,

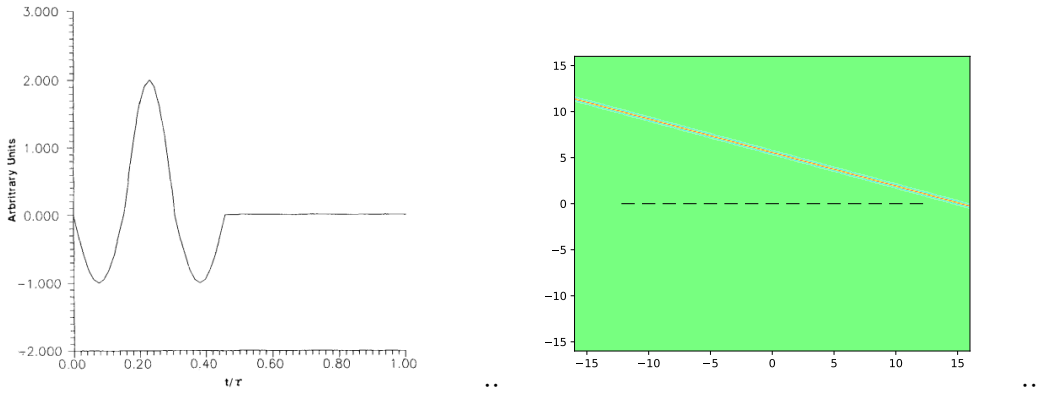

Figure 5.3 In the left figure above, the incidence pulse wave is given. On the left is the orientation of the scatterers and the angle of the plane wave.

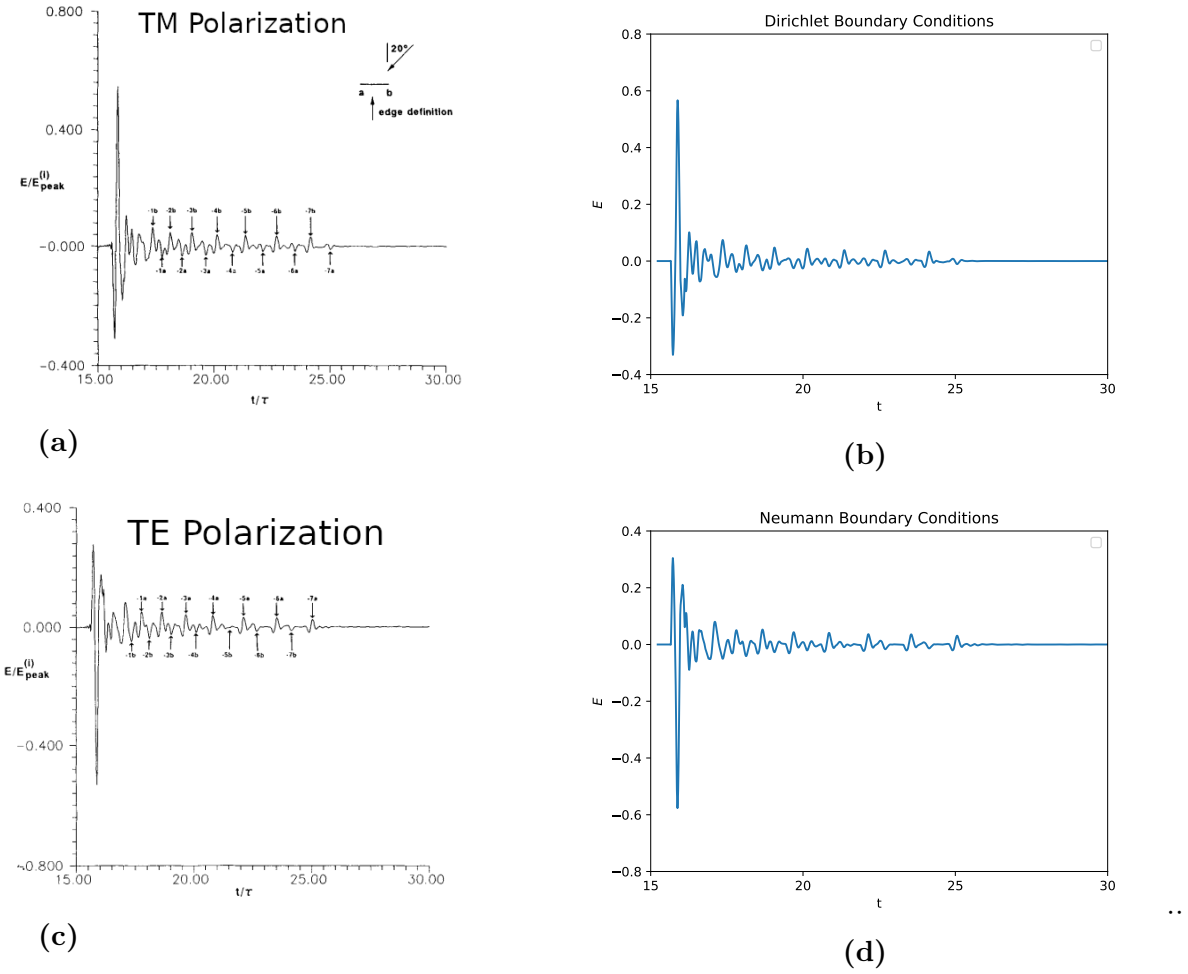

Figure 5.4 Comparisons between the different fields.

The data in Figures 5.4b and 5.4d has been produced with CQ-IRK5 method, while Figures 5.4a and 5.4c has been taken from the paper [23]. Although there are no exact numerical results to compare against, the results seem to match well enough, at least phenomenologically. For the CQ results, 512 points were used to discretize each scatterer and 16384 time steps were used in total, corresponding to $\Delta t \approx 0.0024$. This resolution, in both time and space, is in general not necessary, and lower resolution would also capture the same behavior.

5.2.2 Smooth Incidence with Uniform Grating.

In the previous two sections, the incidences have either been rapidly decaying or compact, respectively. This section deals with a pulse that is smooth but not rapidly decaying:

$$g(t) = \Re\left[\frac{i}{(i+\omega_M t/4)^5}\right] \quad \omega_M = \frac{2\pi}{\lambda_M}. \tag{5.1}$$

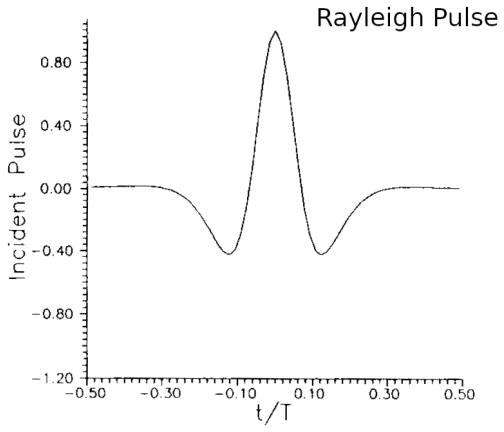

Figure 5.5 The specific pulse to be used in this section from [22]

The parameter ω_M determines the width of the Rayleigh pulse (5.1). The orientation of the scatterers are similar to the previous section, though in this case 20 scatterers are considered and the observation point is at 5/3 above the center of the scatterers as shown in Figure 5.6. We compare our CQ results against the paper [22], which, once again, is only done in phenomenological manner as the raw data and parameters are not explicitly stated.

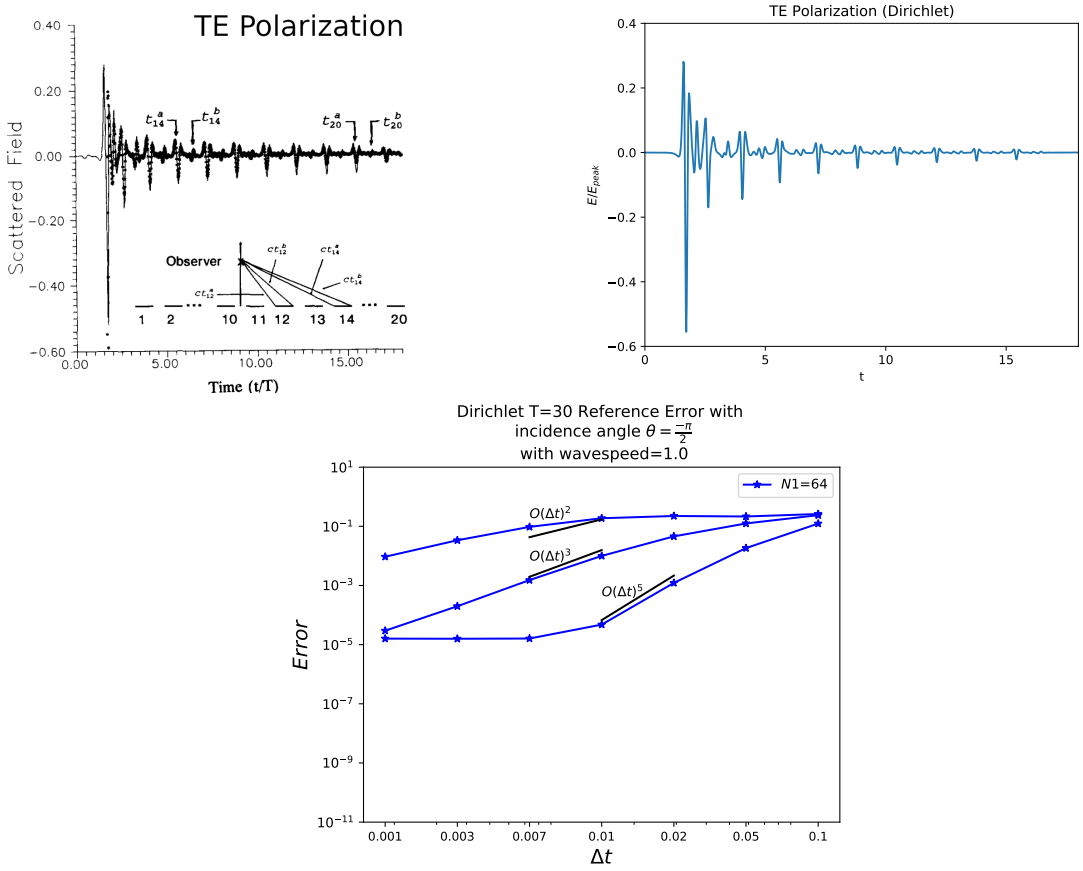

Figure 5.6 Original field from [22] left and CQ field on the right.

5.3 Slotted Cylinder

The Rayleigh pulse (5.1) is considered, once again. For the convergence plots below, ω_M has been chosen in such a way to have the width of the incoming plane wave be approximately the arc length of the aperture opening with angle $\frac{\pi}{2}$ in Figure 5.7b.

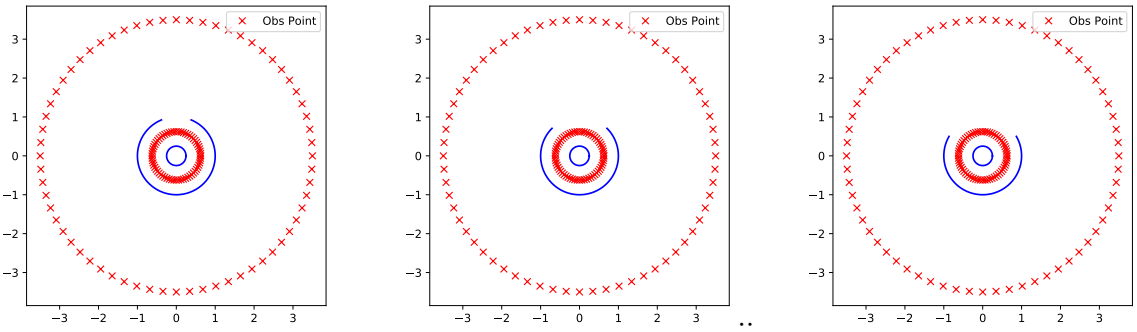

(a) $\frac{\pi}{4}$ **(b)** $\frac{\pi}{2}$ **(c)** $\frac{2\pi}{3}$

Figure 5.7 Different aperture angles.

Three different slotted unit circles are considered, with only the angle of the aperture differing. The circle in the interior has radius of $r = 0.25$. In addition, three different boundary conditions are also imposed on each of the setups: Dirichlet, Neumann, and a mix of the two with the open arc having Dirichlet boundary conditions and in the inner cylinder having Neumann boundary conditions. All other parameters have been kept constant, including spatial discretization, which in this case has been chosen to be 1024 points per scatterer. The effect on convergence of geometry and boundary conditions can be seen in Figure 5.8.

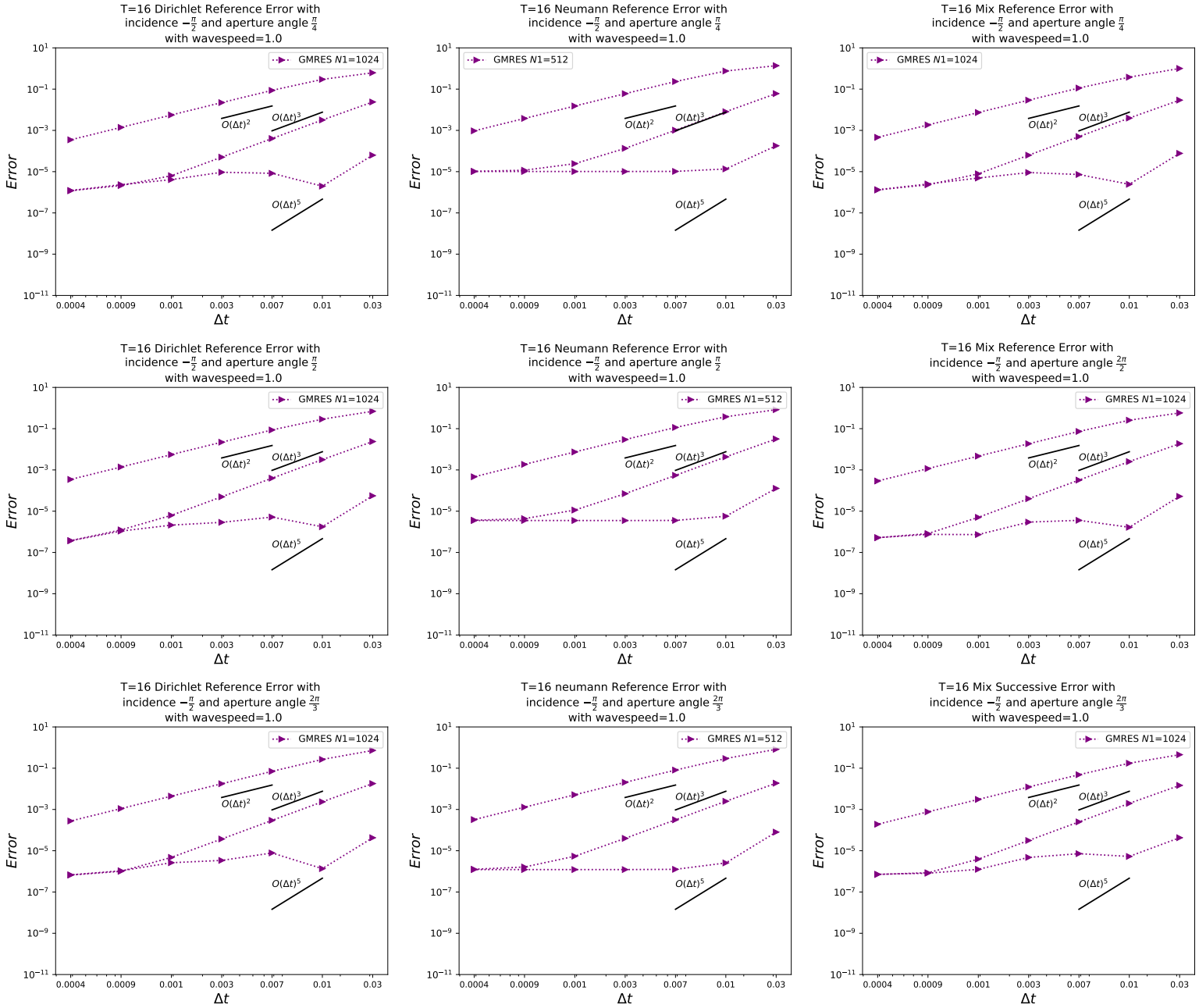

Figure 5.8 Going across a row gives the convergence respectively for Dirichlet, Neumann, and a mix of BC. Going down a column is the convergence as the aperture angle increases.

.

Since the Rayleigh pulse decays slowly, it has been mollified with a smooth cutoff function, and started far enough way, to ensure that at time $t = 0$ the wave does not interact with the scatterers.

5.3.1 Time Traces

Animations from the previous sections are presented here. All the following time traces have been calculated with IRK5 with the same spatial discretization as in Section 5.3 and time discretization $\Delta t \approx 0.007$, which according to the convergence plots results in an absolute time error of about 10^{-5}. For animation purposes, such discretization in both time and space is more than sufficient.

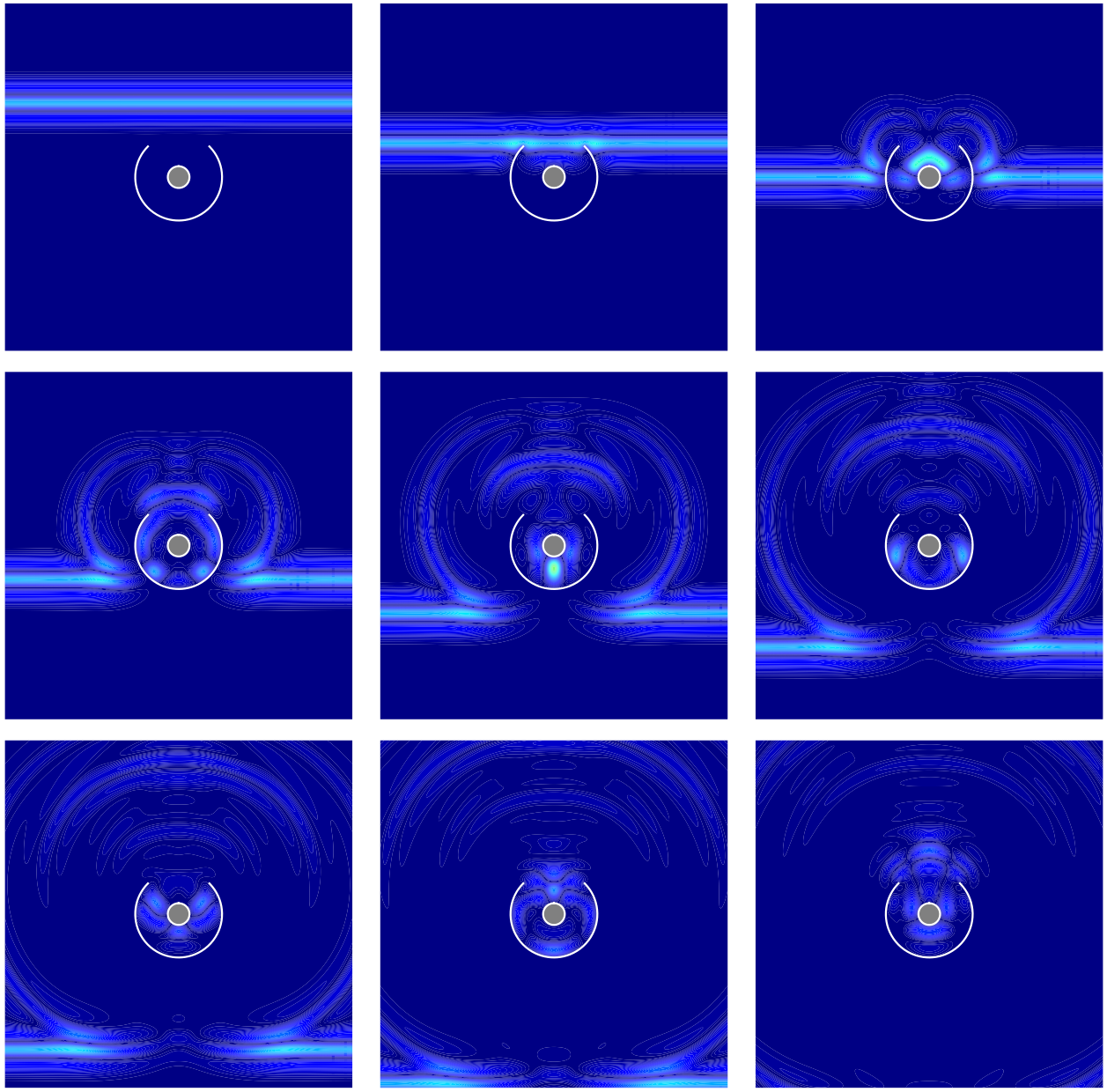

Figure 5.9 Dirichlet time traces of slotted cylinder with an aperture angle of $\frac{\pi}{2}$.

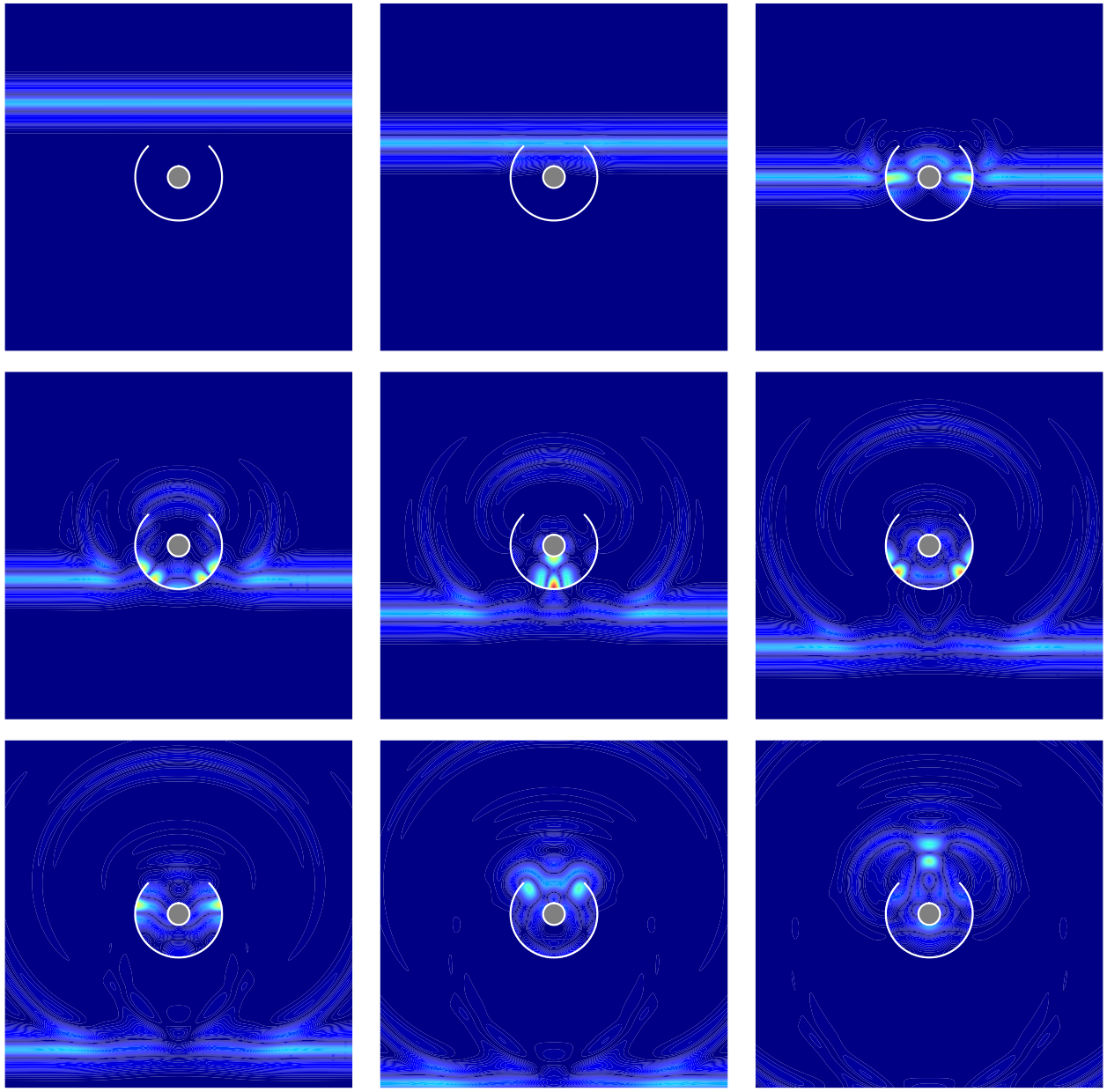

Figure 5.10 Neumann time traces of slotted cylinder with an aperture angle of $\frac{\pi}{2}$.

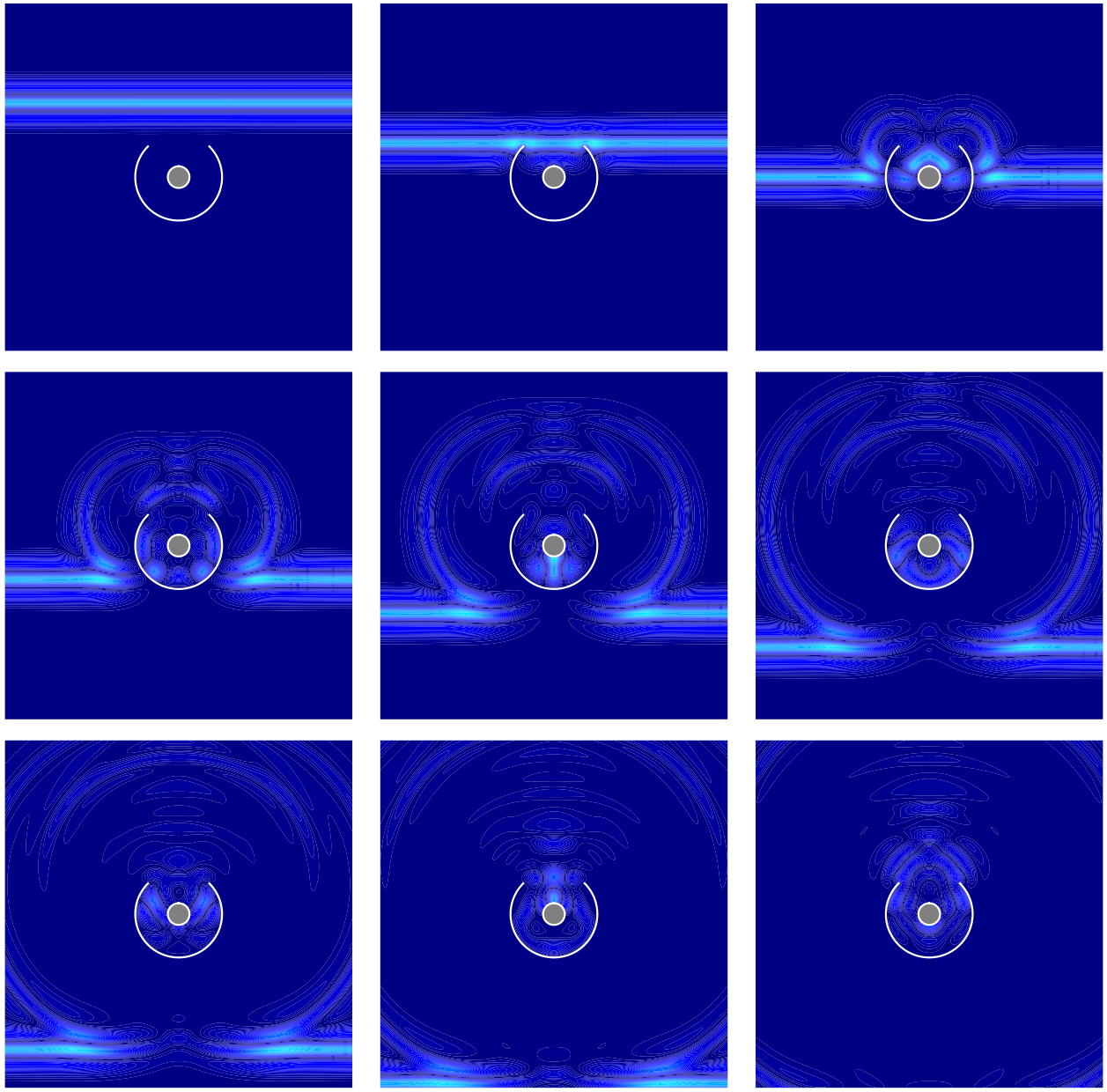

Figure 5.11 Mix BC time traces of slotted cylinder with an aperture angle of $\frac{\pi}{2}$.

CHAPTER 6

CURRENT AND FUTURE WORK

The work presented in the preceeding chapters show the potential to solve large scale time domain scattering problems with CQ and BIE. We have shown the efficiency and accuracy of these methods, especially in the context of scatterers with Lipschitz and open arcs, which are particularly useful for chaff scattering.

Our overall goal has been to explore numerical homogenization to replace a model chaff cloud by a lossy dielectric that produces the same scattered field. While the results towards this end has been promising, the work has been limited in two respects: mainly the number of scatterers but also the dimension of the problems considered.

6.1 Fast Field Evaluation Methods and Scaling

As the scattering system grows, either in number of scatterers or dimension, the computational load to calculate the scattered field to within a prescribed error threshold will grow. The computation time will most likely become intractable making it essential that we have a fast method tailored to work seamlessly with our current setup. One such possibility would be to modify the Fast Multipole method (FMM) to work with the CQ method for two and three dimensions over our complex geometries. Further scaling will also require several parallelization implementations of the method if time domain scattering in three dimensions are to be considered.

6.2 Time Domain Scattering in Three Dimensions

It is possible to extend many of the techniques used thus far to get solutions of the time dependant multiple scattering problem in three dimensions. By considering BIE defined on axisymmetric surfaces in $\mathbb{R}^3$, generated by rotating a curve γ, and under the

restriction that the kernels in the BIE are rotationally invariant, we can via the Fourier transform recast the three dimensional BIE into a sequence of equations defined on the dimensional curve γ [93]. The drawback this method is that scattering surfaces we can consider are somewhat limited, however with the reduction in dimensionality and by making using of Nyström methods, the system that needs to be solved is small and can be inverted directly for a single scatterer. The desire is to couple this method of evaluating three dimensional Helmholtz problems with the CQ method for multiple scatterers.

APPENDIX A

INVERSE RUNGE-KUTTA RADAU-II BUTCHER TABLEAU

In this appendix the Butcher Tableu for the third-order and fifth-order Inverse Runge-Kutta method is given respectively by the following tables:

Table A.1 IRK3 Butcher Tableau

$1/3$	$5/12$	$-1/12$
1	$3/4$	$1/4$
	$3/4$	$1/4$

Table A.2 IRK5 Butcher Tableau

$\frac{2}{5} - \frac{\sqrt{6}}{10}$	$\frac{11}{45} - \frac{7\sqrt{6}}{360}$	$\frac{37}{225} - \frac{169\sqrt{6}}{1800}$	$-\frac{2}{225} + \frac{\sqrt{6}}{75}$
$\frac{2}{5} + \frac{\sqrt{6}}{10}$	$\frac{37}{225} + \frac{169\sqrt{6}}{1800}$	$\frac{11}{45} + \frac{7\sqrt{6}}{360}$	$-\frac{2}{225} - \frac{\sqrt{6}}{75}$
1	$\frac{4}{9} - \frac{\sqrt{6}}{36}$	$\frac{4}{9} + \frac{\sqrt{6}}{36}$	$\frac{1}{9}$
	$\frac{4}{9} - \frac{\sqrt{6}}{36}$	$\frac{4}{9} + \frac{\sqrt{6}}{36}$	$\frac{1}{9}$

APPENDIX B

ALPERT QUADRATURE WEIGHTS AND NODES

Table B.1 gives the various weights and nodes for the desired order of convergence l with Alpert quadrature. For the purposes of combining this method of quadrature with CQ, we have found in practise that the 4th order gives the best mix of speed and accuracy.

Table B.1 Alpert Quadrature Weights and Nodes

l	a	χ_i	w_i
2	1	1.591549430918953e − 01	5.000000000000000e − 01
3	2	1.150395811972836e − 01	3.913373788753340e − 01
		9.365464527949632e − 01	1.108662621124666e + 00
4	2	2.379647284118974e − 02	8.795942675593887e − 02
		2.935370741501914e − 01	4.989017152913699e − 01
		1.023715124251890e + 00	9.131388579526912e − 01
5	3	2.339013027203800e − 02	8.609736556158105e − 02
		2.854764931311984e − 01	4.847019685417959e − 01
		1.005403327220700e + 00	9.152988869123725e − 01
		1.994970303994294e + 00	1.013901778984250e + 00
6	3	4.004884194926570e − 03	1.671879691147102e − 02
		7.745655373336686e − 02	1.636958371447360e − 01
		3.972849993523248e − 01	4.981856569770637e − 01
		1.075673352915104e + 00	8.372266245578912e − 01
		2.003796927111872e + 00	9.841730844088381e − 01
8	5	6.531815708567918e − 03	2.462194198995203e − 02
		9.086744584657729e − 02	1.701315866854178e − 01
		3.967966533375878e − 01	4.609256358650077e − 01
		1.027856640525646e + 00	7.947291148621894e − 01
		1.945288592909266e + 00	1.008710414337933e + 00
		2.980147933889640e + 00	1.036093649726216e + 00
		3.998861349951123e + 00	1.004787656533285e + 00
10	6	1.175089381227308e − 03	4.560746882084207e − 03
		1.877034129831289e − 02	3.810606322384757e − 02
		9.686468391426860e − 02	1.293864997289512e − 01
		3.004818668002884e − 01	2.884360381408835e − 01
		6.901331557173356e − 01	4.958111914344961e − 01
		1.293695738083659e + 00	7.077154600594529e − 01
		2.090187729798780e + 00	8.741924365285083e − 01
		3.016719313149212e + 00	9.661361986515218e − 01
		4.001369747872486e + 00	9.957887866078700e − 01
		5.000025661793423e + 00	9.998665787423845e − 01

APPENDIX C

FOURIER INTERPOLATION FOR ALPERT QUADRATURE

In addition to interpolating onto our discritization with a Lagrange basis we also have the possibility of doing the interpolation via different manner. We have in this section decided to perform a Fourier interpolation. We give a brief derivation, starting with:

$$\int_0^T k(x_i, x')\sigma(x')dx' \approx h\sum_{p=1}^{N-a} k(x_i, x_i + ph)\sigma(x') + h\sum_{p=1}^{2m} k(x_i, x_i + \chi_p h)\sigma(x_i + \chi_p h)$$

The first sum on the right is on our grid, so that part is to be left alone. If we look at the last sum and suppose that

$$\sigma(x) \approx \frac{1}{2\pi}\sum_{n=-\frac{N}{2}+1}^{N/2} \hat{\sigma}_n e^{inx}$$

where

$$\begin{bmatrix} \hat{\sigma}_1 \\ \hat{\sigma_2} \\ \vdots \\ \hat{\sigma}_n \end{bmatrix} = DFT \begin{bmatrix} \sigma_1 \\ \sigma_2 \\ \vdots \\ \sigma_n \end{bmatrix}$$

and $DFT \in \mathbb{C}^{N\times N}$. The operator termed DFT is of course the discrete Fourier transform. Armed with this we can then try to interpolate onto our grid:

$$\begin{aligned} \sigma(x_i + \chi_p h) &\approx \frac{1}{2\pi}\sum_{n=-\frac{N}{2}+1}^{\frac{N}{2}} \hat{\sigma}_n e^{in(x_i+\chi_p h)} \\ &= \frac{1}{2\pi}\sum_{n=-\frac{N}{2}+1}^{\frac{N}{2}} \hat{\sigma}_n e^{inx_i} e^{in\chi_p h} \end{aligned}$$

$$= \frac{1}{2\pi} \sum_{n=-\frac{N}{2}+1}^{\frac{N}{2}} \left(\sum_{j=1}^{N} DFT_{nj}\sigma_j \right) e^{inx_i} e^{in\chi_p h}$$

Meaning that our interpolation can be written as:

$$\sum_{p=1}^{2m} w_p k(x_i, \chi_p h)\sigma(x_i + \chi_p h) \approx \frac{1}{2\pi} \sum_{p=1}^{2m} w_p k(x_i, \chi_p h) \sum_{n=-\frac{N}{2}+1}^{\frac{N}{2}} \left(\sum_{j=1}^{N} DFT_{nj}\sigma_j \right) e^{inx_i} e^{in\chi_p h}$$

The aim is not to turn these sums into some clever matrix products. Towards that end let is define the final entity we are looking for as

$$\begin{aligned} C_{ij} &= \frac{1}{2\pi} \sum_{p=1}^{2m} w_p k(x_i, \chi_p h) \sum_{n=-\frac{N}{2}+1}^{\frac{N}{2}} DFT_{nj} e^{inx_i} e^{in\chi_p h} \\ &= \frac{1}{2\pi} \sum_{n=-\frac{N}{2}+1}^{\frac{N}{2}} DFT_{nj} e^{inx_i} \sum_{p=1}^{2m} w_p k(x_i, x_i + \chi_p h) e^{in\chi_p h} \\ &= \frac{1}{2\pi} \sum_{n=-\frac{N}{2}+1}^{\frac{N}{2}} W_{in} DFT_{nj} \end{aligned}$$

Where we have that

$$W_{in} = \frac{1}{2\pi} e^{inx_i} \sum_{p=1}^{2m} w_p k(x_i, x_i + \chi_p h) e^{in\chi_p h}.$$

We further want to see if we can rewrite this last quatity in an intelligent manner. Let us try to do so be defining:

$$W_{in} = \frac{1}{2\pi} e^{inx_i} U_{in},$$

where we have defined U as

$$U_{in} = \frac{1}{2\pi} \sum_{p=1}^{2m} w_p k(x_i, x_i + \chi_p h) e^{in\chi_p h}$$

We can now further define U as a prdouct of matrices if we let

$$F_{i\rho} = w_p k(x_i, x_i + \chi_p h)$$

$$G_{\rho n} = e^{in\chi_p}.$$

Hence we then have that

$$U_{in} = \frac{1}{2\pi} \sum_{p=1}^{2m} F_{i\rho} G_{\rho n} \quad \text{or rather} \quad U = FG.$$

It should be noted that whenever a entry in a matrix or vector is denoted by n, since there are negative summing entries in the above formulation, the entry actually needs to be $n = n + \frac{N}{2}$. We also need to mention that this formulation only makes sense if the discritization is an even number. It is better still if it is a power of two. Dimensionally we have that $F \in \mathbb{C}^{N \times 2m}$ and $G \in \mathbb{C}^{2m \times N}$. Meaning that $W \in \mathbb{C}^{N \times N}$. Finally this means then that

$$C = \frac{1}{2\pi} W * DFT,$$

as we were looking for.

REFERENCES

[1] Bradley K Alpert. Hybrid gauss-trapezoidal quadrature rules. *Society for Industrial and Applied Mathematics Journal on Scientific Computing*, 20(5):1551–1584, 1999.

[2] Akash. Anand, Jeff Ovall, and Catalin Turc. Well-conditioned boundary integral equations for two-dimensional sound-hard scattering problems in domains with corners. *J. Integral Equations Appl.*, 24(3):321–358, 2012.

[3] Thomas Geoffrey Anderson. Hybrid frequency-time analysis and numerical methods for time-dependent wave propagation. *Dissertation (Ph.D.), California Institute of Technology, Pasadena, California*, (2):185–200, 2021.

[4] Constantin Bacuta, Victor Nistor, and Ludmil Zikatanov. Regularity and well posedness for the Laplace operator on polyhedral domains. *arXiv preprint math/0410207.*, pages 1–8, 2004.

[5] Lehel Banjai. Multistep and multistage convolution quadrature for the wave equation: algorithms and experiments. *Society for Industrial and Applied Mathematics Journal on Scientific Computing*, 32(5):2964–2994, 2010.

[6] Lehel Banjai, Christian Lubich, and Jens Markus Melenk. Runge–kutta convolution quadrature for operators arising in wave propagation. *Numerische Mathematik*, 119(1):1–20, 2011.

[7] Lehel Banjai and Stefan Sauter. Rapid solution of the wave equation in unbounded domains. *Society for Industrial and Applied Mathematics Journal on Numerical Analysis*, 47(1):227–249, 2009.

[8] Alex Barnett, Leslie Greengard, and Thomas Hagstrom. High-order discretization of a stable time-domain integral equation for 3D acoustic scattering. *Journal of Computational Physics*, 402:109047, 2020.

[9] Alvin Bayliss and Eli Turkel. Radiation boundary conditions for wave-like equations. *Communications on Pure and Applied Mathematics*, 33(6):707–725, 1980.

[10] Abderrahmane Bendali, Francis Collino, Mbarek Fares, and Bassam Steif. Extension to nonconforming meshes of the combined current and charge integral equation. *Institute of Electrical and Electronics Engineers transactions on antennas and propagation*, 60(10):4732–4744, 2012.

[11] Jean Pierre Berenger. A perfectly matched layer for the absorption of electromagnetic waves. *Journal of Computational Physics*, 114(2):185–200, 1994.

[12] Timo Betcke, Nicolas Salles, and Wojciech Smigaj. Overresolving in the laplace domain for convolution quadrature methods. *Society for Industrial and Applied Mathematics Journal on Scientific Computing*, 39(1):A188–A213, 2017.

[13] E. H. Bleszynski, M. K. Bleszynski, T. Jaroszewicz, and R. Albanese. Analysis of dispersive effects and enhanced medium penetrability in wide-band pulse propagation through sparse discrete media. In *Proceedings - 2011 International Conference on Electromagnetics in Advanced Applications*, pages 235–238, 2011.

[14] Yassine Boubendir and Catalin Turc. Wave-number estimates for regularized combined field boundary integral operators in acoustic scattering problems with neumann boundary conditions. *IMA Journal of Numerical Analysis*, 33(4):1176–1225, 2013.

[15] Helmut Brakhage and Peter Werner. Über das Dirichletsche Aussenraumproblem für die Helmholtzsche Schwingungsgleichung. *Archiv de Mathematik*, 16:325–329, 1965.

[16] James Bremer. On the nyström discretization of integral equations on planar curves with corners. *Applied and Computational Harmonic Analysis*, 32(1):45–64, 2012.

[17] Oscar P Bruno and Stéphane K Lintner. Second-kind integral solvers for te and tm problems of diffraction by open arcs. *Radio Science*, 47(06):1–13, 2012.

[18] Oscar P Bruno and Stéphane K Lintner. A high-order integral solver for scalar problems of diffraction by screens and apertures in three-dimensional space. *Journal of Computational Physics*, 252:250–274, 2013.

[19] A. J. Burton and G. F. Miller. The application of integral equation methods to the numerical solution of some exterior boundary-value problems. *Proceedings of the Royal Society. London. Series A. Mathematical, Physical and Engineering Sciences*, 323:201–210, 1971. A discussion on numerical analysis of partial differential equations (1970).

[20] Zhiqiang Cai, Seokchan Kim, Sangdong Kim, and Sooryun Kong. A finite element method using singular functions for Poisson equations: Mixed boundary conditions. *Computer Methods in Applied Mechanics and Engineering*, 195(19-22):2635–2648, 2006.

[21] Zhiqiang Cai, Seokchan Kim, and Gyungsoo Woo. A finite element method using singular functions for the Poisson equation: Crack singularities. *Numerical Linear Algebra with Applications*, 9(6-7):445–455, 2002.

[22] L. Carin and L.B. Felsen. Time harmonic and transient scattering by finite periodic flat strip arrays: hybrid (ray)-(floquet mode)-(mom) algorithm. *Institute of Electrical and Electronics Engineers Transactions on Antennas and Propagation*, 41(4):412–421, 1993.

[23] Lawrence Carin and Leopold B. Felsen. Efficient analytical-numerical modeling of ultra-wideband pulsed plane wave scattering from a large strip grating. *International Journal of Numerical Modelling: Electronic Networks, Devices and Fields*, 6(1):3–17, 1993.

[24] Durga Prasad Challa and Mourad Sini. On the justification of the Foldy-lax approximation for the acoustic scattering by small rigid bodies of arbitrary shapes. *Multiscale Modeling and Simulation*, 12(1):55–108, 2014.

[25] Durga Prasad Challa and Mourad Sini. Multiscale analysis of the acoustic scattering by many scatterers of impedance type. *Zeitschrift fur Angewandte Mathematik und Physik*, 67(3):1–31, 2016.

[26] Roman Chapko, Rainer Kress, and Lars Mönch. On the numerical solution of a hypersingular integral equation for elastic scattering from a planar crack. *IMA Journal of Numerical Analysis*, 20(4):601–619, 2000.

[27] David Colton and Rainer Kress. *Integral equation methods in scattering theory*. Pure and Applied Mathematics. John Wiley & Sons Inc., New York, New York, 1983. A Wiley-Interscience Publication.

[28] David Colton and Rainer Kress. *Inverse acoustic and electromagnetic scattering theory*, volume 93 of *Applied Mathematical Sciences*. Springer-Verlag, Berlin, Germany, second edition, 1998.

[29] Penny J. Davies. A stability analysis of a time marching scheme for the general surface electric field integral equation. *Applied Numerical Mathematics*, 27(1):33–57, 1998.

[30] Penny J. Davies and Dugald B. Duncan. Stability and convergence of collocation schemes for retarded potential integral equations. *Society for Industrial and Applied Mathematics Journal on Numerical Analysis*, 42(3):1167–1188, 2004.

[31] Penny J Davies and Dugald B Duncan. Stability and Convergence of Collocation Schemes for Retarded Potential Integral Equations. *Society for Industrial and Applied mathematics Journal on Numerical Analysis*, 42(3):1167–1188, 2004.

[32] Victor Dominguez, Sijiang L Lu, and Francisco-Javier Sayas. A fully discrete calderón calculus for two dimensional time harmonic waves. *arXiv preprint arXiv:1210.7017*, 2012.

[33] Víctor Domínguez, Sijiang L Lu, and Francisco-Javier Sayas. A nyström flavored calderón calculus of order three for two dimensional waves, time-harmonic and transient. *Computers & Mathematics with Applications*, 67(1):217–236, 2014.

[34] Victor Dominguez, Mark Lyon, and Catalin Turc. Well-posed boundary integral equation formulations and nyström discretizations for the solution of helmholtz

transmission problems in two-dimensional lipschitz domains. *Journal of Integral Equations and Applications*, 28(3):395–440, 2016.

[35] Víctor Domínguez, Maria-Luisa Rapún, and Francisco-Javier Sayas. Dirac delta methods for helmholtz transmission problems. *Advances in Computational Mathematics*, 28(2):119–139, 2008.

[36] Víctor Domínguez, Tonatiuh Sánchez-Vizuet, and Francisco-Javier Sayas. A fully discrete calderón calculus for the two-dimensional elastic wave equation. *Computers & Mathematics with Applications*, 69(7):620–635, 2015.

[37] Bjorn Engquist and Andrew Majda. Absorbing boundary conditions for numerical simulation of waves. *Proceedings of the National Academy of Sciences*, 74(5):1765–1766, 1977.

[38] Bjorn Engquist and Andrew Majda. Radiation boundary conditions for acoustic and elastic wave calculations. *Communications on Pure and Applied Mathematics*, 32(3):313–357, 1979.

[39] Charles L. Epstein and Leslie Greengard. Debye sources and the numerical solution of the time harmonic maxwell equations. *Communications on Pure and Applied Mathematics: A Journal Issued by the Courant Institute of Mathematical Sciences*, 63(4):413–463, 2010.

[40] Charles L. Epstein, Leslie Greengard, and Thomas Hagstrom. On the stability of time-domain integral equations for acoustic wave propagation. *Discrete and Continuous Dynamical Systems- Series A*, 36(8):4367–4382, 2016.

[41] Leslie L Foldy. The multiple scattering of waves. i. general theory of isotropic scattering by randomly distributed scatterers. *Physical Review*, 67(3-4):107, 1945.

[42] Kim Green and Kari Lumme. Multiple scattering by the iterative Foldy–Lax scheme. *Journal of the Optical Society of America A*, 22(8):1555, 2005.

[43] Magnus Gustavsson, Gerhard Kristensson, and Niklas Wellander. Multiple scattering by a collection of randomly located obstacles – numerical implementation of the coherent fields. *Journal of Quantitative Spectroscopy and Radiative Transfer*, 185:95–100, 2016.

[44] Bamberger Alain Ha-Duong, Tuong and Jean-Claude Nedelec. Formulation variationnelle espace-temps pour le calcul par potentiel retardé de la diffraction d'une onde acoustique (i). *Mathematical Methods in the Applied Sciences*, 8(1):405–435, 1986.

[45] Tuong Ha-Duong. On Retarded Potential Boundary Integral Equations and their Discretisation. pages 301–336. Springer, Berlin, Heidelberg, 2003.

[46] Thomas Hagstrom and Timothy Warburton. Complete Radiation Boundary Conditions: Minimizing the Long Time Error Growth of Local Methods. *Society for Industrial and Applied Mathematics Journal on Numerical Analysis*, 47(5):3678–3704, 2009.

[47] Sijia Hao, Alex. H. Barnett, Per-Gunnar Martinsson, and Mattew Young. High-order accurate methods for nystrom discretization of integral equations on smooth curves in the plane. *Advances in Computational Mathematics*, 40(1):245–272, 2014.

[48] Matthew Hassell and Francisco Javier Sayas. Convolution Quadrature for wave simulations. In *SEMA SIMAI Springer Series*, volume 9, pages 71–159. Springer International Publishing, 2016.

[49] Johan Helsing and Rikard Ojala. Corner singularities for elliptic problems: Integral equations, graded meshes, quadrature, and compressed inverse preconditioning. *Journal of Computational Physics*, 227(20):8820–8840, 2008.

[50] Hoppe Ronald W. Hiptmair, Ralf and Ulrich Langer. Report No. 11/2004. *Workshop on Computational Electromagnetism*, (36):1–15, 2003.

[51] Kai Huang, Knut Solna, and Hongkai Zhao. Generalized Foldy-Lax formulation. *Journal of Computational Physics*, 229(12):4544–4553, 2010.

[52] Martin Huber. Numerical Solution of the Wave Equation in Unbounded Domains Masterarbeit. *Doctoral dissertation, Universität Zürich, Institut für Mathematik*, 2011.

[53] Berenger Jean-Pierre. A perfectly matched layer for the absorption of electromagnetic waves. *Journal of Computational Physics*, 114(2):185–200, 1994.

[54] Andreas Klöckner, Alexander Barnett, Leslie Greengard, and Michael O'Neil. Quadrature by expansion: A new method for the evaluation of layer potentials. *Journal of Computational Physics*, 252:332–349, 2013.

[55] Dan Kosloff and Ronnie Kosloff. A nonreflectlng boundary condition for discrete acoustic and elastic wave calculations. In *Society of Exploration Geophysicist Annual Meeting*, pages 627–628. Society of Exploration Geophysicists, 1984.

[56] Rainer Kress. A Nyström method for boundary integral equations in domains with corners. *Numerische Mathematik*, 58(1):145–161, 1990.

[57] Rainer Kress. Boundary integral equations in time-harmonic acoustic scattering. *Mathematical and Computer Modelling*, 15(3-5):229–243, 1991.

[58] Rainer Kress. On the numerical solution of a hypersingular integral equation in scattering theory. *Journal of Computational and Applied Mathematics*, 61(3):345–360, 1995.

[59] Rainer Kress. A collocation method for a hypersingular boundary integral equation via trigonometric differentiation. *Journal of Integral Equations and Applications*, 26(2):197–213, 2014.

[60] Gerhard Kristensson. Coherent scattering by a collection of randomly located obstacles - An alternative integral equation formulation. *Journal of Quantitative Spectroscopy and Radiative Transfer*, 164:97–108, 2015.

[61] R. Kussmaul. Ein numerisches Verfahren zur Lösung des Neumannschen Neumannschen Aussenraumproblems für die Helmholtzsche Schwingungsgleichung. *Springer Computing (Arch. Elektron. Rechnen)*, 4:246–273, 1969.

[62] Ignacio Labarca, Luiz M. Faria, and Carlos Pérez-Arancibia. Convolution quadrature methods for time-domain scattering from unbounded penetrable interfaces. *Proceedings of the Royal Society A: Mathematical, Physical and Engineering Sciences*, 475(2227), 2019.

[63] Melvin Lax. Multiple scattering of waves. II. the effective field in dense systems. *Physical Review*, 85(4):621–629, 1952.

[64] Lee Jin-Fa, Lee Robert, and Andreas Cangellaris. Time-domain finite-element methods. *Institute of Electrical and Electronics Engineers Transactions on Antennas and Propagation*, 45(3):430–442, 1997.

[65] Jie Liao and Chao Ji. Extended Foldy-Lax Approximation on Multiple Scattering. *Mathematical Modelling and Analysis*, 19(1):85–98, 2014.

[66] Wangtao Lu and Ya Yan Lu. Efficient high order waveguide mode solvers based on boundary integral equations. *Journal of Computational Physics*, 272:507–525, 2014.

[67] Christian Lubich. Convolution quadrature and discretized operational calculus. II. *Numerische Mathematik*, 52(4):413–425, 1988.

[68] Christian Lubich. On convolution quadrature and Hille-Phillips operational calculus. *Applied Numerical Mathematics*, 9(3-5):187–199, 1992.

[69] Sherman W. Marcus. Electromagnetic wave propagation through chaff clouds. *Institute of Electrical and Electronics Engineers Transactions on Antennas and Propagation*, 55(7):2032–2042, 2007.

[70] Erich Martensen. Über eine Methode zum räumlichen Neumannschen Problem mit einer Anwendung für torusartige Berandungen. *Acta Math.*, 109:75–135, 1963.

[71] Paul A Martin. *Multiple scattering: interaction of time-harmonic waves with N obstacles*, volume 107. Cambridge University Press, New York, New York, 2006.

[72] M. Melenk, Jens and Stefan Sauter. Convergence analysis for finite element discretizations of the Helmholtz equation with Dirichlet-to-Neumann boundary conditions. *Mathematics of Computation*, 79(272):1871–1871, 2010.

[73] Fabian Müller, Dominik Schötzau, and Christoph Schwab. Discontinuous Galerkin Methods for Acoustic Wave Propagation in Polygons. *Journal of Scientific Computing*, 77(3):1909–1935, 2018.

[74] Pelle Olsson. High order finite differences methods on non-smooth domains. *Computer Methods in Applied Mechanics and Engineering*, 116(1-4):265–272, 1994.

[75] C.-J. Ong, D. Miller, L. Tsang, B. Wu, and C.-C. Huang. Application of the Foldy–Lax multiple scattering method to the analysis of vias in ball grid arrays and interior layers of printed circuit boards. *Microwave and Optical Technology Letters*, 49(1):225–231, 2007.

[76] Kailash C. Patidar. On the use of nonstandard finite difference methods. *Journal of Difference Equations and Applications*, 11(8):735–758, 2005.

[77] Carlos Pérez-arancibia. A plane-wave singularity subtraction technique for the classical Dirichlet and Neumann combined field integral equations. *Applied Numerical Mathematics*, 123:221–240, 2018.

[78] Peter P. Petropoulos, Catalin Turc, and Erli Wind-Andersen. Nyström methods for high-order cq solutions of the wave equation in two dimensions. *arXiv preprint arXiv:2111.06829*, 2021.

[79] Youcef Saad and Martin H. Schultz. GMRES: a generalized minimal residual algorithm for solving nonsymmetric linear systems. *Society for Industrial and Applied Mathematics J. Sci. Statist. Comput.*, 7(3):856–869, 1986.

[80] Francisco-Javier Sayas. Retarded potentials and time domain boundary integral equations. 2013.

[81] Daniel Seibel. Boundary Element Methods for the Wave Equation based on Hierarchical Matrices and Adaptive Cross Approximation. *arXiv preprint arXiv:2006.05186*, pages 1–40, 2020.

[82] T. B. A. Senior, K. Sarabandi, and F. T. Ulaby. Measuring and modeling the backscattering cross section of a leaf. *Radio Science*, 22(6):1109–1116, 1987.

[83] D. W. Seo, J. H. Yoo, K. I. Kwon, and N. H. Myung. Generalized equivalent conductor method for a chaff cloud with an arbitrary orientation distribution. *Progress in Electromagnetics Research*, 105:333–346, 2010.

[84] John Strikwerda. *Finite Difference Schemes and Partial Differential Equations*. Society for Industrial and Applied Mathematics, Philadelphia, Pennsylvania, 2004.

[85] A. Taflove and K.R. Umashankar. The finite-difference time-domain (fd-td) method for numerical modeling of electromagnetic scattering. *Institute of Electrical and Electronics Engineers Transactions on Magnetics*, 25(4):3086–3091, 1989.

[86] Allen Taflove, Susan C. Hagness, and Melinda Piket-May. Computational Electromagnetics: The Finite-Difference Time-Domain Method. In *The Electrical Engineering Handbook*, pages 629–670. 2005.

[87] Matti Taskinen and Pasi Yla-Oijala. Current and charge integral equation formulation. *Institute of Electrical and Electronics Engineers Transactions on Antennas and Propagation*, 54(1):58–67, 2006.

[88] Betrand Thierry. A remark on the single scattering preconditioner applied to boundary integral equations. *Journal of Mathematical Analysis and Applications*, 413(1):212–228, 2014.

[89] Vidar Thomée. From finite differences to finite elements. *Journal of Computational and Applied Mathematics*, 128(1-2):1–54, 2001.

[90] L. Nick Trefethen. *Spectral Methods in MATLAB*. Software, Environments, and Tools. Society for Industrial and Applied Mathematics, Philadelphia, Pennsylvania, 2000.

[91] Boping Wu and Leung Tsang. Full-wave modeling of multiple vias using differential signaling and shared antipad in multilayered high speed vertical interconnects. *Progress in Electromagnetics Research*, 97:129–139, 2009.

[92] Ali E. Yilmaz, Jian Ming Jin, and Eric Michielssen. Time domain adaptive integral method for surface integral equations. *Institute of Electrical and Electronics Engineers Transactions on Antennas and Propagation*, 52(10):2692–2708, 2004.

[93] P Young, Sijia Hao, and Per-Gunnar Martinsson. A high-order Nyström discretization scheme for boundary integral equations defined on rotationally symmetric surfaces. *Journal of Computational Physics*, 231:4142–4159, 2012.

[94] Z. D. Zaharis and J. N. Sahalos. On the electromagnetic scattering of a chaff cloud. *Electrical Engineering*, 85(3):129–135, 2003.